

ABSTRACT

Title of Dissertation: NEW METHOD FOR KINETIC ISOTOPE EFFECT MEASUREMENTS

Teodora Kljaic, Doctor of Philosophy, 2023

Dissertation directed by: Myles B. Poulin, Department of Chemistry and Biochemistry

Kinetic isotope effect (KIE) measurements are a powerful tool to interrogate the microscopic steps in enzyme catalyzed reactions and can provide detailed information about transition state structures. However, the application of KIE measurements to study enzymatic reactions is not widely applied due to the tedious and complex analytical workflows required to measure KIEs with sufficient precision. In this thesis I described the development of a novel competitive KIE measurement method using MALDI-TOF-MS and the investigation of the transition state of glycosyltransferase enzyme BshA from *B. subtilis*.

We developed a method for the direct measurement of competitive KIEs using a whole molecule matrix assisted laser desorption ionization (MALDI) time of flight (TOF) mass spectrometry (MS). This approach enabled quantitative measurements of both relative isotope

abundance of an analyte and fractional conversion F in single measurements without the need for purification prior to analysis. The application of this MALDI-TOF MS approach has demonstrated the precision of KIE measurements comparable to those obtained using competitive radioisotope labelling, and NMR based approaches while requiring smaller amounts of stable isotope labelled substrates.

Using two chemoenzymatic approaches, we then synthesized 5 substrates for the application of our method to investigate the transition state of BshA: UDP-GlcNAc (**3.1**), [1''-¹³C]UDP-GlcNAc (**3.2**), [2''-¹³C]UDP-GlcNAc (**3.3**), [¹³C₆]UDP-GlcNAc (**3.4**) and [2''-²H]UDP-GlcNAc (**3.5**). Finally, we have begun to work on the synthesis of [1''-¹⁸O]UDP-GlcNAc and describe an approach to prepare this substrate that is currently underway in the lab.

Application of the quantitative whole molecule MALDI-TOF MS approach enabled us to determine multiple competitive KIEs for the enzymatic reaction catalyzed by BshA. While previous studies suggested a front-face S_{Ni} (D_{NAN}) TS for the conjugation of UDP-GlcNAc and L-malate, our KIE results show that a stepwise mechanism resulting in the formation of a discrete, though likely short lived, oxocarbenium ion intermediate is more likely.

Our method be applied to study other glycosyltransferases whose mechanisms still remain to be elucidated and to design TS based inhibitors for enzymes involved in different bacterial infections. Future work on automation of this method would simplify the KIE measurement process and increase reproducibility making the measurement of KIEs for TS analysis a more experimentally accessible technique for the broader enzymology research community.

LAY ABSTRACT

Bacterial infections are usually treated with antibiotics, that help the immune system clear the infection. But sometimes, bacteria develop a way to protect themselves against antibiotics and the immune system. Bacterial infections which are resistant to antibiotics often lead to sepsis if another antibiotic is not available and are most dangerous for immunocompromised people. People become immunocompromised for many reasons, including advanced age, metabolic disorders like diabetes, cancer treatments, and even cancer itself. Antibiotic resistance in immunocompromised people can often lead to death. But if we can quickly develop molecules that stop these bacteria from being resistant, it would increase the effectiveness of antibiotics currently available on the market. These molecules are called inhibitors because they inhibit the activity of enzymes, which are proteins that bacteria use for many functions that allow their survival.

We developed a method that can quickly, precisely and with relative ease analyze what goes on inside the enzyme. When enzymes consume different molecules called substrates, they go through a transition state before forming a product. Our method obtains information about this transition state that can be used to design inhibitors. While other methods investigating transition states exist, they are mainly performed by only the specialized labs who developed them. These methods often require extensive purification, and separate measurements of the variables important for this analysis. We designed a more user-friendly method that could be applied by a wider community of researchers – a method that does not require purification of molecules being analyzed and measures all important variables simultaneously with a precision comparable to the other methods in this field.

We used our novel method to analyze an enzyme called BshA, which is involved in antibiotic resistance of Fosfomycin, the drug that is used to treat urinary tract and bladder infections and other infections that lead to sepsis in immunocompromised patients. We found new information about the transition state of BshA which could be used to make inhibitors that would stop Fosfomycin resistance. Moreover, our method can be used to investigate other enzymes involved in bacterial and viral infections, and potentially even different types of cancer. As long as an enzyme is important for the progression of a disease, our method could test it to quickly and precisely investigate its transition state. This information could be used to build an inhibitor that would stop the disease of interest.

NEW METHOD FOR KINETIC ISOTOPE EFFECT
MEASUREMENTS

by

Teodora Kljaic

Dissertation submitted to the Faculty of the Graduate School of the
University of Maryland, College Park, in partial fulfillment
of the requirements for the degree of
Doctor of Philosophy
2023

Advisory Committee:

Assistant Professor Myles Poulin, Chair

Professor Jeffrey Davis

Professor Philip DeShong

Professor Daniel Falvey

Professor Ian White

© Copyright by
Teodora Kljaic
2023

Dedication

This thesis is dedicated to my beautiful, brave, and relentless mother Jasna who has given me everything I have.

Acknowledgements

I want to start by thanking my advisor Dr. Myles Poulin. He has been an invaluable mentor to whom I am eternally grateful. His suggestions about my research and my writing have been instrumental in my growth as a scientist. He always showed confidence in my ability and provided valuable guidance with any research issues we encountered. It has been an true honor to work with him, as his intelligence, humility and way of thinking have been a constant inspiration to me since the day I met him. I am really proud of the method we developed together and the scientist I became with his guidance and belief in me.

Next, I would like to appreciate the inspiring work and mentorship from my committee members. I want to express my gratitude for all our interactions. I have had the pleasure of taking classes with all my committee members and I will never forget the subtlety with which they influenced my thinking, learning and research abilities. Dr. DeShong and Dr. Davis have been particularly helpful, supportive and wise during my transition between Master's and Doctorate degree. I would like to thank Dr. Ian White at the University of Maryland, Bioengineering Department for being the Dean's representative for my thesis defense. My great appreciation goes to Dr. Yue Li for his insight and help over the years with MALDI-TOF MS and to Ryan O'Neil for his help with QTOF-BioMS. I also need to acknowledge Dr. Fu Chen for his help with NMR acquisition. I would also like to thank the National Science Foundation (NSF) for financial support for this work, and our collaborator Jim Paulson for sending us plasmids for our KIE work.

I also want to express gratitude to Dr. Lyle Isaacs for his excellent teaching during the classes I have had with him, and his overall approach to ambition and excellence. I have had the honor of being a Teaching Assistant for Dr. Isaacs, Dr. Poulin and Dr. Christopher Capp, and I am grateful to have learned from them the structure, discipline and patience one needs to teach.

I would like to applaud the work of amazing staff members Diane Canter and Faith Johnson who have been helpful beyond belief with all the paperwork, questions, and amazing support a graduate student could ever wish for. I owe a special thanks to Carl Womack for his motivational words of wisdom and genuine care about the wellbeing of all students.

I would like to acknowledge the contributions of the previous Poulin lab members to my projects: Merritt Scott – for her help with enzyme expression and optimization of substrate synthesis, Andrew Liu – for his help with isotopically labeled substrate synthesis, Michal Tyrlic – for his expertise with data analysis using R, and Veronica Guirguis – for her help with MALDI-TOF MS acquisition. It has been a great pleasure and honor to work alongside so many wonderful colleagues in the Poulin lab who have made my PhD experience unforgettable. I am rendered speechless at the immense gratitude I owe Merritt Scott, Dr. Shaochi Wang, Dr. Alexandra Peterson, and Kayla Best for welcoming me to Poulin lab when I first started. They created a joyful and supportive environment to the workplace that I could only dream of and continued to encourage and inspire me after they graduated. My current labmates Luan Vo, Steven Hong, Sashika Fernando, Sureshee Liyanaarachchi, Kwaku Obeng, Prince Tetteh and

Kehinde Joshua have carried on the legacy of a healthy supportive friendly lab atmosphere, and I am very grateful for all the laughter and meaningful conversations we have had. I will never forget the dancing breaks I have had with Alex, Merritt and Sashika, nor will I forget the peaceful writing sessions I had with Kwaku. I want to thank Steven for being a great sounding board whenever I needed him, Luan and Prince for always making me smile, and Sureshee for always making sure I ate something during late nights in the lab.

Other important people I cannot fail to mention are my previous colleagues and mentors. Dr. John (Kitty) Giddens, Dr. Chris Toonstra, Dr. Jared Orwenyo, Dr. Kevin Li, and Dr. Hui Cai have all influenced my knowledge of analytical techniques, enzyme expression and enzymatic reaction optimization that has been a great help when arriving to Poulin lab. I would also like to honor the knowledge and expertise of my past mentors Dr. Mark Levandoski, Dr. Steven Sieck, Dr. Peter Storz, Dr. Jim Lindberg, Dr. Theresa Geller and Mihajlo Kozomora, who have influenced my path towards graduate school.

Next, I would like to thank some of my friends without whose support, encouragement and uplifting talks my experience in graduate school would be nearly impossible. Ioannis Vasilios Voliotis and his family have brought my family and me invaluable contributions. Their insightful, motivational and caring words regularly brought me joy for the last two years of my graduate school, and their belief in my perseverance brought out my strength in my weakest times. I would also like to acknowledge my friends Panayota, Ian and Ariel for their support and healing presence

in my life during the last three years of my graduate school. I am also grateful to the friends I met through dancing in the DMV who supported and motivated me during my PhD journey – Gaby Macias, Kathy Zen, Jamiel Roberson, Daniel Lee, Erick Rivera, Emily Anne, Michael Rosado, Jose R. Fontanez, Warner Wilson, Vincent Emanuele, Jonathan Batista, Wanda, Rita (Ferret), Remi, Kira, Natt, Marymar and Saul. The encouragement and love I received from each one of them cannot be quantified but it immensely contributed to my overall graduate school experience. I also owe gratitude to my roommates Joelle and Caleb who have listened to my troubles throughout the years and could always bring a smile to my face.

I would like to express my immense gratitude for my loyal friends of 15 years who have supported me on my educational journey to the US – Strahinja, Stefan, Miloš, Tijana and particularly Kristina Jovanovic for her fiery support throughout all the years I have known her. Her support during my transition between my Master's and PhD labs has meant to me more than words can describe, and her words of optimistic realism have brought a breath of fresh air to my days. I am very appreciative of my college friends as well, who have hosted me in their homes, given me advice and support when I needed it and always cheered me on – Mani, Tanya, Isaac, Peca, Abraham, Tasnim, Josh, Chike, Erik and Christine. They each contributed to my survival in different ways and each one of them was irreplaceable to me. During my time in the US, I have always been able to count on my host parents from Grinnell, Iowa – Dixie and Doug Hansen. They encouraged and supported me during my educational journey as if I was their own daughter, and I am at a lack of words that would thank them enough for welcoming my family and me into their lives and into their hearts. Additionally, I would like to

show gratitude to my really good friends from graduate school, Dr. Aaron Geller, Dr. Matt Thum, Rebecca Thum, Winston, Louie Coplan and Dr. Sarah Menio for all the motivational and encouraging conversations, healing times spent together and all the laughter since the day I arrived to University of Maryland onward. During my time at Maryland, I was very fortunate to encounter amazing support group called Adventure Club, without whose encouragement, relentless drive, strength and love I could not have stayed sane in graduate school – Aravind, Leo, Yehnara, Kyle, Kevin and Medha. I owe a great deal of gratitude to them for monitoring and nurturing my progress, focus and mental health. Their constant motivation and support were of crucial importance to getting me to my PhD. Finally, I would like to thank and recognize the friends who have become my family who always had belief in my perseverance – Kyle Oliver, Troy (Jaguar) Walker, and Melissa (Margay) Tsai, in chronological order. Kyle has been my best man for my PhD, my relentless champion who always elevated my spirits during tough times and kept me focused on the light at the end of the tunnel. He is the best cheerleader I have ever met, and I owe him a huge amount of gratitude for always knowing what to say and never losing faith in me. Troy has been my source of vigor, love, encouragement, and peace since the first day we studied together and has been an inspiration of strength and resilience throughout the entire time I have known him. Melissa has been my reenergizing power, a beautiful light during my toughest months this past year, a source of laughter during my long nights in lab and a great friend who is always biased in my favor. I owe them all a debt of gratitude for all their love and support.

Most importantly, I would like to acknowledge my family: my grandparents – for inspiration, my father – for determination, my uncle – for never-ending joy, my sister – for the most supportive laughter, and my mother – for my analytical mind, my perseverance and her most unconventional support. I would like to thank my mother Jasna and sister Bojana for everything they have done for me before and during my PhD journey. They were with me via video calls since the moment I arrived to the US. They were with me during my long nights in lab, keeping me awake. They were with me whenever I felt lost and sad. Without their unconditional love, encouragement, wake-up calls, reminders, and video calls, none of this would have been possible. All the hope, drive, resilience and endurance I have developed, I owe to them and for that, I dedicate this PhD to them.

Table of Contents

Dedication	ii
Acknowledgements	iii
Table of Contents	ix
List of Tables	xii
List of Figures	xiii
List of Illustrations	xiv
List of Abbreviations	xiii
Chapter 1: Introduction to Transition State Analysis of Glycosyltransferase via Kinetic Isotope Measurements	1
1.1 Primary and Secondary KIEs	5
1.2 Kinetic Isotope Effect Measurements	9
1.3 Transition State Analysis	12
1.4 Overview of current approaches for KIE measurements	13
1.4.1 Measurement of KIEs by Scintillation Counting/Radiolabeling	14
1.4.2 Measurement of KIEs by Nuclear Magnetic Resonance Spectrometry (NMR)	16
1.4.3 Measurement of KIEs by Mass Spectrometry (MS).....	18
1.4.4 Measurement of KIEs by MALDI-MS	20
1.5 Glycosyltransferases	21
1.5.1 Mechanism nomenclature – chemical vs enzymatic (GT) mechanisms	23
1.6 Bibliography	28
Chapter 2: Direct Competitive Kinetic Isotope Effect Measurement Using Quantitative Whole Molecule MALDI-TOF Mass Spectrometry	44
2.1 Introduction.....	45
2.2 Results and Discussion	49
2.3 Conclusion	54
2.4 Experimental Procedures	54

2.4.1 General.....	54
2.4.2 Protein and substrate preparation.....	55
2.4.3 Sample quenching.....	56
2.4.4 MALDI-TOF MS sample preparation and acquisition.....	57
2.4.5 KIE measurements.....	58
2.4.2 Peak integration and data analysis.....	58
2.5 Bibliography.....	60
Chapter 3: Chemoenzymatic synthesis of isotopically labeled UDP-N-Acetyl Glucosamine substrates.....	69
3.1 Introduction.....	70
3.2 Results and Discussion.....	75
3.3 Conclusion.....	80
3.4 Experimental Procedures.....	81
3.4.1 General.....	81
3.4.2 Protein preparation.....	82
3.4.3 General procedure for Enzymatic Synthesis of UDP-GlcNAc substrates.....	84
3.5 Bibliography.....	91
3.6 Appendix.....	100
Chapter 4: Direct Competitive Kinetic Isotope Effect Measurement of BshA Using Quantitative Whole Molecule MALDI-TOF Mass Spectrometry.....	108
4.1 Introduction.....	109
4.2 Results and Discussion.....	116
4.3 Conclusion.....	119
4.4 Experimental Procedures.....	120
4.4.1 General.....	120

4.4.2 Protein Preparation.....	121
4.4.3 Sample quenching.....	121
4.4.4 MALDI-TOF MS Sample Preparation and Acquisition.....	122
4.4.5 KIE measurements.....	123
4.4.6 Peak integration and data analysis.....	124
2.5 Bibliography.....	125
Chapter 5: Summary and Future Directions.....	138
5.1 Summary and Future Directions.....	139
5.2 Bibliography.....	145

List of Tables

Table 1.1 Approximate ranges of KIEs Measured in TS Analyses	6
Table 2.1 Summary of LacZ KIEs	52
Table 3.1 Summary of isotopically labeled substrates and their application.....	76
Table 4.1 Summary of experimental KIEs for BshA.....	117

List of Figures

Figure 1.1 Reaction rate acceleration in enzymatic reactions.....	3
Figure 1.2 Zero point energy difference between C-H and C-D bond	4
Figure 1.3 Categorization of KIE types	7
Figure 1.4 Energy diagrams of normal KIE vs inverse KIE.....	12
Figure 1.5 Liquid scintillation counting principle of analysis	15
Figure 1.6 Mechanism nomenclature.....	24
Figure 1.7 GT mechanisms	26
Figure 2.1 Quantitative MALDI-TOF MS approach for competitive KIE measurements.....	47
Figure 2.2 Optimization of MALDI-TOF MS conditions for competitive KIE measurements.....	50
Figure 2.3 Quantitative MALDI-TOF MS approach for competitive KIE determination	51
Figure 2.4 Mechanism for LacZ catalyzed hydrolysis of lactose highlighting the first transition state	53
Figure 3.1 Biosynthesis and cellular utilization of UDP-GlcNAc in <i>E. coli</i>	72
Figure 3.2 Enzymatic incorporation of 2''- ² H.....	78
Figure 4.1 The basic chemical reaction mechanisms of glycosylation.....	110
Figure 4.2 Experimental KIEs for BshA glycosyltransferase.....	117
Figure 4.3 Proposed front-face transition state for BshA-catalyzed conjugation of UDP-GlcNAc and L-malate.....	119

List of Illustrations

Scheme 3.1 Overall chemoenzymatic synthesis of the isotopically labeled UDP- GlcNAc substrates	76
Scheme 3.2 Synthesis of [1''- ¹⁸ O] UDP-GlcNAc from GlcNAc	79
Scheme 4.1 Bacillthiol biosynthesis pathway.....	115

List of Abbreviations

nuclear magnetic resonance (NMR)

cryo-electron microscopy (CryoEM)

kinetic isotope effect (KIE)

transition state (TS)

ground state (GS)

vibrational energy (E_n)

bond stretch (ν),

fractional conversion (F)

heavy/light isotope ratio (R)

nucleophilic addition (A_N)

nucleophilic dissociation (D_N)

density functional theory (DFT)

liquid scintillation counting (LSC)

heteronuclear single quantum coherence nuclear magnetic resonance (HSQC-NMR)

mass spectrometry (MS)

isotope-ratio mass spectrometry (IRMS)

whole molecule mass spectrometry (WMMS)

electrospray ionization (ESI)

matrix assisted laser desorption/ionization (MALDI).

time-of-flight (TOF)

high-performance liquid chromatography (HPLC)

glycosyltransferase (GT)

nucleotide diphosphate (NDP)

International Union of Biochemistry and Molecular Biology (IUBMB)

carbohydrate active enzyme database (**CAZy**)

uridinediphosphate-2-acetamido-2-deoxy- β -D-glucopyranose (UDP-GlcNAc)

ultraviolet-visible spectroscopy (UV-Vis)

Escherichia coli (*E.coli*)

β -galactosidase (LacZ)

lactose (Lac)

2,4-dihydroxybenzoic acid (DHB)

Tris hydroxymethyl aminomethane hydrochloride (Tris-HCl)

3-(N-morpholino)-propanesulfonic acid (MOPS)

glutamic acid (Glu)

trifluoroacetic acid (TFA)

β -D-galactopyranoside (PNP-Galactose)

adenosine triphosphate (ATP)

nucleotide triphosphate (NTP)

N-acetylglucosamine-1-phosphate (GlcNAc-1-P)

uridine triphosphate (UTP)

N-acetyl-D-glucosamine (GlcNAc)

N-acetyl-D-galactosamine (GalNAc)

UDP-N-acetyl-hexosamine pyrophosphorylase (AGX1)

GlcNAc-1-phosphate uridyltransferase (GlmU)

UDP-N-acetylglucosamine 2-epimerase (WecB)

uridinediphosphate-N-acetylmannosamine (UDP-ManNAc)

N-acetylhexosamine-1-kinase (NahK)

inorganic pyrophosphate (iPP)

pyruvate kinase (PK)

inorganic pyrophosphorylase (IPPase)

unit (U)

hydrazinoquinoline (2-HQ)

endonuclease from *Neisseria denitrificans* (NdeI)

deoxyribonuclease from *Haemophilus influenzae* (HindIII)

optical density (OD)

isopropyl β -D-1-thiogalactopyranoside (IPTG)

relative centrifugal force (rcf)

units of gravity or times gravity ($\times g$)

sodium dodecyl-sulfate polyacrylamide gel electrophoresis (SDS-PAGE)

nickel nitrilotriacetic acid (Ni-NTA)

ethanol (EtOH)

hydrochloric acid (HCl)

dichloromethane (CH₂Cl₂)
sodium bicarbonate (NaHCO₃)
sodium sulphate (NaSO₄)
ethyl acetate (EtOAc)
aspartic acid (Asp)
histidine (His)
amino acid (AA)
arginine (Arg)
lysine (Lys)
substitution nucleophilic intramolecular (S_Ni)
bacillthiol (BSH)
Bacillus subtilis (*B. subtilis*)
N-acetylglucosaminy-malate (GlcNAc-mal)
uridine diphosphate (UDP)
L-malate (L-mal)

**Chapter 1: Introduction to Transition State Analysis of
Glycosyltransferase via Kinetic Isotope Measurements**

Enzymes are one of the largest categories of biological drug targets, with more than 40% of approved drugs targeting enzymes. One way to target enzymes is through the design of small molecules that inhibit the catalytic function of the enzyme. Traditionally, high-throughput screening approaches and structure-based drug design are used to discover enzyme inhibitors, however each has its limitations. High-throughput screening for example, requires an appropriate assay that is compatible with automated liquid handling that enables sensitive detection of inhibitor binding, and requires access to large libraries of small molecules to screen, which are not always available. Structure-based drug design, on the other hand, utilizes information about protein three-dimensional structure from x-ray crystallography, nuclear magnetic resonance (NMR) spectroscopy, or cryo-electron microscopy (CryoEM). While advances in structural biology techniques have increased access to protein structural information, structural determination of many drug targets remains challenging. This is especially true for membrane proteins and intrinsically disordered proteins that can be resistant to traditional structural biology approaches. Thus, there is a need for alternative methods for drug design. One such alternative involves the design of transition state analogues as enzyme inhibitors by mimicking the geometry and electron distribution at the enzymatic transition state.

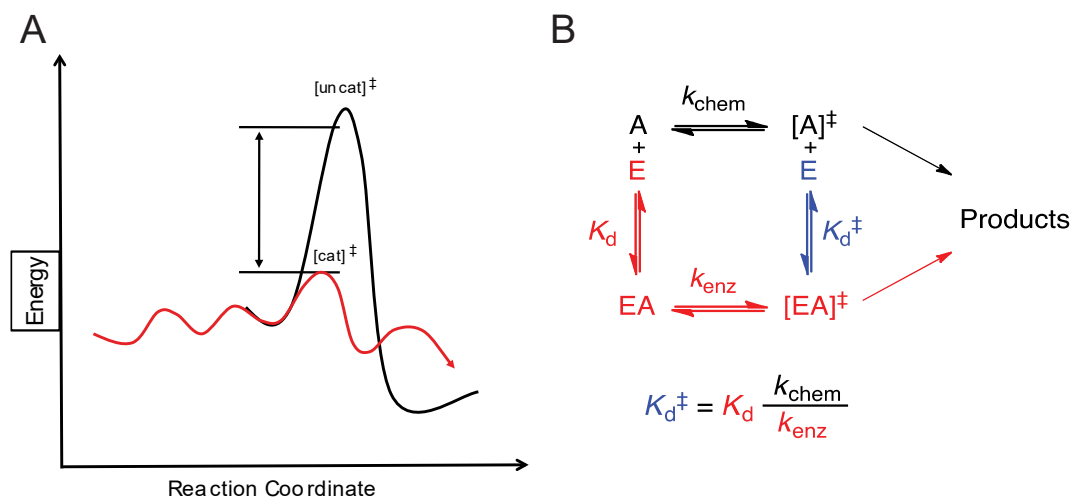


Figure 1.1. Reaction rate acceleration in enzymatic reactions. (A) Energy diagram showing the difference in activation energy between uncatalyzed and enzymatically catalyzed reaction. (B) Diagram of thermodynamic relationship between rate constants of catalyzed and uncatalyzed reaction

We know that enzymes are able to greatly accelerate the rate of chemical reactions by lowering the activation energy needed to reach the transition state (Figure 1.1). Linus Pauling first postulated that enzymes accomplish this rate enhancement by evolving to bind tightly to and stabilize the transition state species of the reaction.¹ Barry Wolfenden formalized the thermodynamics for this hypothesis in 1972, which shows that the enzyme binds tighter to that transition state species than to the substrate of the reaction by a factor of the enzyme rate enhancement.² Since transition states (TS) are chemically unstable species, they exist only for a femtosecond time scale.³⁻⁶ However, chemically stable mimics of these TS could serve as potent inhibitors by exploiting the same binding interactions that lead to TS stabilization. Traditional methods like x-ray crystallography or spectroscopy cannot be used to directly study the TS due to its short lifetime, but we can get indirect information about TS through kinetic isotope effect (KIE) measurements. KIEs are changes in reaction rate observed when an atom of the substrate is replaced by a heavier isotope. Typically, two identical

reactions are measured using substrates that are isotopologues, molecular entities that differ only in their isotopic composition, and the ratio of the rate constants is calculated and reported as KIE.⁷ One isotopologue contains a light isotope (^1H , ^{12}C , ^{14}N , or ^{16}O) near or at the reaction center of the molecule and the other isotopologue contains a stable heavy isotope (^2H , ^{13}C , ^{15}N or ^{18}O) or radioisotope (^3H and ^{14}C) at the same position.

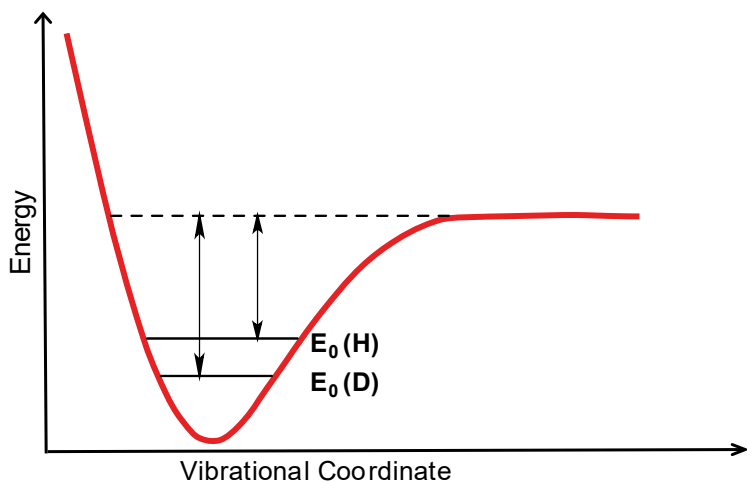


Figure 1.2. Zero-point energy difference between C-H and C-D bond.

Substituting a light isotope with a heavier isotope causes changes in bond vibration frequencies. The energy the molecule possesses in the ground vibrational state is known as the zero-point energy, and it forms the basis for the reactivity differences between isotopologues. The ground state (GS) for a bond vibration lies above the potential energy surface and as a result, heavier isotopes have lower zero-point energy than light isotopes of the same element (Figure 1.2). The sum of bond vibrational energies of the isotopically substituted atom changes as reaction goes from reactant to transition state, resulting in an experimentally measurable isotope effect.⁸

As a bond is being broken, the force constant for the bond is being weakened. As force constant is weakened, the frequency of bond stretch is smaller and consequently, so is the vibrational energy (E_n). The vibrational energy (E_n) is dependent on the frequency of the bond stretch (ν), which is in turn dependent on the reduced mass of the two connected atoms (μ).

Vibrational energy levels are quantized and can be described by:

$$e_n = \left(n + \frac{1}{2}\right) h\nu \quad n = 0, 1, 2 \dots$$

When we change the mass of the atom, we change the frequency of the bond vibration.

$$\nu = \frac{1}{2} \sqrt{\frac{k}{m_r}} \quad \text{where } m_r = \frac{m_1 m_2}{m_1 + m_2}$$

1.1 Primary and Secondary KIEs

Based on the different position of the isotopic substitution placement, kinetic isotope effects could be divided into primary and secondary. Based on the difference in mass between the light and heavy isotope, KIEs have different magnitudes and ranges associated with a particular mechanism (Table 1.1). Hydrogen/deuterium isotope effects (^1H vs $^2\text{H}=\text{D}$) result from a much larger mass change than carbon isotope effects (^{12}C vs ^{13}C). As a result of this mass difference, primary carbon isotope effects vary between 0.99 and 1.07 and primary hydrogen isotope effects vary between less than 1.0 and 1.20, as shown in Table 1.1.

Table 1.1 Approximate ranges of KIEs Measured in TS Analyses⁸

position	type	Approximate range	Interpretation
1-¹³C	primary	> 1.07	Synchronous A _N D _N (S _N 2) ⁹
		1.013 – 1.03	Dissociative A _N D _N (S _N 2) ¹⁰⁻²¹
		1.005 – 1.01	Dissociative D _N A _N (S _N i) ^{20,22,23}
		0.995 – 1.0	Stepwise D _N *A _N (S _N 1) ²³⁻²⁵
1-²H	α-secondary	1.08 – 1.20	Dissociative A _N D _N /D _N A _N or D _N *A _N ^{9,10,12,14-24,26-28}
		< 1.0	Synchronous A _N D _N ⁹
2-²H	β-secondary	>1.07	High oxocarbenium ion character and hyperconjugation ^{10,12,14-24,26-28}
		< 1.035	Low oxocarbenium ion character or lack of hyperconjugation ^{9,23-25}

Primary KIEs are observed when bond to isotopically labeled atom is breaking in TS of the slow rate determining step of the reaction. More detailed description of this type of KIE is described in the review by Shiner and Wilgis.²⁹ Primary isotope effects could be measured for carbon of the reaction center, leaving group or nucleophile (Figure 1.3A). For leaving group KIEs, for example, the bonding, vibrational energy to an isotopically labeled atom in the leaving group is reduced going to the TS, so the resulting KIE will be larger than 1 (i.e. the light isotopologue will react faster). Traditionally, it was considered that the amount of C_α-LG bond rupture

was directly correlated with the magnitude of these LG KIEs. Thus, it could be inferred that the KIE provides detailed information about the length of the C α -LG bond at the TS.⁸ For primary carbon KIEs, larger values are associated with TS of a synchronous or dissociative bimolecular reaction (Table 1.1). Large values (KIE > 1) signify a faster reaction rate of the lighter isotope reactant/substrate due to smaller activation energy of the lighter isotope. This activation energy entering the TS decreases more for lighter isotope due to bond weakening compared to that of a heavier carbon isotope. Values close to or less than 1 signify bond strengthening to the light isotope compared to the heavy isotope, resulting in slower reaction rate for the light isotope compared to the heavy isotope. These values could be expected for S_N1 and S_Ni-like reactions as shown in Table 1.1.

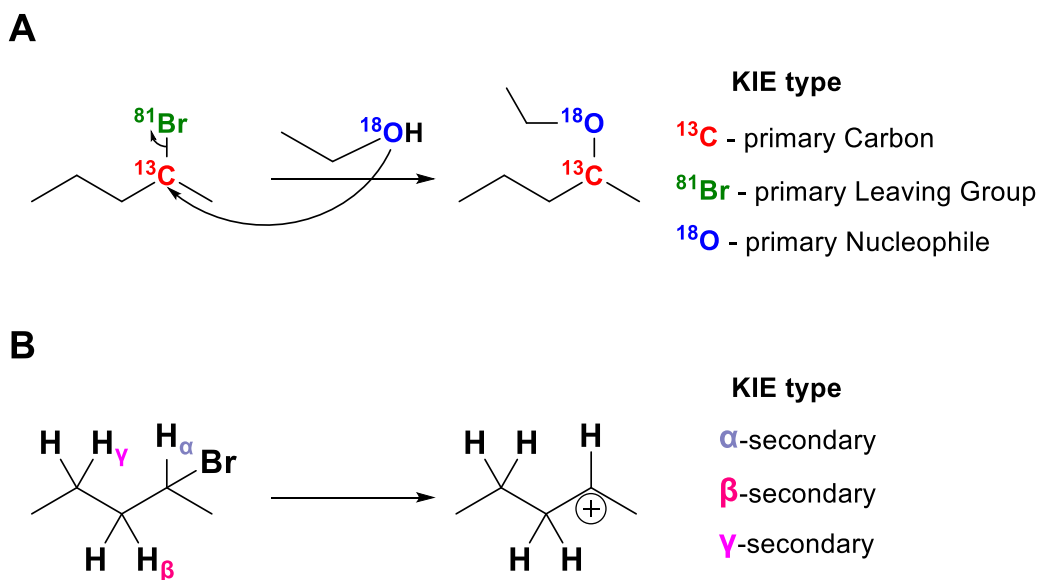


Figure 1.3. Categorization of KIE types. A. Primary isotope effects based on mechanistic role B. Secondary H isotope effects based on the distance between the position of isotopic substitution and the reaction center.

Secondary KIEs are observed when the bond to the isotopically substituted atom is not broken or formed in the transition state of the rate-determining step of the reaction. Based on the distance between the position of isotopic substitution and the reaction center, secondary KIEs are referred to as α , β , γ , etc. (Figure 1.3B). An α -secondary effect is measured for isotopically labeled atoms bonded directly to the reacting atom, β -secondary effect is measured for isotopically labeled atoms two bonds away from the reaction center and γ -secondary effect is measured for isotopically labeled atoms three bonds away from the reaction center. Due to the small magnitude of secondary KIEs, only alpha-secondary and beta-secondary hydrogen atom isotope effects have been studied in detail (Table 1.1). Secondary α -deuterium KIEs are observed when hydrogen is substituted for a deuterium isotope at the reacting carbon. Large normal α -deuterium KIEs are found for solvolysis reactions proceeding through a carbenium ion intermediate, while smaller α -deuterium KIEs are observed for reactions proceeding via S_N2 mechanism.^{11,20,30} Small normal or inverse α -deuterium KIE is observed as a result of the $C\alpha-H(D)$ stretching vibrations becoming stronger due to rehybridization of the $C\alpha$ from sp^3 into a sp^2 hybridized center.⁸ Therefore, we can see that the change in the $C\alpha-H(D)$ out-of-plane bending vibrations on going from the reactants to the transition state largely dictate the magnitude of the secondary KIE.

Secondary β -deuterium KIEs are observed when hydrogen is substituted for a deuterium isotope at the β -carbon. While these KIEs are slightly affected by steric effects ($C\beta-D$ bonds are shorter than the $C\beta-H$ bonds), and inductive effects (D is more electron donating than H), secondary β -deuterium KIEs are mainly the result of hyperconjugative effects related to the amount of cationic charge that develops on the

α -carbon in the TS (the weaker C β -H bonds stabilize the transition state more than C β -D bonds via hyperconjugation).³¹ Hyperconjugation weakens the C β -H/D bond and lowers its associated vibrational frequency.³² Since the deuterium labelled molecule has a stronger bond to carbon, it participates in the hyperconjugation to a lesser extent than the protonated molecule, giving a small normal KIE (Table 1.1).

1.2 Kinetic Isotope Effect Measurements

The measurement of KIEs can be carried out in either a non-competitive or competitive manner. In non-competitive KIE measurements, the kinetic constants are measured from separate experiments with light and heavy isotopologue substrates, after which the ratio of rate constants are compared to give the experimental KIEs. Although in theory it is possible to measure isotope effects on every kinetic parameter individually through non-competitive KIE measurements, many factors, such as light differences in temperature, pH, concentration, can influence the observed rate constant in a way that is independent of the true isotope effect value of such a small magnitude. By comparison, in competitive KIE measurements, both light and heavy isotopologue substrates are combined in a mixture and allowed to react as competitive substrates. The KIE is calculated using the ratio between light and heavy isotopologue substrate concentrations (R/R_0) and fractional conversion (F). Competitive KIEs are calculated using eq. 1:

$$(R/R_0) = (1 - F)^{(1/k_{ie}-1)}$$

where R is the heavy/light isotope ratio measured for the unreacted substrate at F , R_0 is the initial heavy/light isotope ratio for the substrate at time zero, F is the fraction of

substrate that has been converted to product (ie. fractional conversion), and k_{ie} is the isotope effect. In this thesis, we will be focusing on competitive isotope effects, as they provide sturdier measurements and human error will be minimized to a higher degree through these types of measurements.

KIEs probe the individual atom bond vibrational environment at enzyme transition state. Over the past 80 years, KIEs have been used to study the mechanism and inform the structure of the transition states of chemical and enzymatic reactions. The Bigeleisen treatment, based on Eyring absolute rate theory, assumes there is a single potential energy surface along which the reaction takes place, and that there is a potential energy barrier between reactants and products.^{33,34} For each stage of the reaction, the reaction occurs along the minimal energy path. The transition state is assumed to be in equilibrium with reactants and products except that one vibrational degree of freedom has become imaginary and that its energy is converted into motion along the reaction coordinate.³¹

Since energy at a state (Ground or Transition) is a function of vibrational frequency, this energy is a function of the strength of a bond, and the mass of the vibrating atoms. The decrease of force constants to an isotopically labeled atom at the TS compared to ground state (GS) weakens the bond in the transition state, so its energy decreases *more* for the light isotope than the heavy isotope. This means that the activation energy for the light isotope is smaller for the heavy isotope and therefore light isotope reacts faster, resulting in a normal KIE > 1 ($k_{\text{light}} > k_{\text{heavy}}$), reflecting a “looser” TS (Figure 1.4 – left).^{8,31} Here, the sum of vibrational energies is closer in value between heavy and light isotopes at the TS compared to the GS.

If the bond to the isotopically labeled atom is broken in a reaction, but bond breaking has not occurred at the transition state of the rate-determining step of the overall reaction, there is no change in force constants involving the isotopic atom between ground state and TS. In this case, the KIE is at unity and it equals to 1 (ie. the light and heavy isotopologues react with the same rate).

However, increase of force constants to isotopically labeled atom at TS strengthens the bond in the transition state, so its energy increases *more* for the light isotope than the heavy isotope. This means that the activation energy for the light isotope is bigger than for the heavy isotope and therefore it reacts slower, resulting in an inverse KIE < 1 ($k_{\text{light}} < k_{\text{heavy}}$), reflecting a “tighter” TS (Figure 1.4 – right).^{8,31} Here, the sum of vibrational energies is farther in value between heavy and light isotopes at the TS compared to the GS. The transition from sp^3 to sp^2 hybridization includes a decrease in coordination number and more s character, which results in a higher bending frequency and tighter hold to the atoms, meaning more force is needed to break the bonds. Change in force constants to isotopically labeled atom on going to TS of rate determining step and changes in bond length to the isotopically substituted atom in TS both contribute to KIE magnitude, and thus reflect the amount of bonding to isotopically labeled atoms of TS. As KIEs can identify bonds that are changing in TS of rate determining steps, they are useful for determining mechanisms of a reaction.

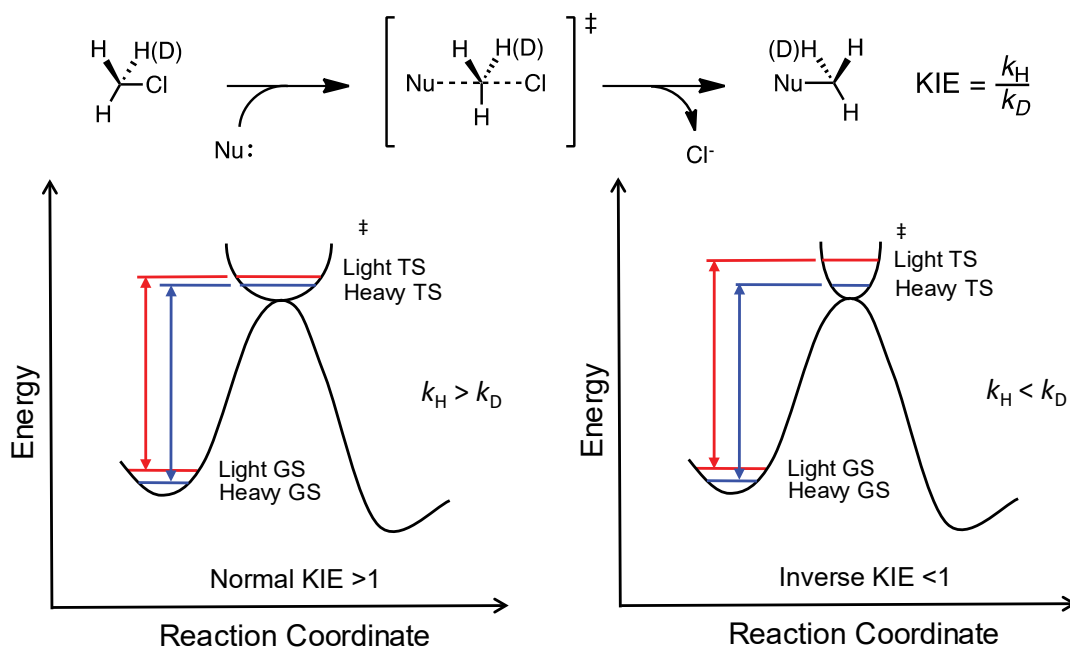


Figure 1.4. Energy diagrams of normal KIE vs inverse KIE showing energy differences between different isotopes of the same atom at ground state and transition state.

1.3 Transition State Analysis

In statistical mechanics, the definition of the transition state is the point where the energetics of bond making or breaking have equal probability of moving from the transition state toward either the reactant or the product basins. The transition state in chemistry is defined by the time for atoms to move apart or together to form a new bond and thus is known to occur on the time scale of bond vibrations.³⁵⁻³⁷ Enzymes accelerate chemical reactions by binding to and stabilizing the TS.³⁸ Wolfenden proposed a thermodynamic explanation by assuming that the increased binding affinity of the transition state species compared to the reactants is proportional to the catalytic rate enhancement imposed by the enzyme.² These proposals imply that chemically stable TS analogues that mimic the geometry and charge localization of the enzymatic TS would be potent enzyme inhibitors.

TS structure refers to the atomic composition, bond geometry and electrostatics of the TS as a fixed object.³⁹ If we define the TS as such, we can then extrapolate its interactions with other molecules based on that TS image. Despite the femtosecond scale lifetime of TS, TS structure can be indirectly determined through a combination of intrinsic kinetic isotope effects (KIE) and computational chemistry.³⁶ TS structure information obtained through this approach has led to the design of TS analogues for enzymatic reactions.^{35,36} The overall approach to TS analysis involves: 1) selection of the enzymatic target 2) synthesis of the isotopically labeled substrates 3) measurement of intrinsic KIEs 4) use of quantum chemical density functional theory (DFT) calculations to match a transition state structure to the experimentally determined intrinsic KIEs 5) solving the wave function of the static model of the TS and using it for construction of an electrostatic potential surface map, which can be used as the blueprint for design of a stable mimic of the transition state 6) application of synthetic organic chemistry to the chemical synthesis of the mimics and 7) testing the proposed analogues against the target enzyme.^{35,36} However, such an approach requires precise experimental KIEs, and thus a number of experimental approaches have emerged to measure these precise KIEs.

1.4 Overview of current approaches for KIE measurements

Experimental approaches for KIE measurement have been evolving in different directions over the course of the last century. There are three general strategies for determination of KIEs: 1) direct comparison of reaction rates^{40,41} 2) equilibrium perturbation measurements⁴²⁻⁴⁴ and 3) measurement by internal competition.⁴³⁻⁴⁵ The first two strategies are generally applicable for the measurement of primary hydrogen

atom KIEs but lack the precision necessary to reproducibly measure heavy atom KIEs (ie. KIEs of carbon, nitrogen, oxygen, phosphorus, etc), or secondary hydrogen atom KIEs, which are smaller in magnitude. For the investigation of such small kinetic isotope effects, the most commonly used method is internal competition because of its high precision. The competitive method avoids systematic errors present in measurements that directly compare reaction rates by directly measuring changes in the isotope ratio of the two isotopologues present within the same reaction.⁴⁶ In this chapter, I will focus mainly on the competitive methods for KIE measurements.

1.4.1 Measurement of KIEs by Scintillation Counting/Radiolabeling

Liquid scintillation counting (LSC) quantifies the radioactive activity of low energy radioisotopes. In order to absorb the energy into detectable light pulses, LSC technique requires the analyte to be mixed with an aromatic solvent, and a scintillator (fluor).⁴⁷ The energy released from a radioactive decay of the analyte excites the aromatic solvent and is further transferred to the scintillator. The scintillant emits a flash of light when high energy electrons (β -particles) are released upon decay of the radioactive isotope. The resultant photon emissions are recorded by a photomultiplier tube within the liquid scintillation counter (Figure 1.5).

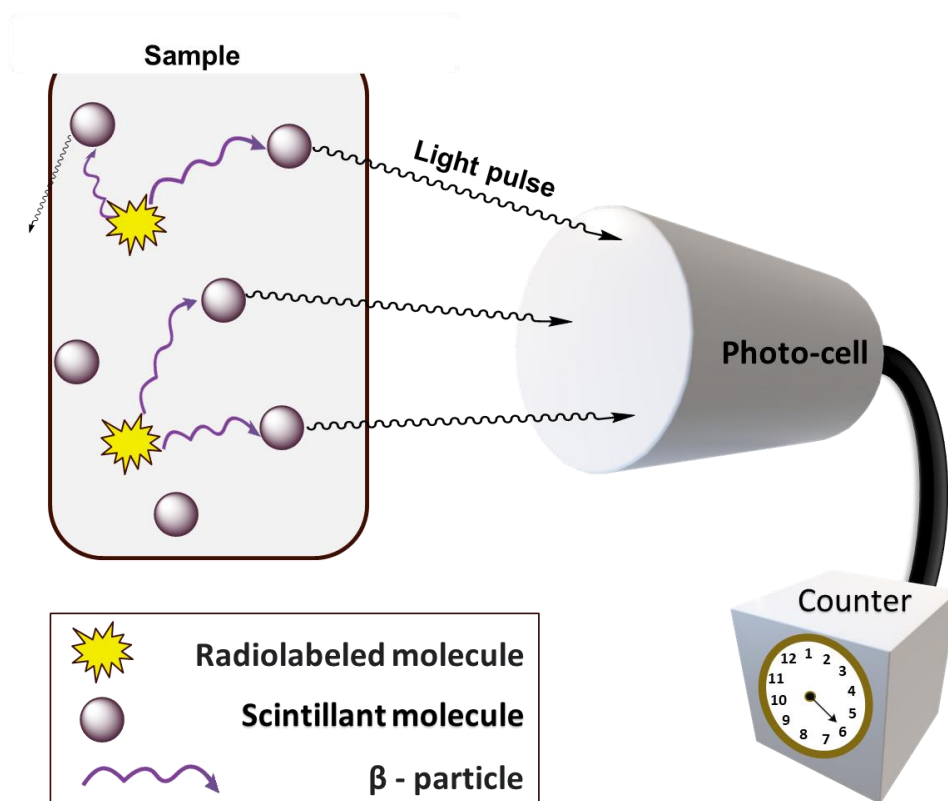


Figure 1.5 Liquid scintillation counting principle of analysis

LSC of radioisotope-labeled molecules was initially the dominant method for measuring competitive KIEs since it can achieve high precision up to $\pm 0.3\%$.²⁶ However, the requirement for radioisotopes limits its use to reactions using radio-labeled substrates that are either commercially available or that can be easily prepared from commercially available radio-labeled reagents.⁴⁸⁻⁵⁰ This method now is mainly used to analyze hydrogen tunneling by comparing $^1\text{H}/^3\text{H}$ and $^2\text{H}/^3\text{H}$ isotope effects and heavy atom KIEs via competitive methods⁴⁶. Furthermore, synthesis of radiolabeled isotopes can be limited due to degradation of intermediates and extensive purification of the labeled substrates is needed to remove any labeled contaminants. Because LSC detects all radioactive labeled compounds – substrates, products, and intermediates,

any labeled contaminants can introduce large errors in calculating a precise KIE.⁴⁸ For example, when measuring KIEs using the ratio of $^{14}\text{C}/^3\text{H}$ present in the reaction product, the presence of a 0.2% contaminant can generate greater than a 1% error in the measured KIE value.²⁶

The dual-radiolabel competitive method for the determination of KIEs was applied by Schramm and co-workers for TS analysis of human and bovine purine nucleoside phosphorylases to demonstrate that bovine and human nucleoside phosphorylases stabilize different TS structures⁵¹⁻⁵³. The approach has also been applied by the Klinman laboratory to examine enzymatic hydride transfer reactions of thermophilic alcohol dehydrogenase and soybean lipoxygenase-1.^{39,54}

1.4.2 Measurement of KIEs by Nuclear Magnetic Resonance Spectrometry (NMR)

Competitive NMR methods for KIE measurements were first reported in 1986 by the Pascal group who measured deuterium KIEs in organic and biological reactions by natural abundance NMR.⁵⁵ Pascal used natural abundance of deuterium in 2-bromoethyl benzene and styrene dibromide to calculate KIEs. While all NMR-active nuclei can be theoretically determined at natural abundances, it is difficult to quantify accurately their abundances using early NMR instruments. However, NMR cannot be directly used to measure ^{18}O KIEs since it lacks a nuclear spin, using NMR at natural abundance to determine KIEs bypasses the synthesis of isotopically enriched substrates.⁴⁶ More accurate and precise KIE measurements are possible by NMR if stable isotope labeled substrates are used. Consequently, accurate measurements of the

small KIEs were hard to measure because of the very low natural isotope abundances. However, the instrument sensitivity of NMR spectroscopy has been dramatically improved by increases in field strength and the introduction of cryoprobes.

Dan Singleton in 1995 expanded on this approach to enable the measurement of natural abundant ^{13}C and ^2H isotope effects for all carbon and non-exchangeable hydrogen within a molecule.⁵⁶ The method simultaneously measures KIEs for all carbon positions from one experiment, but it requires large reactions with multiple gram quantities of starting material in order to obtain sufficiently quantitative results.^{57,58} A remote ^{13}C signal, used as a reference, is assumed to have a KIE of 1 and the change in signal intensity for all other ^{13}C positions within the molecule are measured relative to that reference. This approach works best for small molecules in which we can assume that only a single ^{13}C isotope is present in each individual molecule. Because of the requirement of gram quantities of reactants, the method has limited application for the measurement of enzymatic kinetic isotope effects.⁵⁹

The Bennett group built on the work by Singleton and developed a method including a ^{13}C reporter to track the isotope ratio of an adjacent atom using quantitative ^{13}C NMR.⁶⁰ Using isotope labeled substrates allowed for the continuous monitoring of isotope ratios as a function of reaction progress. However, this approach requires the presence of multiple isotopic labels within a single reactant and still required large amounts of sample (> 2 mg) for each analysis or the use of a cryogenic NMR probe to boost sensitivity.^{46,60,61} The low sensitivity limitation was later overcome by the development of 2D [^{13}C , ^1H]-heteronuclear single quantum coherence (HSQC) NMR technique that allows for a continuous measurement of unpurified reaction mixture.⁶²

Murkin group improved the sensitivity by indirectly measuring ^{13}C signals,⁶² but this technique requires synthesis of large quantities of the isotopically labeled substrates, one of which contains two isotopic labels at adjacent atomic positions, which limits the general application of this approach.

1.4.3 Measurement of KIEs by Mass Spectrometry (MS)

Mass spectrometry (MS) is an analytical technique that determines the molecular weight of the analyte molecules through the separation of ionized analytes by the differences in the ratios of their charges to their respective masses (mass/charge; m/z), to determine the molecular weight of those molecules. Since mass spectrometry can distinguish multiple isotopes simultaneously at high sensitivity, it has been widely used to study of isotope effects.⁶³ Mass spectrometry-based approaches have been used to measure KIEs in enzyme systems, typically by quenching the reaction at various time points and determining the relative quantities of labeled and unlabeled reactant/product.⁶⁴⁻⁶⁶

Two MS based approaches have been developed for competitive kinetic isotope effect measurements using stable isotopic labeling of substrates: isotope-ratio mass spectrometry (IRMS) and whole molecule mass spectrometry (WMMS). IRMS allows for the accurate measurement of small differences in the abundances of isotopes such as $^2\text{H}/^1\text{H}$, $^{13}\text{C}/^{12}\text{C}$, $^{15}\text{N}/^{14}\text{N}$, and $^{18}\text{O}/^{16}\text{O}$. Through interaction with the electron beam in the ion source, samples are converted into gases such as H_2 , CO_2 , N_2 , and CO depending on their chemical composition.⁶⁷ Isotope ratio mass spectrometry is very sensitive and could obtain high precision on the order of 0.01%. However, IRMS is

highly dependent on sample purity and limited to the analysis of small gaseous molecules or to analytes where the isotopically labeled atom can be quantitatively converted to one of the aforementioned gases.⁴⁶ The Cleland group introduced a remote label method coupled with IRMS for the first time, which they used for determining KIEs for a variety of enzymatic reactions with high precision.⁶⁸ This method was effective in analyzing glucose-6-phosphate dehydrogenase reaction, adenosine deaminase and aspartate transcarbamylase.^{69–72} However, this method requires extensive purification of the mixture of unlabeled and isotope labeled molecules because contaminants lead to generation of artefactual isotope effects. Another limitation is that fractional conversion had to be measured using an alternative technique such as UV-vis spectroscopy.

Whole molecule mass spectrometry (WMMS), on the other hand, involves the analysis of intact molecular ions by mass spectrometry without breaking down the analyte molecule into a gas, using ionization techniques like electrospray ionization (ESI) or matrix assisted laser desorption/ionization (MALDI). WMMS has the advantage of requiring only pmole–nmole quantities of single stable isotope labeled substrates. Advances in MS have allowed for increasingly precise measurement of isotope ratios. In 1978, Cooks group reported the first use of isotope effect measurements using WMMS to determine chlorine isotope effects in elimination reactions with standard error of less than 5%.⁷³ In the 1990s, Anderson group developed a method applying WMMS to measure the enzymatic catalyzed KIEs with a precision similar to the radioactive-labeled method.^{74,75} Schramm group applied this method to their own research showing similar experimental values with WMMS (0.991 ± 0.003)

as with the radioactive label model (0.986 ± 0.003).¹⁸ While WMMS shows promising precision, these methods typically require complex analytical workflows that involve purification of the analyte through techniques such as high-performance liquid chromatography (HPLC) before isotope ratios can be measured. As a result, fractional conversions (F) are not measured directly and must be estimated using an alternative approach.⁷⁶⁻⁷⁹ These approaches are time consuming and labor intensive as they require numerous sample handling and purification steps before analysis, which have the potential to introduce errors in the measured KIE because of the purification method. This limitation calls for improvement to include measurement of both fractional conversion and isotopic ratio in a single experiment.

1.4.4 Measurement of KIEs by MALDI-MS

Matrix-Assisted Laser Desorption/Ionization Mass Spectrometry (MALDI-MS) is a soft ionization method that uses laser irradiation to ionize intact (bio)-molecules which have been co-crystallized in a matrix.⁸⁰⁻⁸² In MALDI, analytes are incorporated into organic matrices in a solid or viscous phase and are then irradiated with a laser to facilitate the ionization/desorption reactions as they enter the gas phase. The molecules enter an excited state which enables a proton transfer between excited matrix ions and vaporized analyte molecules, thereby ionizing them. Analyte ions are then accelerated by an electric field to enter the mass analyzer, in most cases, a time-of-flight (TOF) mass spectrometer. A TOF analyzer works on the principle that accelerated ions from the laser pulse in the MALDI source will enter a long, field-free tube in vacuum.^{83,84} As the ions are accelerated in the same electric field, they will separate in the field-free region according to their mass-to-charge (m/z) ratio. Thus,

when ions hit the detector at the end of the flight-tube, the m/z ratio of the ions can be determined by calculating the time it takes them to fly through the tube.

The analysis of large biomolecules as intact groups was made possible by the development of MALDI in the 1980s.⁸² After the development of ESI, the use of MALDI in the analysis of biomolecules initially declined, however, because of the development of high sensitivity instruments, the low sample consumption, and limited sample processing requirements, the use of MALDI has significantly increased over the last decade.

The laboratory of Minkui Luo used a MALDI-TOF MS method to measure KIEs for the reaction catalyzed by the protein lysine methyltransferase enzymes SET8 in 2013.⁸⁵ However, in their approach it required separate experiments to analyze isotopic ratios and fractional conversion, and required prior purification of the analytes prior to analysis, all of which can introduce errors in the measurement of highly precise KIEs. Thus, there is still a need for precise WMMS based KIE approaches that can be used to simultaneously measure both isotope ratios and fractional conversion of enzyme reactions in a single experiment with minimal sample purification and handling.

1.5 Glycosyltransferases

KIE measurements have been one of the best tools for determining transition state structure of enzymatic reactions, as they are very sensitive to changes in TS structure. For many enzymatic reactions the observed KIEs can be reasonably interpreted, once the intrinsic values are known on the chemical steps.^{44,86} The problem is that the

chemical step (or steps) of an enzymatic reaction is often not completely rate limiting. In those cases one has to either find a way to make this step rate limiting (by changing substrate, changing pH, or mutating the enzyme) or find a way to calculate the intrinsic isotope effect.⁸⁷ Enzymologists aim to determine transition state structures for enzymatic reactions for several reasons. For example: (1) to compare the mechanisms of enzymatic and nonenzymatic reactions in order to understand better the factors involved in enzymatic catalysis and (2) to determine transition states of these enzymes and create analogs as potential powerful drugs.

One family of enzymes that would be particularly suitable for TS analysis via KIE measurements are glycosyltransferase (GT) enzymes. Despite their suitability for TS analysis, only a few examples of GT enzyme KIE measurements have been reported. GTs are responsible for the biosynthesis of complex glycan structures, which play significant roles in various processes in nature ranging from bacterial toxicity to mammalian development.⁸⁸⁻⁹⁰ Glycosyltransferases catalyze glycosidic bond formation reactions using sugar donors containing a nucleoside phosphate or a lipid phosphate leaving group.⁹¹ Leloir glycosyltransferases utilize carbohydrates linked to a nucleotide diphosphate (NDP) typically through an α -linked glycosidic bond, where non-Leloir glycosyl transferase utilize glycolipids, such as polyprenyl-pyrophosphate-sugars, or phosphorylated sugar as glycosyl donors.⁹²

Glycosyltransferases can be classified as either retaining or inverting enzymes according to the stereochemistry of the substrates and reaction products^{93,94}. The recommendations of the International Union of Biochemistry and Molecular Biology (IUBMB) do not indicate the intrinsic structural features of the enzymes, nor do they

adequately accommodate enzymes which act on several distinct substrates. However, the carbohydrate active enzyme (CAZy) database proposes the continuously updated classification of glycosyltransferases using nucleotide diphospho-sugar, nucleotide monophospho-sugars and sugar phosphates and related proteins into distinct sequence-based families as first described by Campbell *et al.*⁹⁵ and then by Coutinho *et al.*⁹⁶ While this classification is useful and can provide mechanistic insight into a protein's function, single GT families often include enzymes that utilize different NDP-sugar substrates and different glycosyl acceptor substrates, limiting their use in predicting GT enzyme function based on family classification. For example, the GT2 family includes enzymes responsible for the synthesis of chitin and mycobacterial galactofuranosides.⁹¹ While these enzymes utilize different substrates, they do share many mechanistic similarities.

1.5.1 Mechanism nomenclature – chemical vs. enzymatic (GT) mechanisms

Prior to going through different mechanisms in glycosyltransferases, I want to introduce you to the different nomenclature used in chemistry that describe TSs also shown in GT mechanisms. IUPAC nomenclature dictates that a reaction mechanism is divided into two key steps: A_N – nucleophilic addition and D_N – nucleophilic dissociation. Bimolecular S_N2 reaction is represented as $A_N D_N$ (Figure 1.6 – top). This is a concerted mechanism which goes through a TS with coordination to both the nucleophile and leaving group. In GT mechanisms, $A_N D_N$ TS is seen in a single or a double displacement mechanism as described below (Figure 1.7A-B).

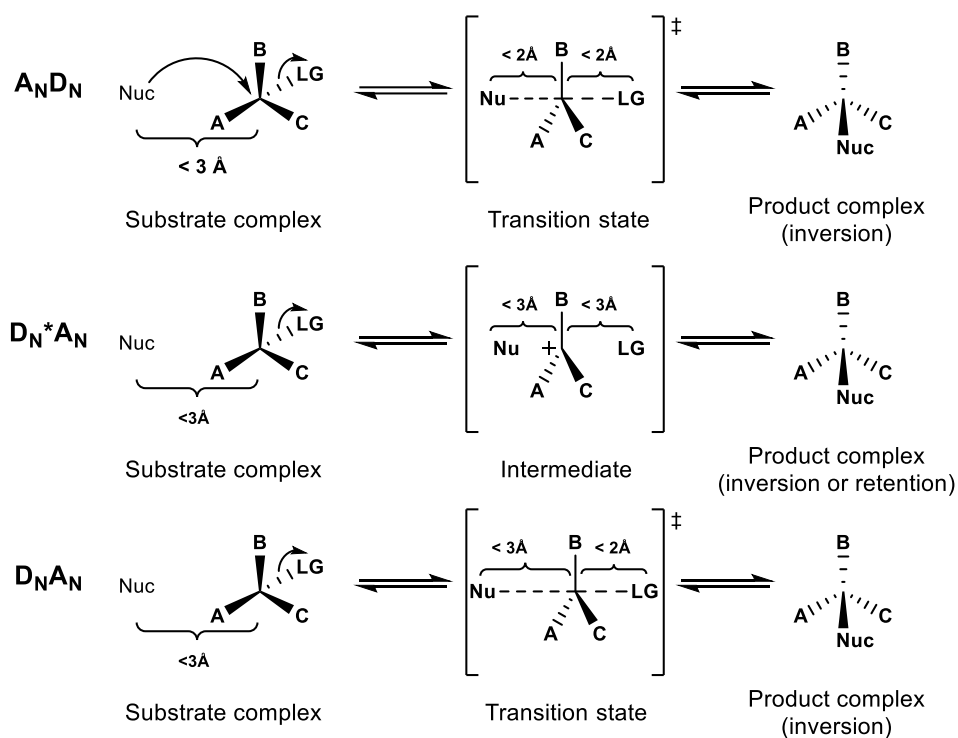


Figure 1.6 Mechanism nomenclature for reactions involving nucleophilic addition and leaving group dissociation.

Stepwise S_N1 reaction is represented as $D_N + A_N$ and $D_N * A_N$. Reactions characterized as $D_N * A_N$ include an intermediate which cannot be chemically recognized or isolated due to its short lifetime (Figure 1.6 – middle). Reactions characterized as $D_N + A_N$ include an intermediate with longer lifetime allowing it to be chemically separated. In glycosyltransferase enzymatic reactions, mechanism including sufficiently long-lived oxocarbenium ion formation falls in the category of S_N1 -like mechanism because oxocarbenium ions are bound to the enzyme and cannot diffuse away from it (Figure 1.7C – top).⁹⁷

Finally, S_Ni reaction is represented as $D_N A_N$. It is a highly dissociative bimolecular reaction called an internal return S_Ni -like mechanism in which leaving group departure and nucleophilic attack occur in a concerted but asynchronous manner

(Figure 1.6 – bottom). In GT mechanisms, they are proposed to happen on the same face of the glycoside (Figure 1.7C – bottom).

GT enzyme mechanisms can be categorized as retaining or inverting depending on if the stereochemistry of the anomeric carbon in the product glycoside is the same or differs from the stereochemistry of the original nucleotide-sugar or phospholipid-sugar donor, respectively.⁹¹ Inverting glycosyltransferases are generally accepted to utilize a direct displacement S_N2 -like mechanism involving general base catalysis (Figure 1.7).^{98–100} Leaving group departure is typically facilitated via electrostatic stabilization by a divalent metal cation (ie. Mg^{2+} or Mn^{2+})¹⁰¹ coordinating to two aspartates or via stabilization of the anionic charge that develops during leaving group departure by cationic amino acid sidechains and/or hydroxyls and helix dipoles.¹⁰² The mechanism of retaining glycosyltransferases was originally thought to proceed via a two-step double-displacement mechanism with the intermediacy of a covalent glycosyl–enzyme intermediate, similar to the accepted mechanism of retaining glycosyl hydrolase enzymes. This mechanism for retaining GT enzymes however has been questioned in recent years due to the lack of conserved architecture in the region where a catalytic nucleophile would be expected in these enzymes. A plausible S_N1 mechanism involves the formation of a short-lived oxocarbenium ion intermediate, followed by nucleophilic addition of the glycosyl acceptor with the leaving phosphate serving as a base.^{103,104} Alternatively, an internal return S_Ni -like mechanism has also been proposed, in which leaving group departure and nucleophilic attack occur in a concerted but asynchronous manner on the same face of the glycoside.^{105–108}

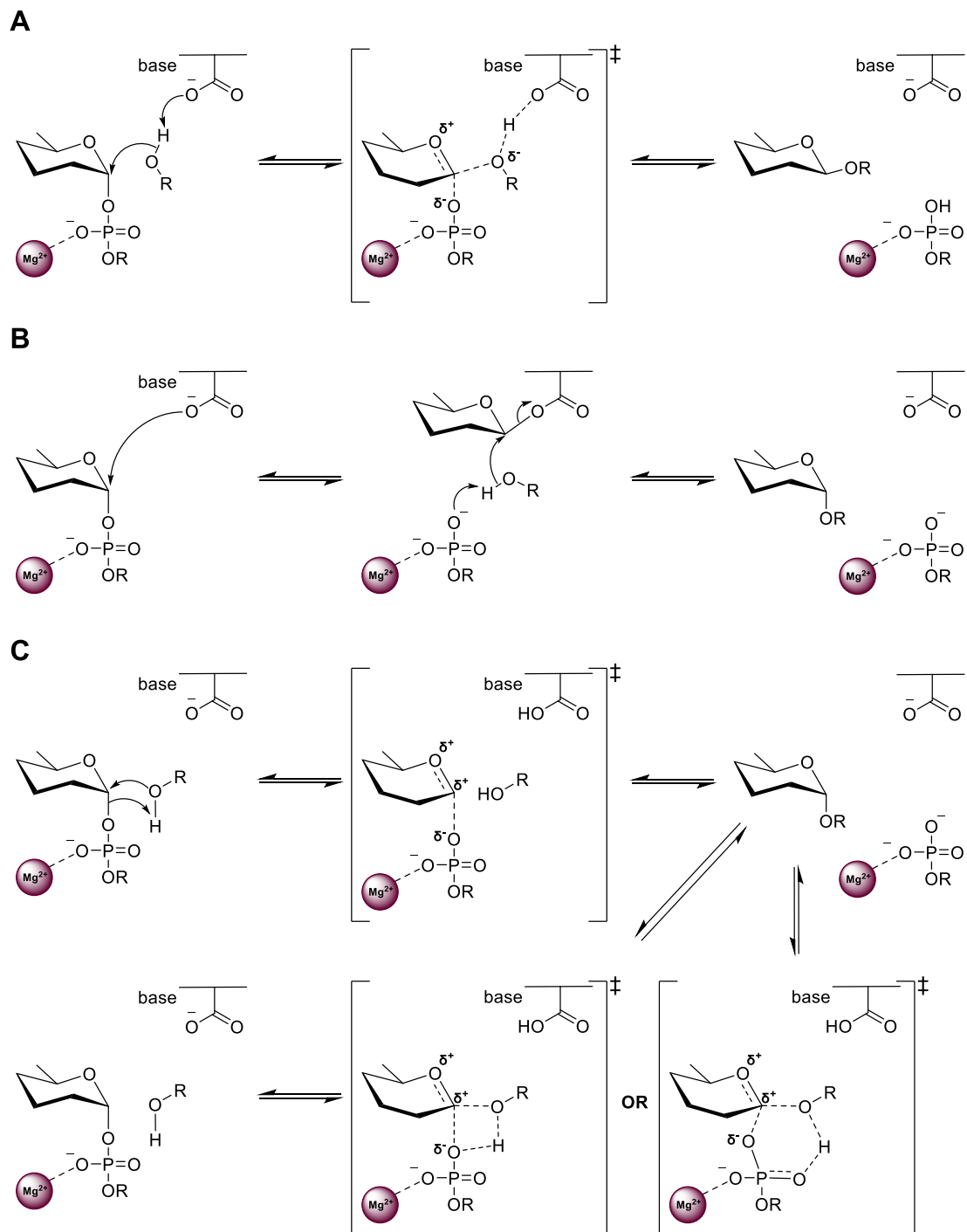


Figure 1.7. GT mechanisms (A) Inverting GT – single displacement mechanism, (B) Retaining GT – double displacement mechanism, (C) Retaining GT (alternative mechanisms) S_N1 – stepwise and S_Ni – concerted but asynchronous LG departure and Nucleophilic attack.

In this thesis I will describe the development of a quantitative method for analysis of experimental KIEs of carbohydrate active enzymes using whole molecule MALDI-TOF mass spectrometry and stable isotope labeled substrates. This method allows for analysis of unpurified mixtures while simultaneously analyzing isotopic ratios and fractional conversions within the same experiment resulting in highly precise measurements. In Chapter 2, I will describe the method development as applied to the glycosyl hydrolase enzyme β -galactosidase. The application of this approach to measure KIEs for GT enzymes requires access to appropriately isotope labeled sugar nucleotide substrates. In Chapter 3, I used a chemoenzymatic approach to synthesize isotopically labeled uridinediphosphate-2-acetamido-2-deoxy- β -D-glucopyranose (UDP-GlcNAc) substrates for the retaining GT enzyme BshA. Chapter 4 will describe the application of the whole molecule MALDI-TOF MS method to measure KIEs for the reaction catalyzed by BshA using the isotope labeled substrates described in Chapter 3. Finally, Chapter 5 will summarize the contents of this thesis while putting the value of this research in a broader context and outline the future directions for application of this KIE measurement method.

1.6 BIBLIOGRAPHY

- (1) Pauling, L. Molecular Architecture and Biological Reactions. *Chemical and Engineering News* **1946**, 24 (10), 1375–1377.
- (2) Wolfenden, R. Transition State Analog Inhibitors and Enzyme Catalysis. *Annu. Rev. Biophys. Bioeng.* **1976**, 5 (1), 271–306.
- (3) Bolhuis, P. G.; Chandler, D.; Dellago, C.; Geissler, P. L. Transition Path Sampling: Throwing Ropes over Rough Mountain Passes, in the Dark. *Annu. Rev. Phys. Chem.* **2002**, 53 (1), 291–318.
- (4) Dellago, C.; Bolhuis, P. G.; Chandler, D. Efficient Transition Path Sampling: Application to Lennard-Jones Cluster Rearrangements. *J. Chem. Phys.* **1998**, 108 (22), 9236–9245.
- (5) Antoniou, D.; Schwartz, S. D. Protein Dynamics and Enzymatic Chemical Barrier Passage. *J. Phys. Chem. B* **2011**, 115 (51), 15147–15158.
- (6) Basner, J. E.; Schwartz, S. D. How Enzyme Dynamics Helps Catalyze a Reaction in Atomic Detail: A Transition Path Sampling Study. *J. Am. Chem. Soc.* **2005**, 127 (40), 13822–13831.
- (7) Bennet, A. J. Kinetic Isotope Effects for Studying Post-Translational Modifying Enzymes. *Curr. Opin. Chem. Biol.* **2012**, 472–478.
<https://doi.org/10.1016/j.cbpa.2012.10.024>.
- (8) Berti, P. J.; McCann, J. A. B. Toward a Detailed Understanding of Base Excision Repair Enzymes: Transition State and Mechanistic Analyses of N-Glycoside

Hydrolysis and N-Glycoside Transfer. *Chem. Rev.* **2006**, 506–555.

<https://doi.org/10.1021/cr040461t>.

- (9) Birck, M. R.; Schramm, V. L. Nucleophilic Participation in the Transition State for Human Thymidine Phosphorylase. *J. Am. Chem. Soc.* **2004**, *126* (8), 2447–2453.
- (10) Kline, P. C.; Schramm, V. L. Purine Nucleoside Phosphorylase. Catalytic Mechanism and Transition-State Analysis of the Arsenolysis Reaction. *J. Biochem.* **1993**, *32* (48), 13212–13219.
- (11) Parkin, D. W.; Schramm, V. L. Catalytic and Allosteric Mechanism of AMP Nucleosidase from Primary, . Beta.-Secondary, and Multiple Heavy Atom Kinetic Isotope Effects. *J. Biochem.* **1987**, *26* (3), 913–920.
- (12) Horenstein, B. A.; Parkin, D. W.; Estupinan, B.; Schramm, V. L. Transition-State Analysis of Nucleoside Hydrolase from *Crithidia Fasciculata*. *J. Biochem.* **1991**, *30* (44), 10788–10795.
- (13) Parkin, D. W.; Mentch, F.; Banks, G. A.; Horenstein, B. A.; Schramm, V. L. Transition-State Analysis of a Vmax Mutant of AMP Nucleosidase by the Application of Heavy-Atom Kinetic Isotope Effects. *J. Biochem.* **1991**, *30* (18), 4586–4594.
- (14) Kline, P. C.; Schramm, V. L. Pre-Steady-State Transition-State Analysis of the Hydrolytic Reaction Catalyzed by Purine Nucleoside Phosphorylase. *J. Biochem.* **1995**, *34* (4), 1153–1162.

- (15) Scheuring, J.; Schramm, V. L. Pertussis Toxin: Transition State Analysis for ADP-Ribosylation of G-Protein Peptide Ai3C20. *J. Biochem.* **1997**, *36* (27), 8215–8223.
- (16) Scheuring, J.; Berti, P. J.; Schramm, V. L. Transition-State Structure for the ADP-Ribosylation of Recombinant Gi α 1 Subunits by Pertussis Toxin. *J. Biochem.* **1998**, *37* (9), 2748–2758.
- (17) Parikh, S. L.; Schramm, V. L. Transition State Structure for ADP-Ribosylation of Eukaryotic Elongation Factor 2 Catalyzed by Diphtheria Toxin. *J. Biochem.* **2004**, *43* (5), 1204–1212.
- (18) Berti, P. J.; Blanke, S. R.; Schramm, V. L. Transition State Structure for the Hydrolysis of NAD⁺ Catalyzed by Diphtheria Toxin. *J. Am. Chem. Soc.* **1997**, *119* (50), 12079–12088.
- (19) Rising, K. A.; Schramm, V. L. Transition State Analysis of NAD⁺ Hydrolysis by the Cholera Toxin Catalytic Subunit. *J. Am. Chem. Soc.* **1997**, *119* (1), 27–37.
- (20) Parkin, D. W.; Schramm, V. L. Effects of Allosteric Activation on the Primary and Secondary Kinetic Isotope Effects for Three AMP Nucleosidases. *J. Biol. Chem.* **1984**, *259* (15), 9418–9425.
- (21) Hunt, C.; Gillani, N.; Farone, A.; Rezaei, M.; Kline, P. C. Kinetic Isotope Effects of Nucleoside Hydrolase from Escherichia Coli. *Biochim. Biophys. Acta. Proteins Proteom.* **2005**, *1751* (2), 140–149.

- (22) Werner, R. M.; Stivers, J. T. Kinetic Isotope Effect Studies of the Reaction Catalyzed by Uracil DNA Glycosylase: Evidence for an Oxocarbenium Ion–Uracil Anion Intermediate. *J. Biochem.* **2000**, *39* (46), 14054–14064.
- (23) Chen, X.-Y.; Berti, P. J.; Schramm, V. L. Transition-State Analysis for Depurination of DNA by Ricin A-Chain. *J. Am. Chem. Soc.* **2000**, *122* (28), 6527–6534.
- (24) Lewandowicz, A.; Schramm, V. L. Transition State Analysis for Human and Plasmodium Falciparum Purine Nucleoside Phosphorylases. *J. Biochem.* **2004**, *43* (6), 1458–1468.
- (25) Singh, V.; Lee, J. E.; Núñez, S.; Howell, P. L.; Schramm, V. L. Transition State Structure of 5'-Methylthioadenosine/S-Adenosylhomocysteine Nucleosidase from Escherichia Coli and Its Similarity to Transition State Analogues. *J. Biochem.* **2005**, *44* (35), 11647–11659.
- (26) Parkin, D. W. Methods for the Determination of Competitive and Noncompetitive Kinetic Isotope Effects. *Enzyme mechanism from isotope effects* 1991, *10*, 269–289.
- (27) Scheuring, J.; Schramm, V. L. Pertussis Toxin: Transition State Analysis for ADP-Ribosylation of G-Protein Peptide Ai3C20. *J. Biochem.* **1997**, *36* (27), 8215–8223.
- (28) Berti, P. J.; Schramm, V. L. Transition State Structure of the Solvolytic Hydrolysis of NAD⁺. *J. Am. Chem. Soc.* **1997**, *119* (50), 12069–12078.
- (29) Shiner, V. J.; Wilgis, F. P.; Buncl, E.; Saunders Jr, W. H. Isotopes in Organic Chemistry *Elsevier*, New York 1992. (8) 239–335.

- (30) Dudkin, V. Y.; Miller, J. S.; Dudkina, A. S.; Antczak, C.; Scheinberg, D. A.; Danishefsky, S. J. Toward a Prostate Specific Antigen-Based Prostate Cancer Diagnostic Assay: Preparation of Keyhole Limpet Hemocyanin-Conjugated Normal and Transformed Prostate Specific Antigen Fragments. *J. Am. Chem. Soc.* **2008**, *130* (41), 13598–13607. <https://doi.org/10.1021/ja8028137>.
- (31) Westaway, K. C. Using Kinetic Isotope Effects to Determine the Structure of the Transition States of SN2 Reactions. *Adv. Phys. Org. Chem.* **2006**, pp 217–273. [https://doi.org/10.1016/S0065-3160\(06\)41004-2](https://doi.org/10.1016/S0065-3160(06)41004-2).
- (32) Sponsler, M. B.; Anslyn, E. V; Dougherty, D. A. *Modern Physical Organic Chemistry*. 2005.
- (33) Bigeleisen, J. W.; Wolfsberg, M. *Adv. Phys. Chem.* **1958**, *1*, 33.
- (34) Bigeleisen, J. The Relative Reaction Velocities of Isotopic Molecules. *J. Chem. Phys.* **1949**, *17* (8), 675–678.
- (35) Berti, P. J.; Tanaka, K. S. E. Transition State Analysis Using Multiple Kinetic Isotope Effects: Mechanisms of Enzymatic and Non-Enzymatic Glycoside Hydrolysis and Transfer. *Adv. Phys. Org. Chem.* **2002**, 239–314. [https://doi.org/10.1016/S0065-3160\(02\)37004-7](https://doi.org/10.1016/S0065-3160(02)37004-7).
- (36) Schramm, V. L. Enzymatic Transition States, Transition-State Analogs, Dynamics, Thermodynamics, and Lifetimes. *Annu. Rev. Biochem.* **2011**, *80*, 703–732. <https://doi.org/10.1146/annurev-biochem-061809-100742>.

- (37) Schramm, V. L. Transition States, Analogues, and Drug Development. *ACS Chem. Biol.* January 18, 2013, pp 71–81. <https://doi.org/10.1021/cb300631k>.
- (38) Zewail, A. H. Femtochemistry: Atomic-scale Dynamics of the Chemical Bond Using Ultrafast Lasers (Nobel Lecture). *Angew. Chem. Int. Ed.* **2000**, *39* (15), 2586–2631.
- (39) Pauling, L. Chemical Achievement and Hope for the Future. *Am. Sci.* **1948**, *36* (1), 51–58.
- (40) Welsh, K. M.; Creighton, D. J.; Klinman, J. P. Transition-State Structure in the Yeast Alcohol Dehydrogenase Reaction: The Magnitude of Solvent and «-Secondary Hydrogen Isotope Effects, *Biochemistry ©* 1970.
- (41) Northrop, D. B. Isotope Effects on Enzyme-Catalyzed Reactions by WW Cleland, *MH OLeary & DB Northrop, University Park Press, Baltimore 1977*, 122.
- (42) Simon, H.; Palm, D. Isotope Effects in Organic Chemistry and Biochemistry. *Angew. Chem. Int. Ed.* **1966**, *5* (11), 920–933.
- (43) Cleland, W. W. Determining the Chemical Mechanisms of Enzyme-Catalyzed Reactions by Kinetic Studies. *Adv. Enzymol. Relat. Areas Mol. Biol.* **1977**, *45*, 273–387.
- (44) Cleland, W. W. [13] Isotope Effects: Determination of Enzyme Transition State Structure. *Meth. Enzymol.* **1995**, *249*, 341–373.
- (45) Cleland, W. W. Use of Isotope Effects to Determine Enzyme Mechanisms. *J. Label. Compd. Radiopharm.* **2007**, 1006–1015. <https://doi.org/10.1002/jlcr.1390>.

- (46) Cook, P. F.; Cleland, W. W. *Enzyme Kinetics and Mechanism*; *Garland Science*, 2007.
- (47) Gu, H.; Zhang, S. Advances in Kinetic Isotope Effect Measurement Techniques for Enzyme Mechanism Study. *Molecules*. **2013**, 9278–9292.
<https://doi.org/10.3390/molecules18089278>.
- (48) *Perkin Elmer Liquid Scintillation Counting Page*. <https://www.perkinelmer.com/lab-products-and-services/application-support-knowledgebase/radiometric/liquid-scintillation-counting.html#Liquidscintillationcounting-Liquidscintillationcountingtheory> (accessed 2023-07-14).
- (49) Parkin, D. W. Methods for the Determination of Competitive and Noncompetitive Kinetic Isotope Effects. *Enzyme mechanism from isotope effects* 1991, *10*, 269–289.
- (50) Schwartz, P. A.; Vetticatt, M. J.; Schramm, V. L. Transition State Analysis of the Arsenolytic Depyrimidination of Thymidine by Human Thymidine Phosphorylase. *J. Biochem.* **2011**, *50* (8), 1412–1420.
- (51) Belen Cassera, M.; Zhang, Y.; Z Hazleton, K.; L Schramm, V. Purine and Pyrimidine Pathways as Targets in Plasmodium Falciparum. *Curr. Top. Med. Chem.* **2011**, *11* (16), 2103–2115.
- (52) Parkin, D. W.; Leung, H. B.; Schramm, V. L. Synthesis of Nucleotides with Specific Radiolabels in Ribose. Primary ¹⁴C and Secondary ³H Kinetic Isotope Effects on Acid-Catalyzed Glycosidic Bond Hydrolysis of AMP, DAMP, and Inosine. *J. Biol. Chem.* **1984**, *259* (15), 9411–9417. [https://doi.org/10.1016/s0021-9258\(17\)42716-5](https://doi.org/10.1016/s0021-9258(17)42716-5).

- (53) Schwartz, P. A.; Vetticatt, M. J.; Schramm, V. L. Transition State Analysis of the Arsenolytic Depyrimidination of Thymidine by Human Thymidine Phosphorylase. *J. Biochem.* **2011**, *50* (8), 1412–1420. <https://doi.org/10.1021/bi101900b>.
- (54) Belén Cassera, M.; Zhang, Y.; Hazleton, K. Z.; Schramm, V. L. Purine and Pyrimidine Pathways as Targets in Plasmodium Falciparum, 2011.
- (55) Knapp, M. J.; Klinman, J. P. Environmentally Coupled Hydrogen Tunneling: Linking Catalysis to Dynamics. *Eur. J. Biochem.* **2002**, pp 3113–3121. <https://doi.org/10.1046/j.1432-1033.2002.03022>.
- (56) Pascal, R. A.; Baum, M. W.; Wagner, C. K.; Rodgers, L. R.; Huang, D. S. Measurement of Deuterium Kinetic Isotope Effects in Organic and Biochemical Reactions by Natural Abundance Deuterium NMR Spectroscopy. *J. Am. Chem. Soc.* **1986**, *108* (21), 6477–6482.
- (57) Singleton, D. A.; Thomas, A. A. High-Precision Simultaneous Determination of Multiple Small Kinetic Isotope Effects at Natural Abundance. *J. Am. Chem. Soc.* **1995**, *117* (36), 9357–9358.
- (58) Singleton, D. A.; Szymanski, M. J. Simultaneous Determination of Intermolecular and Intramolecular ¹³C and ²H Kinetic Isotope Effects at Natural Abundance. *J. Am. Chem. Soc.* **1999**, *121* (40), 9455–9456.
- (59) Singleton, D. A.; Merrigan, S. R.; Beno, B. R.; Houk, K. N. Isotope Effects for Lewis Acid Catalyzed Diels-Alder Reactions. The Experimental Transition State. *Tetrahedron Lett.* **1999**, *40* (32), 5817–5821.

- (60) Lee, J. K.; Bain, A. D.; Berti, P. J. Probing the Transition States of Four Glucoside Hydrolyses with ^{13}C Kinetic Isotope Effects Measured at Natural Abundance by NMR Spectroscopy. *J. Am. Chem. Soc.* **2004**, *126* (12), 3769–3776.
- (61) Chan, J.; Lewis, A. R.; Gilbert, M.; Karwaski, M. F.; Bennet, A. J. A Direct NMR Method for the Measurement of Competitive Kinetic Isotope Effects. *Nat. Chem. Biol.* **2010**, *6* (6), 405–407. <https://doi.org/10.1038/nchembio.352>.
- (62) Chan, J.; Lewis, A. R.; Indurugalla, D.; Schur, M.; Wakarchuk, W.; Bennet, A. J. Transition State Analysis of *Vibrio Cholerae* Sialidase-Catalyzed Hydrolyses of Natural Substrate Analogues. *J. Am. Chem. Soc.* **2012**, *134* (8), 3748–3757.
- (63) Manning, K. A.; Sathyamoorthy, B.; Eletsy, A.; Szyperski, T.; Murkin, A. S. Highly Precise Measurement of Kinetic Isotope Effects Using ^1H -Detected 2D [^{13}C , ^1H]-HSQC NMR Spectroscopy. *J. Am. Chem. Soc.* **2012**, *134* (51), 20589–20592. <https://doi.org/10.1021/ja310353c>.
- (64) Hunt, C.; Gillani, N.; Farone, A.; Rezaei, M.; Kline, P. C. Kinetic Isotope Effects of Nucleoside Hydrolase from *Escherichia Coli*. *Biochim. Biophys. Acta. Proteins Proteom.* **2005**, *1751* (2), 140–149. <https://doi.org/10.1016/j.bbapap.2005.06.001>.
- (65) Werner, R. A.; Brand, W. A. Referencing Strategies and Techniques in Stable Isotope Ratio Analysis. *Rapid Commun. in Mass Spectrom.* **2001**, pp 501–519. <https://doi.org/10.1002/rcm.258>.

- (66) Bates, C.; Kendrick, Z.; McDonald, N.; Kline, P. C. Transition State Analysis of Adenosine Nucleosidase from Yellow Lupin (*Lupinus Luteus*). *Phytochemistry* **2006**, *67* (1), 5–12. <https://doi.org/10.1016/j.phytochem.2005.10.006>.
- (67) Liuni, P.; Olkhov-Mitsel, E.; Orellana, A.; Wilson, D. J. Measuring Kinetic Isotope Effects in Enzyme Reactions Using Time-Resolved Electrospray Mass Spectrometry. *Anal. Chem.* **2013**, *85* (7), 3758–3764. <https://doi.org/10.1021/ac400191t>.
- (68) O’Leary, M. H.; Marlier, J. F. Application of a Novel Double-Labeling Procedure to Measurement of Carbonyl Oxygen Isotope Effects on the Alkaline Hydrolysis and Hydrazinolysis of Methyl Benzoate. *J. Am. Chem. Soc.* **1978**, *100* (8), 2582–2583.
- (69) Hermes, J. D., Cleland, W. W.; Evidence from Multiple Isotope Effect Determinations for Coupled Hydrogen Motion and Tunneling in the Reaction Catalyzed by Glucose-6-phosphate Dehydrogenase **1984**, *106* (23) 7263-7264.
- (70) Weiss, P. M.; Garcia, G. A.; Kenyon, G. L.; Cleland, W W; Cook, P. F. Kinetics and Mechanism of Benzoylformate Decarboxylase Using ¹³C and Solvent Deuterium Isotope Effects on Benzoylformate and Benzoylformate Analogues, *J. Biochem.* **1988**, *27* (6), 2197-2205.
- (71) Weiss, P. M.; Cook, P. F.; Hermes, J. D.; Cleland, W. W. Evidence from Nitrogen-15 and Solvent Deuterium Isotope Effects on the Chemical Mechanism of Adenosine Deaminase1 **1987**, *26* (23) 7378-7384.

- (72) Weiss, P.M., Chen, C.Y., Cleland, W.W. and Cook, P.F., Use of primary deuterium and nitrogen-15 isotope effects to deduce the relative rates of steps in the mechanisms of alanine and glutamate dehydrogenases. *J. Biochem.*, **1988**, 27(13), 4814-4822.
- (73) Hermes, J.D., Roeske, C.A., O'Leary, M.H. and Cleland, W.W., 1982. Use of multiple isotope effects to determine enzyme mechanisms and intrinsic isotope effects. Malic enzyme and glucose 6-phosphate dehydrogenase. *J. Biochemistry*, **1982**, 21(20), 5106-5114.
- (74) Zakett, D.; Flynn, R. G. A.; Cooks, R. G. Chlorine Isotope Effects In Mass Spectrometry Chlorine Isotope Effects in Mass Spectrometry by Multiple Reaction Monitoring; *J. Phys. Chem.* **1978**; 82 (22) 2359-2362.
- (75) Bahnson, B. J.; Anderson, V. E. Crotonase-Catalyzed. Beta.-Elimination Is Concerted: A Double Isotope Effect Study. *J. Biochem.* **1991**, 30 (24), 5894–5906.
- (76) Gawlita, E.; Paneth, P.; Anderson, V. E. Equilibrium Isotope Effect on Ternary Complex Formation of [1-18O] Oxamate with NADH and Lactate Dehydrogenase. *J. Biochem.* **1995**, 34 (18), 6050–6058.
- (77) Huang, S.-M.; Xu, S.-Y.; Belopolski, I.; Lee, C.-C.; Chang, G.; Chang, T.-R.; Wang, B.; Alidoust, N.; Bian, G.; Neupane, M. New Type of Weyl Semimetal with Quadratic Double Weyl Fermions. *Proc. Nat. Acad. Sci.* **2016**, 113 (5), 1180–1185.
- (78) Harris, M. E.; Dai, Q.; Gu, H.; Kellerman, D. L.; Piccirilli, J. A.; Anderson, V. E. Kinetic Isotope Effects for RNA Cleavage by 2'-O-Transphosphorylation:

- Nucleophilic Activation by Specific Base. *J. Am. Chem. Soc.* **2010**, *132* (33), 11613–11621.
- (79) Rosenberg, S.; Kirsch, J. F. Measurement of Heavy Atom Kinetic Isotope Effects by Direct Mass Spectrometric Analysis. *Anal. Chem.* **1979**, *51* (9), 1375–1379.
- (80) Rosenberg, S.; Kirsch, J. F. Oxygen-18 Leaving Group Kinetic Isotope Effects on the Hydrolysis of Nitrophenyl Glycosides. 1. Beta.-Galactosidase-Catalyzed Hydrolysis. *J. Biochem.* **1981**, *20* (11), 3189–3196.
- (81) Singhal, N.; Kumar, M.; Kanaujia, P. K.; Viridi, J. S. MALDI-TOF Mass Spectrometry: An Emerging Technology for Microbial Identification and Diagnosis. *Front. Microbiol.* Frontiers Research Foundation 2015.
<https://doi.org/10.3389/fmicb.2015.00791>.
- (82) Lay, J. O. MALDI-TOF Mass Spectrometry of Bacteria. *Mass Spectrom. Rev.* **2001**, 172–194. <https://doi.org/10.1002/mas.10003>.
- (83) Zenobi, R.; Knochenmuss, R. Ion Formation in Maldi Mass Spectrometry. *Mass Spectrom. Rev.* **1998**, *17* (5), 337–366. [https://doi.org/10.1002/\(sici\)1098-2787\(1998\)17:5<337::aid-mas2>3.0.co;2-s](https://doi.org/10.1002/(sici)1098-2787(1998)17:5<337::aid-mas2>3.0.co;2-s).
- (84) Burlingame, A. L.; Boyd, R. K.; Gaskell, S. J. *Mass Spectrom.* **1998**.
- (85) Karas, M.; Glückmann, M.; Schäfer, J. Ionization in Matrix-Assisted Laser Desorption/Ionization: Singly Charged Molecular Ions Are the Lucky Survivors. *J. Mass Spectrom.* **2000**, *35* (1), 1–12. [https://doi.org/10.1002/\(SICI\)1096-9888\(200001\)35:1<1::AID-JMS904>3.0.CO;2-0](https://doi.org/10.1002/(SICI)1096-9888(200001)35:1<1::AID-JMS904>3.0.CO;2-0).

- (86) Linscott, J. A.; Kapilashrami, K.; Wang, Z.; Senevirathne, C.; Bothwell, I. R.; Blum, G.; Luo, M. Kinetic Isotope Effects Reveal Early Transition State of Protein Lysine Methyltransferase SET8. *Proc. Natl. Acad. Sci.* **2016**, *113* (52), E8369–E8378. <https://doi.org/10.1073/pnas.1609032114>.
- (87) Cleland, W. W. The Use of Isotope Effects to Determine Enzyme Mechanisms. *Arch. Biochem. Biophys.* **2005**, 2–12. <https://doi.org/10.1016/j.abb.2004.08.027>.
- (88) Cleland, W. W. Isotope Effects: Determination of Enzyme Transition State Structure; Enzyme Transition State Structure **1995**. 341-369.
- (89) Ünligil, U. M., & Rini, J. M. Glycosyltransferase structure and mechanism. *Current opinion in structural biology*, 2000, *10*(5), 510-517.
- (90) Busch, C.; Hofmann, F.; Selzer, J.; Munro, S.; Jeckel, D.; Aktories, K. A Common Motif of Eukaryotic Glycosyltransferases Is Essential for the Enzyme Activity of Large Clostridial Cytotoxins. *J. Biol. Chem.* **1998**, *273* (31), 19566–19572.
- (91) Pedersen, L. C.; Tsuchida, K.; Kitagawa, H.; Sugahara, K.; Darden, T. A.; Negishi, M. Heparan/Chondroitin Sulfate Biosynthesis: Structure and Mechanism of Human Glucuronyltransferase I. *J. Biol. Chem.* **2000**, *275* (44), 34580–34585.
- (92) Lairson, L. L.; Henrissat, B.; Davies, G. J.; Withers, S. G. Glycosyl Transferases: Structures, Functions, and Mechanisms. *Annu. Rev. Biochem.* **2008**, pp 521–555. <https://doi.org/10.1146/annurev.biochem.76.061005.092322>.
- (93) Mestrom, L.; Przypis, M.; Kowalczykiewicz, D.; Pollender, A.; Kumpf, A.; Marsden, S. R.; Bento, I.; Jarzębski, A. B.; Szymańska, K.; Chruściel, A.; Tischler, D.;

- Schoevaart, R.; Hanefeld, U.; Hagedoorn, P. L. Leloir Glycosyltransferases in Applied Biocatalysis: A Multidisciplinary Approach. *Int. J. Mol. Sci.* **2019**.
<https://doi.org/10.3390/ijms20215263>.
- (94) Lombard, V.; Golaconda Ramulu, H.; Drula, E.; Coutinho, P. M.; Henrissat, B. The Carbohydrate-Active Enzymes Database (CAZy) in 2013. *Nucleic Acids Res.* **2014**, *42* (D1), D490–D495.
- (95) *Cazy Carbohydrate-Active Enzymes Home Page*. <http://www.cazy.org/>.
- (96) Campbell, R. E.; Mosimann, S. C.; Tanner, M. E.; Strynadka, N. C. J. The Structure of UDP-N-Acetylglucosamine 2-Epimerase Reveals Homology to Phosphoglycosyl Transferases. *J. Biochem.* **2000**, *39* (49), 14993–15001.
<https://doi.org/10.1021/bi001627x>.
- (97) Coutinho, P. M.; Deleury, E.; Davies, G. J.; Henrissat, B. An Evolving Hierarchical Family Classification for Glycosyltransferases. *J. Mol. Biol.* **2003**, *328* (2), 307–317.
[https://doi.org/10.1016/S0022-2836\(03\)00307-3](https://doi.org/10.1016/S0022-2836(03)00307-3).
- (98) Chiu, C. P. C.; Lairson, L. L.; Gilbert, M.; Wakarchuk, W. W.; Withers, S. G.; Strynadka, N. C. J. Structural Analysis of the α -2, 3-Sialyltransferase Cst-I from *Campylobacter Jejuni* in Apo and Substrate-Analogue Bound Forms. *J. Biochem.* **2007**, *46* (24), 7196–7204.
- (99) Chiu, C. P. C.; Watts, A. G.; Lairson, L. L.; Gilbert, M.; Lim, D.; Wakarchuk, W. W.; Withers, S. G.; Strynadka, N. C. J. Structural Analysis of the Sialyltransferase CstII

- from *Campylobacter Jejuni* in Complex with a Substrate Analog. *Nat. Struct. Mol. Biol.* **2004**, *11* (2), 163–170.
- (100) Kozmon, S.; Tvaroška, I. Catalytic Mechanism of Glycosyltransferases: Hybrid Quantum Mechanical/Molecular Mechanical Study of the Inverting N-Acetylglucosaminyltransferase I. *J. Am. Chem. Soc.* **2006**, *128* (51), 16921–16927. <https://doi.org/10.1021/ja065944o>.
- (101) Larivière, L.; Gueguen-Chaignon, V.; Moréra, S. Crystal Structures of the T4 Phage β -Glucosyltransferase and the D100A Mutant in Complex with UDP-Glucose: Glucose Binding and Identification of the Catalytic Base for a Direct Displacement Mechanism. *J. Mol. Biol.* **2003**, *330* (5), 1077–1086.
- (102) Lairson, L. L.; Chiu, C. P. C.; Ly, H. D.; He, S. M.; Wakarchuk, W. W.; Strynadka, N. C. J.; Withers, S. G. An Active Site Mutant of the Retaining Glycosyltransferase LgtC from *Neisseria Meningitidis* Contains a Covalently Bound Galactosyl-Enzyme Intermediate and Reveals an Alternative Candidate Catalytic Nucleophile. In *Glycobiology*; Oxford Univ Press Inc Journals Dept, 2004, 14, 1087.
- (103) Guthrie, R. D., & Jencks, W. P. IUPAC recommendations for the representation of reaction mechanisms. *Acc. Chem. Res.* **1989**, *22*(10), 343-349.
- (104) Jencks, W. P. Quantitative Approaches to Reaction Mechanisms and Catalysis. Substitution at Carbon. *J. Phys. Org. Chem.* **1996**, *9* (6), 337–340.
- (105) Winstein, S.; Clippinger, E.; Fainberg, A. H.; Heck, R.; Robinson, G. C. Salt Effects and Ion Pairs in Solvolysis and Related Reactions. III. 1 Common Ion Rate

- Depression and Exchange of Anions during Acetolysis^{2, 3}. *J. Am. Chem. Soc.* **1956**, 78 (2), 328–335.
- (106) Carey, F. A.; Sundberg, R. J. *Advanced Organic Chemistry: Part A: Structure and Mechanisms*; Springer Science & Business Media, 2007.
- (107) Lee, S. S.; Hong, S. Y.; Errey, J. C.; Izumi, A.; Davies, G. J.; Davis, B. G. Mechanistic Evidence for a Front-Side, S_Ni -Type Reaction in a Retaining Glycosyltransferase. *Nat. Chem. Biol.* **2011**, 7 (9), 631–638.
<https://doi.org/10.1038/nchembio.628>.
- (108) Jencks, W. P. When Is an Intermediate Not an Intermediate? Enforced Mechanisms of General Acid-Base, Catalyzed, Carbocation, Carbanion, and Ligand Exchange Reaction. *Acc. Chem. Res.* **1980**, 13 (6), 161–169.

Chapter 2: Direct Competitive Kinetic Isotope Effect Measurement Using Quantitative Whole Molecule MALDI-TOF Mass Spectrometry

Parts of this chapter have been submitted for publication as:

Teodora Kljaic, Scott, M. A.; Guirguis, V.; Tyrlic, M.; Liu, A.; Poulin, M. B. Direct Competitive Kinetic Isotope Effect Measurement Using Quantitative Whole Molecule MALDI-TOF Mass Spectrometry. *JACS Comm.* **2023**.

Contributions of other authors:

Merritt Scott was involved in the initial conception of the development of the approach on PgaCD system, not shown here. Andrew Liu ran standards of UDP-GlcNAc needed for application of the initial concept of the method on PgaCD. Veronica Guirguis was involved in the method development using DHB. Their data collections were not reported in this thesis, as the method was further developed and improved since then. Michael Tyrlic designed MALDI-TOF MS peak data analysis in RStudio for all samples analyzed in this chapter.

2.1 INTRODUCTION

The measurement of kinetic isotope effect (KIEs) is among the most powerful tools available for the study enzyme reaction mechanisms.¹⁻⁴ Highly precise KIE measurements can provide unique insight into the rate limiting microscopic steps of enzyme catalyzed reactions,^{1,5} and can facilitate detailed atomistic characterization of transition state structures to guide the design of incredibly potent transition state analogue enzyme inhibitors.⁶⁻⁹ Despite the utility of KIE measurements for examining enzyme mechanisms, they are not been widely used by the broader enzymology research community. This is, at least in part, due to the complex analytical workflows required to measure heavy atom KIEs using available approaches, and difficulty obtaining suitably labeled substrates for these KIE measurements. While primary hydrogen atom and solvent KIEs are more common, few labs conduct the precise heavy atom KIEs required for detailed analysis of enzyme transition state structures.

KIEs for heavy atoms (ie. C, N, O, S, etc...) are of low magnitude with typical values falling in the range of 0.95–1.05, necessitating highly precise analytical measurements.^{3,10,11} Typically these are measured under competitive conditions giving isotope effects on the enzyme specificity constant V/K that report on all isotopically sensitive steps up to and including the first irreversible step of the reaction. Competitive KIEs are calculated using eq. 1:

$$(R/R_0) = (1 - F)^{(1/kie-1)}$$

where R is the heavy/light isotope ratio measured for the unreacted substrate at F , R_0 is the initial heavy/light isotope ratio for the substrate at time zero, F is the fraction of substrate that has been converted to product (ie. fractional conversion), and kie is the

V/K isotope effect. Thus, the determination of competitive KIEs requires precise measurement of both the analyte concentration (to determine F) and heavy/light isotope ratios (to determine R and R_0).

The most common approaches to measure heavy atom KIEs utilize direct competitive isotope ratio measurements using a pair of isotope labelled substrates by liquid-scintillation counting,^{12–19} isotope ratio mass spectrometry,^{20–24} or more recently nuclear magnetic resonance (NMR) spectroscopy.^{25–29} While these approaches can be successfully employed to measure heavy atom KIEs for enzymatic reactions, they require complex analytical workflows to purify and isolate the analyte prior to analysis, or in the case of competitive NMR KIE measurements, they require high concentrations of multiple isotopically labeled reactants.

As an alternative, direct whole molecule mass spectrometry (MS) has emerged as a promising approach for heavy atom KIE measurements due to its high sensitivity and ability to distinguish multiple isotopes simultaneously.^{3,30–38} Generally, isotopologues of an analyte ionize with the same ionization efficiency allowing for relative quantification of their isotope ratios. Another advantage of whole molecule MS measurements is that they enable the analysis of stable isotope labeled analytes that are generally more easily available and more affordable than radioisotope labeled materials required for scintillation counting. However, the technique is not without its limitations. First, MS-based KIE measurements have traditionally examined enzyme reaction at partial conversion to quantify isotope ratio R for the reactant or product that have already been purified from the reaction mixture,^{30,32,33,35,36,38,39} necessitating complex analytical workflows for the isolation and purification of the analyte prior to

analysis. Second, slight variations in sample composition can effect ionization efficiency of and analyte making the precise quantification of analyte concentrations required for determining fractional conversion F challenging. Thus, an alternative approach like UV-Vis spectroscopy, or high-performance liquid chromatography (HPLC) is carried out parallel to quantify the analyte concentration for the calculation of F . We sought to simplify the procedure to enable both R and F to be determined in a single measurement.

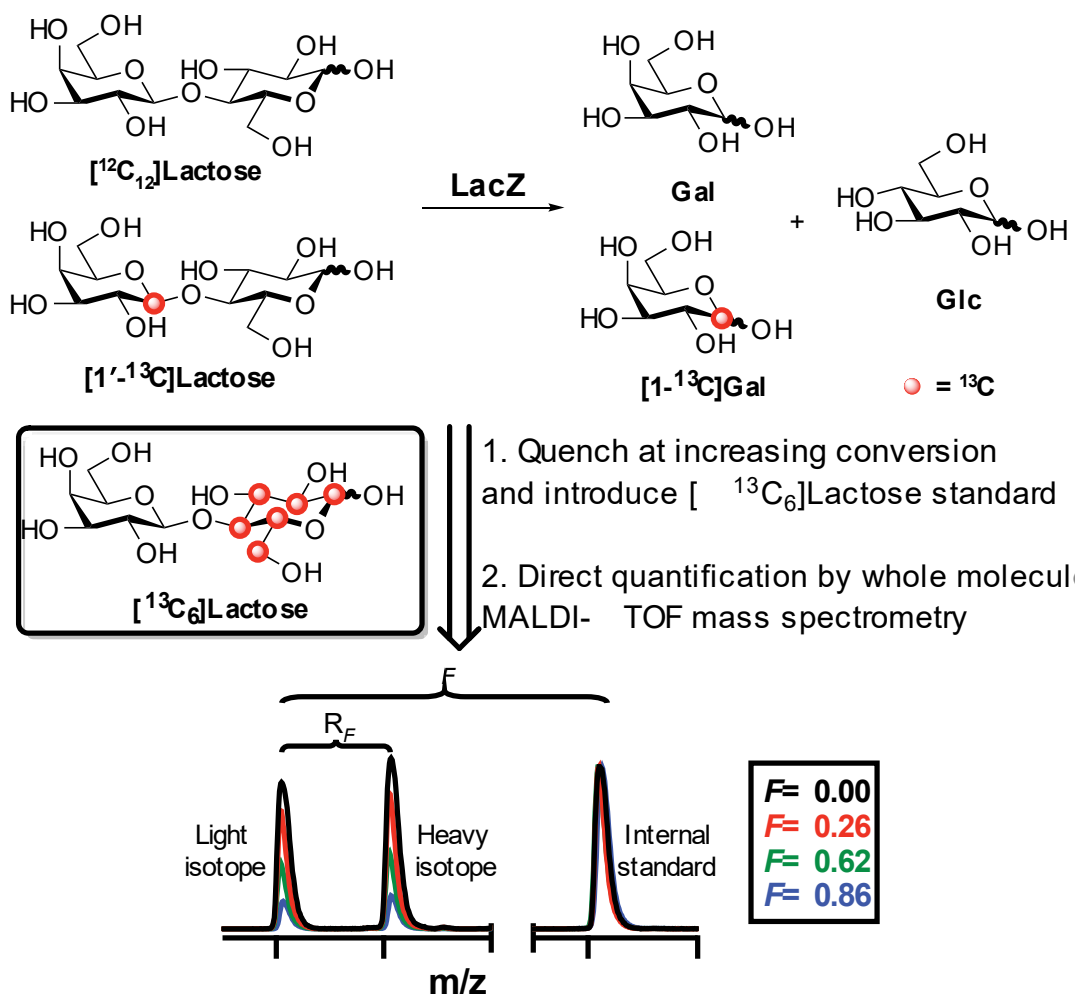


Figure 2.1. Quantitative MALDI-TOF MS approach for competitive KIE measurements. An enzymatic reaction containing light ($[^{12}\text{C}_{12}]$ lactose) and heavy ($[1'-^{13}\text{C}]$ lactose) is allowed to proceed and aliquots are quenched at increasing fractional

conversion. An internal standard ($[^{13}\text{C}_6]$ lactose) is added during the quench. Isotope ratios (R_F) and fractional conversion (F) are determined at each time point from the heavy/light isotope peak area and the light/internal standard peak area, respectively.

Here, we report a method that enables the direct measurement of competitive KIEs using a quantitative whole molecule matrix assisted laser desorption ionization (MALDI) time of flight (TOF) MS approach that does not require isolation and purification of the reactants prior to analysis (Figure 2.1). This approach enables quantitative measurements of both relative isotope abundance of an analyte and fractional conversion F in single measurements. This is accomplished by introducing a known concentration of internal standard to quenched samples of the enzyme reaction that has the same structure as the analyte but a different isotope labeling pattern. By quenching the enzyme reaction at multiple time points it enables us to measure R and F relative to the internal standard for each sample as the reaction progresses. These values can then be fit using eq. 1 to obtain highly precise V/K KIEs. MALDI was selected as the ionization source for these measurement as it is more tolerant of salts and buffer composition than electrospray ionization (ESI) enabling the direct analysis of enzyme reaction mixtures without requiring isolation or purification of the analyte prior to the analysis. While, MALDI-TOF MS has been previously employed for KIE measurements,^{39,40} what distinguishes our approach is the inclusion of an internal standard during sample quenching, which enables the simultaneous determination of R and F in a single measurement.

2.2 RESULTS AND DISCUSSION

To evaluate the utility of this MALDI-TOF MS approach for enzymatic KIE measurements, we chose to examine the hydrolysis of lactose catalyzed by *E. coli* β -galactosidase (LacZ) as a model system. The structure and chemical mechanism of LacZ have been extensively studied,^{41–46} and ^{18}O , secondary- ^2H , and solvent KIE measurements have been previously reported.^{33,41,47} LacZ is a retaining glycosyl hydrolase that catalyzes the hydrolysis of lactose with an overall retention of the anomeric configuration. Despite the substantial efforts that have been made to elucidate the mechanism of LacZ, there have been no previous KIE studies that have used the native lactose as the substrate. Here, we used our quantitative MALDI-TOF MS approach to measure both 1'- ^{13}C and 6'- ^{13}C KIEs for the LacZ catalyzed hydrolysis of lactose.

Our initial application of this MALDI-TOF MS approach to measure LacZ KIEs made use of 2,4-dihydroxybenzoic acid (DHB) as a matrix compound. However, the use of DHB produced inefficient ionization of lactose resulting from matrix ion interference and detector saturation, limiting the accurate quantification of lactose concentration (Figure 2.2A). To overcome these limitations, we switched to the use of graphene as a macromolecular matrix compound (Figure 2.2B). This led to the reproducible ionization of a lactose- Na^+ adduct as the major peak within our mass spectra. Samples of lactose prepared in 20 mM Tris-HCl buffer (pH 7.4) with 100 mM NaCl demonstrated optimum ionization of a lactose- Na^+ adduct without signal suppression and provides a stable pH for efficient LacZ enzyme activity. We found that averaging the peak areas from at least five technical replicates of the same sample

improved the overall precision of the isotope ratio measurements (data not shown). Increasing the number of technical replicates beyond five did not significantly improve precision of the measurements and so the average peak areas from five technical replicates were used to calculate analyte concentrations in all subsequent experiments.

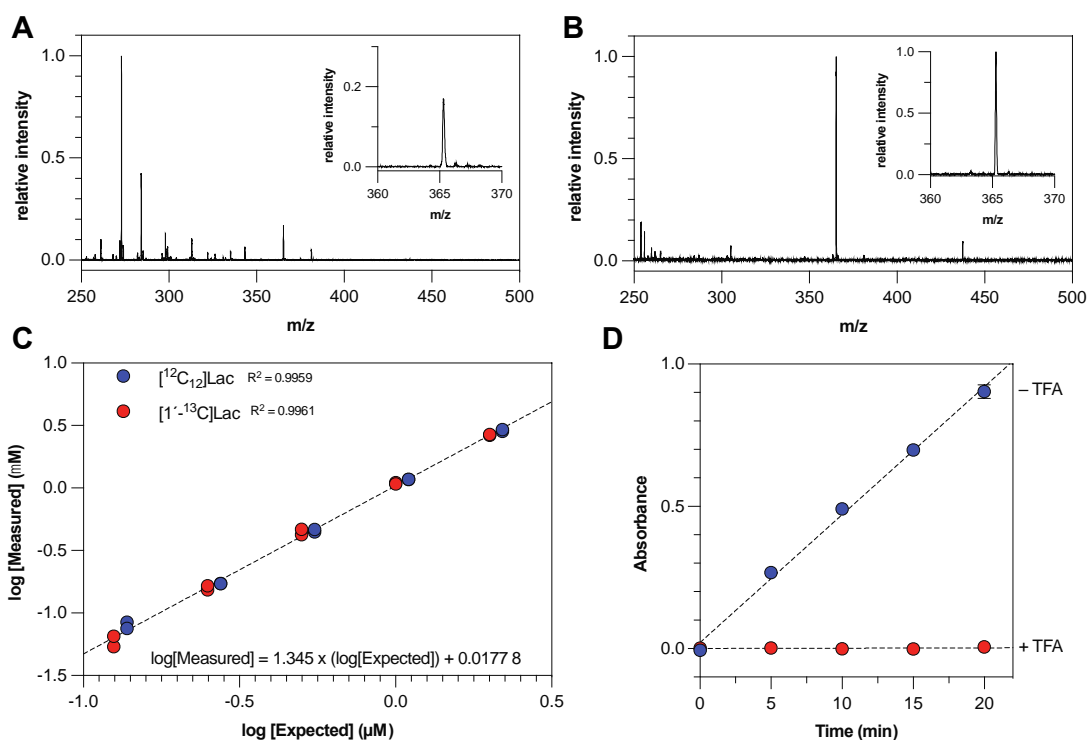


Figure 2.2. Optimization of MALDI-TOF MS conditions for competitive KIE measurements. (A) A sample of $[^{12}\text{C}_{12}]$ -lactose analyzed using DHB as the matrix. (B) The same sample of $[^{12}\text{C}_{12}]$ -lactose analyzed using graphene as the matrix. The spectra were normalized to the intensity of the largest ion peak within the m/z window analyzed. (C) Standard curves for $[^{12}\text{C}_{12}]$ -lactose and $[1'-^{13}\text{C}]$ -lactose concentrations measured relative to a fixed 500 μM concentration of $[^{13}\text{C}_6]$ -lactose internal standard. (D) Measurement of LacZ quenching efficiency. Samples of PNP-Gal and LacZ were either pre-quenched with TFA or quenched at the times indicated. The absorbance of the pre-quenched samples was compared to the unquenched at each time point.

To ensure precise and accurate analyte concentrations could be measured using this approach, we prepared standard curves for both $[^{12}\text{C}_{12}]$ -lactose and $[1'-^{13}\text{C}]$ -lactose

measured relative to a fixed concentration of [Glc- $^{13}\text{C}_6$]-lactose. Interestingly, we observed a non-linear relationship between the peak area and analyte concentration that was consistent for both [$^{12}\text{C}_{12}$]-lactose and [$1'-^{13}\text{C}$]-lactose. A linear correlation was obtained by plotting the $\log(\text{peak area})$ vs. $\log(\text{analyte concentration})$ (Figure 2.2C-D), and this standard curve was used to calculate analyte concentrations based on peak area in all subsequent KIE experiments.

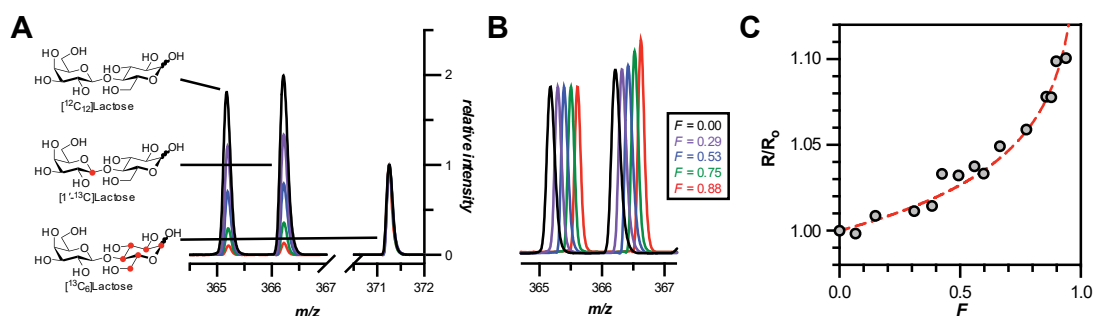


Figure 2.3. Quantitative MALDI-TOF MS approach for competitive KIE determination. (A) Representative mass spectra normalized to the peak intensity of [$^{13}\text{C}_6$]lactose internal standard for the measurement of a LacZ [$1'-^{13}\text{C}$] KIE measured at different F . The peaks for [$^{12}\text{C}_{12}$]lactose, [$1'-^{13}\text{C}$]lactose, and [$^{13}\text{C}_6$]lactose are indicated. (B) The same mass spectra normalized relative to the [$^{12}\text{C}_{12}$]lactose peak intensity. (C) Representative plot of R/R_0 vs. F fit to eq. 1 using 15 time points derived from a single LacZ reaction.

Using the optimized MALDI-TOF MS conditions, LacZ KIEs using [$1'-^{13}\text{C}$]-lactose and [$6'-^{13}\text{C}$]-lactose were measured. For each KIE measurement, a minimum of fifteen time points were analyzed from each individual reaction mixture at varying fractional conversion F , where the enzymatic activity of LacZ was quenched through the addition of 3 mM trifluoroacetic acid (TFA). At the same time 500 μM of [$^{13}\text{C}_6$]lactose internal standard was introduced. These conditions were found to effectively quench LacZ activity without interfering with subsequent MALDI-TOF MS analysis. Figure 2.3A shows representative mass spectra measured at F ranging from

0.0 to 0.88 that have been normalized to the peak intensity of the [$^{13}\text{C}_6$]lactose standard. The peaks for unlabeled [$^{12}\text{C}_{12}$]lactose (m/z 365.1) and [$1'-^{13}\text{C}$]lactose (m/z 366.1) decrease as a function of increasing F relative to that of the [$^{13}\text{C}_6$]-lactose internal standard (m/z 371.1). When these same spectra are instead normalized to the intensity of the [$^{12}\text{C}_{12}$]-lactose peak, a clear increase in the [$1'-^{13}\text{C}$]lactose relative to the [$^{12}\text{C}_{12}$]lactose is observed as a function of increasing F (Figure 2.3B) consistent with a normal KIE value. The data from all 15 time points were fit using eq. 1 as shown in Figure 2.3C to calculate individual V/K KIE values. Four individual KIE measurements were carried out on separate days and the individual KIEs determined by fitting to eq. 1 are summarized in Table 2.1, resulting in an average primary [$1'-^{13}\text{C}$] KIE of 1.034 ± 0.005 . The precision of these KIE measurements is comparable to those obtained using competitive radioisotope labelling, and NMR based approaches.

Table 2.1. Summary of LacZ KIEs

KIE	Experimental KIE ^a	Average ^b
$1'-^{13}\text{C}$	1.034 ± 0.005	1.034 ± 0.005
	1.028 ± 0.002	
	1.039 ± 0.002	
	1.036 ± 0.002	
$6'-^{13}\text{C}$	0.999 ± 0.007	1.001 ± 0.002
	1.001 ± 0.003	
	1.003 ± 0.005	
	1.002 ± 0.009	

^a Error is the standard error for the nonlinear regression fit

^b Mean and standard deviation for four KIE experiments.

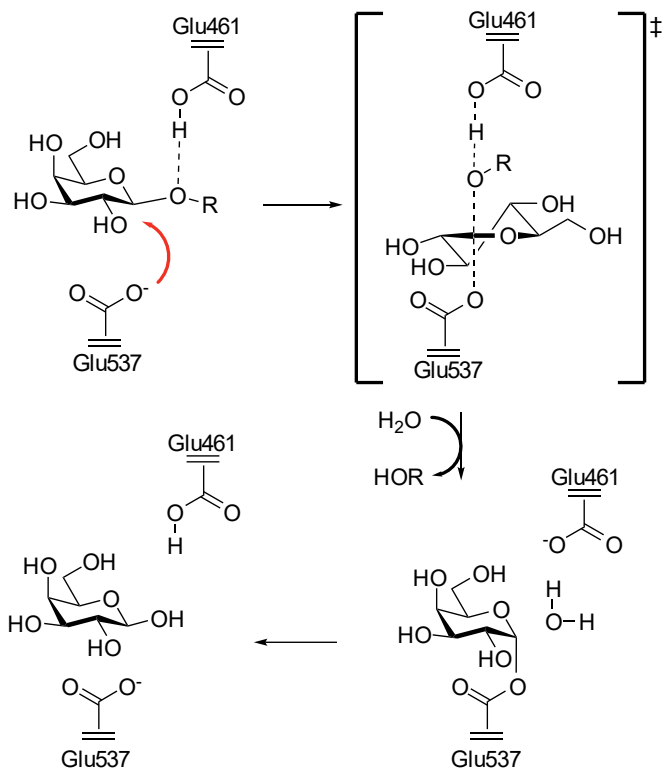


Figure 2.4. Mechanism for LacZ catalyzed hydrolysis of lactose highlighting the first TS.

To verify the primary [$1'-^{13}\text{C}$] KIE is not an artifact of the MALDI-TOF MS analysis method, we additionally measured a LacZ KIE using [$6'-^{13}\text{C}$]-lactose. The 6'-carbon of lactose is positioned distal from the reaction center and not isotopically sensitive to the reaction catalyzed by LacZ. As summarized in Table 2.1, we observed an average [$6'-^{13}\text{C}$]-lactose KIE of 1.001 ± 0.002 , which is not significantly different from the expected value of 1.

Both the [$1'-^{13}\text{C}$]-lactose and [$6'-^{13}\text{C}$]-lactose KIE are consistent with the accepted mechanism for LacZ, which involves an initial $\text{S}_{\text{N}}2$ attack of Glu537 to form a covalent glycosyl-enzyme intermediate and release glucose, followed by hydrolysis of the glycosyl-enzyme intermediate via a nucleophilic attack by water (Figure 2.4).⁴⁴ Previous leaving group ^{18}O and secondary ^2H KIE measurements measured for LacZ

using phenyl-glycoside analogs show that the initial attack of Glu537 is substantially rate limiting, and represents the first “irreversible” step in the reaction.^{33,41} The magnitude of the [1'-¹³C]-lactose KIE measured here is also consistent with an effectively irreversible attack of Glu537 being substantially rate determining under these experimental conditions.

2.3 CONCLUSION

These results demonstrate the utility of this MALDI-TOF MS based KIE measurement approach. This approach can easily be adapted for the analysis of different analytes and enables simultaneous measurement of heavy/light isotope ratio R and fractional conversion F in a single measurement without requiring isolation and purification of the analyte prior to analysis. This enables the use of easily accessible stable isotope labeled samples, while obtaining KIEs with comparable precision to competitive radioisotope labelling methods. While we used MALDI as an ionization source to enable the direct analysis of enzyme reaction mixtures without requiring isolation and purification of the analyte, in principle this quantitative whole molecule MS approach can be applied using any ionization method.

2.4 EXPERIMENTAL PROCEDURES

2.4.1 General

Unless otherwise noted, all chemicals were purchased as analytical or reagent grade and used without further purification. Isotopically labeled [¹³C₆]-lactose, [1'-

^{13}C]-lactose, and [$6'$ - ^{13}C]-lactose were purchased from Omicron Biochemicals, Inc and prepared as described below. MALDI-TOF mass spectrometry measurements were recorded on a Bruker Autoflex Speed spectrometer equipped with a 2KHz smartbeam II laser, with a time of flight (TOF)-analyzer capable of both positive and negative ion mode as described in detail below. Matrix solutions of 2,5-dihydroxybenzoic acid (DHB) were prepared in a 50:50 mixture of acetonitrile:1% aqueous trifluoroacetic acid (TFA) at a final concentration of 10 mg/mL. Graphene matrix samples were prepared as described previously.⁴⁸ Briefly, graphite oxide was prepared following the Hummers method,⁴⁹ starting from commercial graphite powder. Graphene was then prepared via the reduction of graphite oxide with hydrazine.⁵⁰ The reduced graphene was obtained as a black precipitate that were prepared fresh for MALDI-TOF MS by suspending in 100% ethanol to a final concentration of 0.1 mg/mL.⁴⁸

2.4.2 Protein and substrate preparation

Commercial β -galactosidase (LacZ) from *Escherichia coli* was obtained as a lyophilized powder and prepared in 20 mM sodium phosphate buffer pH 7.1 to a concentration of 1 mU/ μL , where 1U is defined as the amount of enzyme required to hydrolyze 1.0 μM of 2-nitrophenol β -D-galactopyranoside (PNP-Galactose) per minute at pH 7.1 and 37 °C. Individual aliquots of enzyme were flash frozen and stored at -80 °C until use.

Lactose substrate samples, both isotopically labeled and unlabeled, were prepared by dissolving the solid in water to a concentration of 10 mM.

2.4.3 Sample quenching

Quenching conditions that enable the rapid inactivation of enzyme activity were tested using a colorimetric LacZ activity assay using 4-nitrophenol β -D-galactopyranoside (PNP-Gal) as a substrate, by measuring the absorbance of the PNP product at 410 nm. First, a 500 μ L reaction mixture was prepared containing 1 mM PNP-Galactose, 1 mM MgCl₂ in 20 mM Tris-HCl buffer pH 7.1. A second 500 μ L reaction mixture containing 1 mM PNP-Galactose, 1 mM MgCl₂, 20 mM Tris-HCl buffer pH 7.1, was set up in parallel and pre-quenched with 6 mM TFA. A 100 μ L fraction from each reaction mixture was removed prior to initiating the reaction to allow for measurement of background absorbance at time zero. Reactions were initiated through the addition of 833 μ U of β -galactosidase to each reaction mixture and allowed to proceed at 22 °C. At 5 min time intervals, 100 μ L aliquots were removed from each reaction mixture and diluted with an equal volume of quench solution. For the first reaction mixture the quench solution consisted of 6 mM aqueous TFA, whereas the quench solution for the second reaction mixture contained only water. The appropriate quench solution was also added to the time zero time points. Immediately before measuring the absorbance at 410 nm, the pH of all of the samples were adjusted by adding 100 μ L of 1M NaOH and samples were transferred to a clear bottom 96 well microtiter plate. End point absorbance measurements were recorder on a Spectramax M5 multimode plate reader (Molecular Devices, USA) and reaction was repeated in triplicate.

2.4.4 MALDI-TOF MS sample preparation and acquisition

For MALDI-TOF measurements using DHB as the matrix, samples were prepared by spotting 1 μL DHB per spot on the target plate followed by drying for 10 minutes at room temperature. Next, 1 μL of analyte, prepared as outlined below, was spotted over the dry matrix and allowed to dry for an additional 10 minutes at room temperature and humidity of 45-50%. For MALDI-TOF measurements using graphene as the matrix, 10 μL of analyte sample was directly mixed with 10 μL of graphene suspension and subsequently dispersed for 10 minutes in a sonication bath. 1 μL samples of the graphene–analyte mixture were spotted on the target plate and allowed to dry for 10 minutes at room temperature and humidity of 45-50%.

Mass spectra were recorded in positive-ion reflectron mode to achieve optimal baseline peak resolution. A spectral window from 280 to 580 m/z was used for analyzing lactose samples. Sodium chloride (25 mM) was included in the analyte sample buffer to boost the sensitivity for detection of lactose + Na^+ molecular ions. A total of five technical replicate spots were analyzed for each analyte sample to minimize variability in sample concentration or isotope composition resulting from sample spotting. Summed spectrum from a minimum of 3000 shots for each sample spot were recorded and exported in mzXML format and further processed in R using the MaldiQuant package,^{51,52} as described below.

2.4.5 KIE measurements

Reaction mixtures for LacZ KIE measurements were prepared containing 2 mM total lactose substrate (in a ~ 1:1 ratio of “heavy” to “light” sample) in 20 mM Tris-HCl pH 7.1 with 10 mM MgCl₂ and 100 mM NaCl in a final volume of 120 μL. Prior to initiation of the reaction, a time zero time point consisting of 20 μL of the reaction mixture was removed and diluted to a final volume of 22 μL to measure initial lactose concentrations and isotope ratios (R_0). Reactions were carried out at 30 °C and initiated through the addition of 10 μL of 166 mU/mL β-galactosidase. At regular time intervals 5 μL aliquots of the reaction mixture were removed and the LacZ activity was quenched by mixing with an equal volume of quench solution consisting of 0.5 mM [Glc-¹³C₆]lactose standard in 6 mM aqueous TFA. These conditions were found to rapidly inactivate β-galactosidase without any degradation of the lactose substrate, as described in the section 2.4.3. Quenched fractions were centrifuged at 17,000 × g for 2 min to remove any solid precipitates and stored at -20 °C prior to MALDI-TOF analysis as described above. A reaction mixture containing only “light” lactose was analyzed in the same fashion to account for concentration of natural abundance ¹³C present in the “light” lactose sample.

2.4.6 Peak integration and data analysis

Relative peak areas for the sodium adducts of [¹²C₁₂]Lac (light, m/z = 365.2), [¹³C₁]Lac (heavy, m/z = 366.2) and [¹³C₆]Lac (standard, 371.2) were determined for each mass spectrum using a numerical peak integration script developed in RStudio. Briefly, mass spectral mzXML files were imported in RStudio using the MALDIquant

package.^{51,52} A 10 m/z window containing the peaks of interest was selected for further analysis. The 25th percentile of all intensity values within this segment was used as a baseline and subtracted from all intensities within the segment. Subsequently, the boundaries of each relevant peak were identified. Initial guesses of outer integration boundaries were provided by the user and were identical for all mass spectra analyzed from the same enzyme-substrate combination. Subsequently, an approximate first derivative was calculated for the entire spectrum segment and smoothed using an “SMA” moving average calculation. A difference in treatment of the left and right boundaries was necessitated by the peak asymmetry. The left boundary was selected as the highest mass number lower than the 20th percentile of smoothed derivatives within the segment bound by the initial guess and the peak maximum. The left boundary was selected as the lowest mass number lower than the 5th percentile of smoothed derivatives within the segment bound by the peak maximum and the initial guess. The total peak intensity was determined after boundary selection from the sum of all intensities within these boundaries. A plot of spectra with overlaid final integration boundaries was manually examined for each measurement to verify accurate boundary detection. An integration was considered successful if the boundaries included the entire target peak, excluded all other peaks, and divided overlapping peaks at a local minimum between them.

2.5 BIBLIOGRAPHY

- (1) Cleland, W. W. The Use of Isotope Effects to Determine Enzyme Mechanisms. *Arch. Biochem. and Biophys.* 2005, 433 (1), 2–12.
<https://doi.org/10.1016/j.abb.2004.08.027>.
- (2) Bennet, A. J. Kinetic Isotope Effects for Studying Post-Translational Modifying Enzymes. *Curr. Opin. Chem. Biol.* 2012, 16 (5–6), 472–478.
<https://doi.org/10.1016/j.cbpa.2012.10.024>.
- (3) Gu, H.; Zhang, S. Advances in Kinetic Isotope Effect Measurement Techniques for Enzyme Mechanism Study. *Molecules* 2013, 18 (8), 9278–9292.
<https://doi.org/10.3390/molecules18089278>.
- (4) Northrop, D. B. Uses of Isotope Effects in the Study of Enzymes. *Methods* 2001, 24 (2), 117–124. <https://doi.org/10.1006/meth.2001.1173>.
- (5) Cook, P. F.; Cleland, W. W. Mechanistic Deductions from Isotope Effects in Multireactant Enzyme Mechanisms. *J. Biochem.* 1981, 20 (7), 1790–1796.
<https://doi.org/10.1021/bi00510a013>.
- (6) Schramm, V. L. Transition States, Analogues, and Drug Development. *ACS Chemical Biology* 2013, 8 (1), 71–81. <https://doi.org/10.1021/cb300631k>.
- (7) Schramm, V. L. Enzymatic Transition States, Transition-State Analogs, Dynamics, Thermodynamics, and Lifetimes. *Annu. Rev. Biochem* 2011, 80 (1), 703–732. <https://doi.org/10.1146/annurev-biochem-061809-100742>.

- (8) Horenstein, B. A.; Schramm, V. L. Correlation of the Molecular Electrostatic Potential Surface of an Enzymic Transition State with Novel Transition-State Inhibitors. *J. Biochem.* 1993, 32 (38), 9917–9925.
<https://doi.org/10.1021/bi00089a007>.
- (9) Cleland, W. W. Isotope Effects: Determination of Enzyme Transition State Structure. *Methods in enzymology* 1995, 249, 341–373.
- (10) Dale, H. J. A.; Leach, A. G.; Lloyd-Jones, G. C. Heavy-Atom Kinetic Isotope Effects: Primary Interest or Zero Point? *J. Am. Chem. Soc.* 2021, 143 (50), 21079–21099. <https://doi.org/10.1021/jacs.1c07351>.
- (11) Paneth, P. Some Analytical Aspects of the Measurement of Heavy-Atom Kinetic Isotope Effects. *Talanta* 1987, 34 (10), 877–883. [https://doi.org/10.1016/0039-9140\(87\)80118-2](https://doi.org/10.1016/0039-9140(87)80118-2).
- (12) Parkin, D. W.; Leung, H. B.; Schramm, V. L. Synthesis of Nucleotides with Specific Radiolabels in Ribose. Primary ¹⁴C and Secondary ³H Kinetic Isotope Effects on Acid-Catalyzed Glycosidic Bond Hydrolysis of AMP, DAMP, and Inosine. *J. Biol. Chem.* 1984, 259 (15), 9411–9417.
- (13) Parkin, D. W.; Schramm, V. L. Effects of Allosteric Activation on the Primary and Secondary Kinetic Isotope Effects for Three AMP Nucleosidases. *J Biological Chem* 1984, 259 (15), 9418–9425.

- (14) Markham, G. D.; Parkin, D. W.; Mentch, F.; Schramm, V. L. A Kinetic Isotope Effect Study and Transition State Analysis of the S-Adenosylmethionine Synthetase Reaction. *J. Biol. Chem.* 1987, 262 (12), 5609–5615.
- (15) Mentch, F.; Parkin, D. W.; Schramm, V. L. Transition-State Structures for N-Glycoside Hydrolysis of AMP by Acid and by AMP Nucleosidase in the Presence and Absence of Allosteric Activator. *J. Biochem.* **1987**, 26 (3), 921–930.
<https://doi.org/10.1021/bi00377a037>.
- (16) Merkler, D. J.; Kline, P. C.; Weiss, P.; Schramm, V. L. Transition-State Analysis of AMP Deaminase. *J. Biochem.* **1993**, 32 (48), 12993–13001.
<https://doi.org/10.1021/bi00211a007>.
- (17) Schramm, V. L.; Horenstein, B. A.; Kline, P. C. Transition State Analysis and Inhibitor Design for Enzymatic Reactions. *J. Biol. Chem.* 1994, 269 (28), 18259–18262.
- (18) Schramm, V. L. [13] Enzymatic Transition-State Analysis and Transition-State Analogs. *Methods Enzym.* 1999, 308, 301–355. [https://doi.org/10.1016/s0076-6879\(99\)08015-5](https://doi.org/10.1016/s0076-6879(99)08015-5).
- (19) Schramm, V. L. ENZYMATIC TRANSITION STATES AND TRANSITION STATE ANALOG DESIGN. *Annu. Rev. Biochem.* 1998, 67 (1), 693–720.
<https://doi.org/10.1146/annurev.biochem.67.1.693>.

- (20) O’Leary, M. H.; Richards, D. T.; Hendrickson, D. W. Carbon Isotope Effects on the Enzymic Decarboxylation of Glutamic Acid. *J. Am. Chem. Soc.* 1970, *92* (14), 4435–4440. <https://doi.org/10.1021/ja00717a048>.
- (21) O’Leary, M. H.; Marlier, J. F. Application of a Novel Double-Labeling Procedure to Measurement of Carbonyl Oxygen Isotope Effects on the Alkaline Hydrolysis and Hydrazinolysis of Methyl Benzoate. *Journal of the American Chemical Society* 1978, *100* (8), 2582–2583. <https://doi.org/10.1021/ja00476a070>.
- (22) O’Leary, M. H. [4] Determination of Heavy-Atom Isotope Effects on Enzyme-Catalyzed Reactions. *Methods Enzym.* 1980, *64*, 83–104. [https://doi.org/10.1016/s0076-6879\(80\)64006-3](https://doi.org/10.1016/s0076-6879(80)64006-3).
- (23) Rendina, A. R.; Hermes, J. D.; Cleland, W. W. Use of Multiple Isotope Effects to Study the Mechanism of 6-Phosphogluconate Dehydrogenase. *J. Biochem.* **1984**, *23* (25), 6257–6262. <https://doi.org/10.1021/bi00320a056>.
- (24) Cleland, W. W. Secondary ¹⁸O Isotope Effects as a Tool for Studying Reactions of Phosphate Mono-, Di-, and Triesters¹. *FASEB J.* 1990, *4* (11), 2899–2905. <https://doi.org/10.1096/fasebj.4.11.2199287>.
- (25) Singleton, D. A.; Thomas, A. A. High-Precision Simultaneous Determination of Multiple Small Kinetic Isotope Effects at Natural Abundance. *J. Am. Chem. Soc.* 1995, *117* (36), 9357–9358. <https://doi.org/10.1021/ja00141a030>.

- (26) Chan, J.; Lewis, A. R.; Gilbert, M.; Karwaski, M.-F.; Bennet, A. J. A Direct NMR Method for the Measurement of Competitive Kinetic Isotope Effects. *Nature Chemical Biology* 2010, 6 (6), 405–407. <https://doi.org/10.1038/nchembio.352>.
- (27) Manning, K. A.; Sathyamoorthy, B.; Eletsky, A.; Szyperski, T.; Murkin, A. S. Highly Precise Measurement of Kinetic Isotope Effects Using ^1H -Detected 2D [^{13}C , ^1H]-HSQC NMR Spectroscopy. *Journal of the American Chemical Society* 2012, 134 (51), 20589–20592. <https://doi.org/10.1021/ja310353c>.
- (28) Sannikova, N.; Lewis, A. R.; Bennet, A. J. Chapter Nineteen Measurement of Kinetic Isotope Effects by Continuously Monitoring Isotopologue Ratios Using NMR Spectroscopy. *Methods Enzym.* 2017, 596, 547–571. <https://doi.org/10.1016/bs.mie.2017.06.034>.
- (29) Lee, J. K.; Bain, A. D.; Berti, P. J. Probing the Transition States of Four Glucoside Hydrolyses with ^{13}C Kinetic Isotope Effects Measured at Natural Abundance by NMR Spectroscopy. *Journal of the American Chemical Society* 2004, 126 (12), 3769–3776. <https://doi.org/10.1021/ja0394028>.
- (30) Rosenberg, S.; Kirsch, J. F. Measurement of Heavy Atom Kinetic Isotope Effects by Direct Mass Spectrometric Analysis. *Analytical Chemistry* 1979, 51 (9), 1375–1379. <https://doi.org/10.1021/ac50045a009>.
- (31) Liuni, P.; Olkhov-Mitsel, E.; Orellana, A.; Wilson, D. J. Measuring Kinetic Isotope Effects in Enzyme Reactions Using Time-Resolved Electrospray Mass

Spectrometry. *Analytical Chemistry* 2013, 85 (7), 3758–3764.

<https://doi.org/10.1021/ac400191t>.

(32) Harris, M. E.; Dai, Q.; Gu, H.; Kellerman, D. L.; Piccirilli, J. A.; Anderson, V. E.

Kinetic Isotope Effects for RNA Cleavage by 2'-O- Transphosphorylation:

Nucleophilic Activation by Specific Base. *Journal of the American Chemical Society*

2010, 132 (33), 11613–11621. <https://doi.org/10.1021/ja103550e>.

(33) Rosenberg, S.; Kirsch, J. F. Oxygen-18 Leaving Group Kinetic Isotope Effects

on the Hydrolysis of Nitrophenyl Glycosides. 1. .Beta.-Galactosidase-Catalyzed

Hydrolysis. *J. Biochem.* 1981, 20 (11), 3189–3196.

<https://doi.org/10.1021/bi00514a031>.

(34) Gu, H.; Zhang, S.; Wong, K.-Y.; Radak, B. K.; Dissanayake, T.; Kellerman, D.

L.; Dai, Q.; Miyagi, M.; Anderson, V. E.; York, D. M.; Piccirilli, J. A.; Harris, M. E.

Experimental and Computational Analysis of the Transition State for Ribonuclease

A-Catalyzed RNA 2'-O-Transphosphorylation. *Proc. Natl. Acad. Sci.* 2013, 110 (32),

13002–13007. <https://doi.org/10.1073/pnas.1215086110>.

(35) Bahnson, B. J.; Anderson, V. E. Crotonase-Catalyzed .Beta.-Elimination Is

Concerted: A Double Isotope Effect Study. *J. Biochem.* **1991**, 30 (24), 5894–5906.

<https://doi.org/10.1021/bi00238a013>.

(36) Gawlita, E.; Paneth, P.; Anderson, V. E. Equilibrium Isotope Effect on Ternary

Complex Formation of [1-18O]Oxamate with NADH and Lactate Dehydrogenase. *J.*

Biochem. **1995**, 34 (18), 6050–6058. <https://doi.org/10.1021/bi00018a007>.

- (37) Kline, P. C.; Rezaee, M.; Lee, T. A. Determination of Kinetic Isotope Effects for Nucleoside Hydrolases Using Gas Chromatography/Mass Spectrometry. *Anal. Biochem.* 1999, 275 (1), 6–10. <https://doi.org/10.1006/abio.1999.4308>.
- (38) Berti, P. J.; Blanke, S. R.; Schramm, V. L. Transition State Structure for the Hydrolysis of NAD⁺ Catalyzed by Diphtheria Toxin †. *J. Am. Chem. Soc.* 1997, 119 (50), 12079–12088. <https://doi.org/10.1021/ja971317a>.
- (39) Linscott, J. A.; Kapilashrami, K.; Wang, Z.; Senevirathne, C.; Bothwell, I. R.; Blum, G.; Luo, M. Kinetic Isotope Effects Reveal Early Transition State of Protein Lysine Methyltransferase SET8. *Proceedings of the National Academy of Sciences* 2016, 113 (52), E8369–E8378. <https://doi.org/10.1073/pnas.1609032114>.
- (40) Mingroni, M. A.; Momaney, V. C.; Barlow, A. N.; Maisonet, I. J.; Knapp, M. J. Measurement of Kinetic Isotope Effects on Peptide Hydroxylation Using MALDI-MS. *Methods Enzym.* 2022, 679, 363–380. <https://doi.org/10.1016/bs.mie.2022.08.019>.
- (41) Sinnott, M. L.; Souchard, I. J. L. The Mechanism of Action of β -Galactosidase. Effect of Aglycone Nature and α -Deuterium Substitution on the Hydrolysis of Aryl Galactosides. *Biochem J* 2005, 133 (1), 89–98. <https://doi.org/10.1042/bj1330089>.
- (42) WITHERS, S. G.; SINNOTT, M. L.; JULLIEN, M.; YON, J. M.; VIRATELLE, O. M. Dependence upon PH of Steady-State Parameters for the B-Galactosidase-Catalysed Hydrolyses of B-D-Galactopyranosyl Derivatives of Different Chemical

- Types. *Eur. J. Biochem.* 1978, 87 (2), 249–256. <https://doi.org/10.1111/j.1432-1033.1978.tb12373.x>.
- (43) Sinnott, M. L. Ions, Ion-pairs and Catalysis by the LacZ B-galactosidase of Escherichia Coli. *Febs Lett* 1978, 94 (1), 1–9. [https://doi.org/10.1016/0014-5793\(78\)80894-1](https://doi.org/10.1016/0014-5793(78)80894-1).
- (44) Juers, D. H.; Matthews, B. W.; Huber, R. E. LacZ β -Galactosidase: Structure and Function of an Enzyme of Historical and Molecular Biological Importance. *Protein Science* 2012, 21 (12), 1792–1807. <https://doi.org/10.1002/pro.2165>.
- (45) Juers, D. H.; Heightman, T. D.; Vasella, A.; McCarter, J. D.; Mackenzie, L.; Withers, S. G.; Matthews, B. W. A Structural View of the Action of Escherichia Coli (LacZ) β -Galactosidase † , ‡. *J. Biochem.* **2001**, 40 (49), 14781–14794. <https://doi.org/10.1021/bi011727i>.
- (46) Juers, D. H.; Jacobson, R. H.; Wigley, D.; Zhang, X.; Huber, R. E.; Tronrud, D. E.; Matthews, B. W. High Resolution Refinement of B-galactosidase in a New Crystal Form Reveals Multiple Metal-binding Sites and Provides a Structural Basis for A-complementation. *Protein Sci.* 2000, 9 (9), 1685–1699. <https://doi.org/10.1110/ps.9.9.1685>.
- (47) Selwood, T.; Sinnott, M. L. A Solvent-Isotope-Effect Study of Proton Transfer during Catalysis by Escherichia Coli (LacZ) β -Galactosidase. *Biochem J* 1990, 268 (2), 317–323. <https://doi.org/10.1042/bj2680317>.

- (48) Dong, X.; Cheng, J.; Li, J.; Wang, Y. Graphene as a Novel Matrix for the Analysis of Small Molecules by MALDI-TOF MS. *Anal. Chem.* 2010, 82 (14), 6208–6214. <https://doi.org/10.1021/ac101022m>.
- (49) Hummers, W. S.; Offeman, R. E. Preparation of Graphitic Oxide. *J. Am. Chem. Soc.* 1958, 80 (6), 1339–1339. <https://doi.org/10.1021/ja01539a017>.
- (50) Chang, H.; Tang, L.; Wang, Y.; Jiang, J.; Li, J. Graphene Fluorescence Resonance Energy Transfer Aptasensor for the Thrombin Detection. *Anal. Chem.* 2010, 82 (6), 2341–2346. <https://doi.org/10.1021/ac9025384>.
- (51) Gibb, S.; Strimmer, K. MALDIquant: A Versatile R Package for the Analysis of Mass Spectrometry Data. *Bioinform.* 2012, 28 (17), 2270–2271. <https://doi.org/10.1093/bioinformatics/bts447>.
- (52) Gibb, S.; Strimmer, K. Mass Spectrometry Analysis Using MALDIquant. *Arxiv* 2016.

Chapter 3: Chemoenzymatic synthesis of isotopically labeled UDP-N-Acetyl Glucosamine substrates

Contributions of other authors:

Merritt Scott expressed and purified NahK and GlmU, and optimized UDP-GlcNAc enzymatic synthesis protocol, all of which I used for the synthesis of UDP-GlcNAc, [2''-¹³C]UDP-GlcNAc and [¹³C₆]UDP-GlcNAc. Andrew Liu used this protocol to synthesize and purify [1''-¹³C]UDP-GlcNAc. Sashika Fernando expressed and purified WecB which I used for synthesis of [2''-²H]UDP-GlcNAc.

3.1 INTRODUCTION

Sugar nucleotides consist of a monosaccharide connected to a nucleotide mono- or diphosphate moiety. The term often refers specifically to structures where the nucleotide is attached to the anomeric carbon of the monosaccharide. Monosaccharides are activated by nucleosides through mono- or diphosphate, forming sugar nucleotides to serve as the glycosylation donors of glycosyltransferases.¹⁰⁹ These sugar nucleotides function as glycosyl or phosphoglycosyl donors used by glycosyltransferases (GTs) in the biosynthesis of glycans, polysaccharides and glycoconjugates essential for the correct function and survival of living organisms, communication, and interactions of cells.^{91,110}

Due to the importance of sugar nucleotides, many chemical methods have been developed for their synthesis.¹¹¹ Chemical methods can be divided into two categories: (1) those involving the condensation of a sugar-1-phosphate with an activated nucleoside monophosphate, and (2) those involving the direct coupling of an activated sugar with a nucleoside diphosphate.¹¹² The many polar and ionic functional groups in sugar nucleotides, and the labile nature of the sugar nucleotide glycosidic bond are responsible for the low solubility of sugar nucleotides in organic solvents, making chemical synthesis very challenging.¹¹¹⁻¹¹³ These approaches often require multiple protection and deprotection reactions just to access the required sugar-1-phosphate for the pyrophosphate coupling reaction, and often results in low yields.

On the other hand, the enzymatic synthesis of sugar nucleotides exclusively gives products with only the natural-type anomer configuration.¹¹⁴ In living cells, sugar

nucleotides are produced by salvage or *de novo* biosynthetic pathways.¹¹⁴ Salvage pathways typically involve phosphorylation of the monosaccharide via a ATP dependent kinase enzyme to generate the sugar-1-phosphate, followed by a reaction with the NTP substrate by a pyrophosphorylase enzyme.¹¹⁵ There are, however, only a select few natural sugar nucleotides can be prepared through such salvage pathways, since salvage pathways for most sugars simply do not exist largely cause of lack of suitable pyrophosphorylases.¹¹⁶⁻¹¹⁸ Alternatively, *de novo* biosynthesis from central metabolic intermediates produces the majority of sugar nucleotides found in nature.¹¹⁹⁻¹²² The process involves single or multiple reactions including dehydration, isomerization, epimerization, oxidation, reduction, amination, and acetylation reactions.¹¹⁹⁻¹²² Nevertheless, it is widely accepted that such complicated bioconversions are not practical for synthetic use due to the complex reaction routes, great purification difficulties, and high preparation cost.¹²³ Additionally, the branching observed for natural bioconversion pathways would lead to isotope scrambling when using *de novo* biosynthesis of isotopically labeled sugar nucleotides, lowering yields (Figure 3.1).

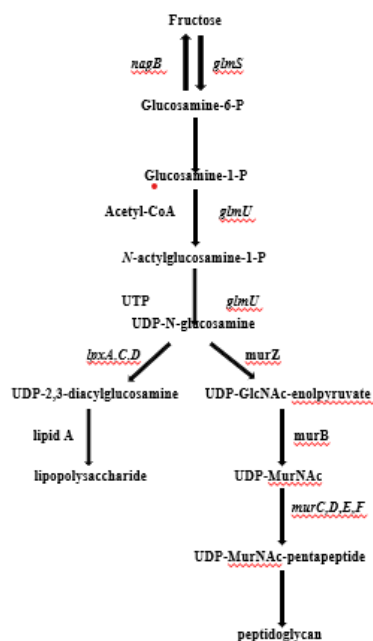


Figure 3.1 Biosynthesis and cellular utilization of UDP-GlcNAc in *E. coli*.

We are particularly interested in studying the mechanism of glycosyltransferase enzymes that utilize UDP-GlcNAc as a glycosyl donor substrate. These enzymes are important for the assembly of complex carbohydrates and glycoconjugate that govern diverse biological processes ranging from energy storage to cell-cell signaling and host–pathogen interactions.⁹¹ One method that is particularly powerful for the study of enzyme mechanisms is the use of kinetic isotope effect (KIE) measurements. These measurements can provide insight into the microscopic steps of enzymatic reactions and can be used to provide detailed information on the structure of enzymatic transition states. However, KIE methods require access to substrate analogs containing isotope labels.

To synthesize isotopically labeled UDP-GlcNAc substrates, we should consider how UDP-GlcNAc has been previously synthesized. UDP-GlcNAc is one of the main

cytoplasmic precursors of bacterial cell wall of *E. coli* and most related Gram-negative bacteria¹²⁴⁻¹²⁶. UDP-GlcNAc is synthesized from fructose 6-phosphate by four enzyme-catalyzed reactions.¹²⁷⁻¹²⁹ In *E. coli*, the first step involves the synthesis of glucosamine-6-phosphate through the amination of fructose-6-phosphate by the glucosamine-6-phosphate synthase enzyme GlmS.¹³⁰ This is followed by the formation of UDP-GlcNAc from N-acetylglucosamine-1-phosphate (GlcNAc-1-P) and uridine-tri-phosphate (UTP). It is catalyzed by the GlcNAc-1-P uridyltransferase (UDP-GlcNAc pyrophosphorylase).¹³¹

The development of salvage pathway like enzyme cascades including monosaccharide-1 phosphate kinases and UDP-sugar pyrophosphorylases was a breakthrough in the field of enzymatic nucleotide sugar synthesis and analogues thereof.^{114,132-138} The salvage pathway synthesis of UDP-N-acetylglucosamine (UDP-GlcNAc) was enabled by the discovery of an *N*-acetylhexosamine-1-kinase from *Bifidobacterium longum* (NahK).¹³⁹ NahK is the first example of anomeric kinases acting on a carbohydrate substrate.¹⁴⁰ This enzyme catalyzes the phosphorylation of sugars *N*-acetyl-D-glucosamine (GlcNAc) or *N*-acetyl-D-galactosamine (GalNAc) at the anomeric C1 position with ATP.

Different pyrophosphorylases have been used for the addition of second phosphate group to GlcNAc-1-phosphate. UDP-*N*-acetyl-hexosamine pyrophosphorylase (AGX1)^{141,142} and GlcNAc-1-phosphate uridyltransferase GlmU^{124,134,143} have been successfully applied to synthesize multi-milligram quantities of UDP-GlcNAc in relatively high yield. While the Chen lab has done amazing work combining NahK and GlmU for synthesis of UDP-GlcNAc, this method is contingent upon availability of

isotopically labeled starting material, GlcNAc. Some isotopically labeled GlcNAc, for example, [2-²H] and [1-¹⁸O]GlcNAc, are not commercially available requiring an alternative synthesis of their UDP-GlcNAc product targets.

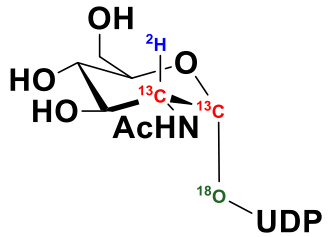
Purely chemical synthesis of [2''-²H]UDP-Glc (80% yield) and [1''-¹⁸O]UDP-Glc (54% yield) was previously achieved from 2,3,4,6-tetra-*O*-acetyl-[2-²H] D-glucopyranose and 2,3,4,6-tetra-*O*-acetyl-D-glucopyranose, respectively.¹⁴⁴ However, enzymatic incorporation [2''-²H] isotope label in UDP-GlcNAc has been reported using UDP-N-acetylglucosamine 2-epimerase (WecB), while chemical enrichment of ¹⁸O at anomeric position was reported in a yield of 82%.^{145,146}

WecB catalyzes the interconversion of UDP-N-acetylglucosamine (UDP-GlcNAc) and UDP-N-acetylmannosamine (UDP-ManNAc) in both Gram-positive and Gram-negative bacteria.^{145,147-149} This enzyme is critical in providing the bacteria with activated ManNAc residues for use in the biosynthesis of cell wall surface polysaccharides.¹⁵⁰⁻¹⁵³ Unlike most known racemases and epimerases, WecB inverts a stereogenic center that is not adjacent to an electron-withdrawing carbonyl or carboxylate group, so it does not go through a simple deprotonation-reprotonation reaction mechanism.¹⁵⁴ Reports suggest that the enzyme oxidizes the C-3 hydroxyl of the GlcNAc residue, forming a ketone intermediate, and acidifying the proton at C-2. Deprotonation at C-2, followed by reprotonation on the opposite face and finally reduction of the ketone, produces the epimeric sugar nucleotide.^{155,156} An alternative mechanism has been proposed in which the epimerization proceeds via cleavage of the anomeric C-O bond, with 2-acetamidoglucal and UDP as enzyme-bound intermediates.^{95,157}

3.2 RESULTS AND DISCUSSION

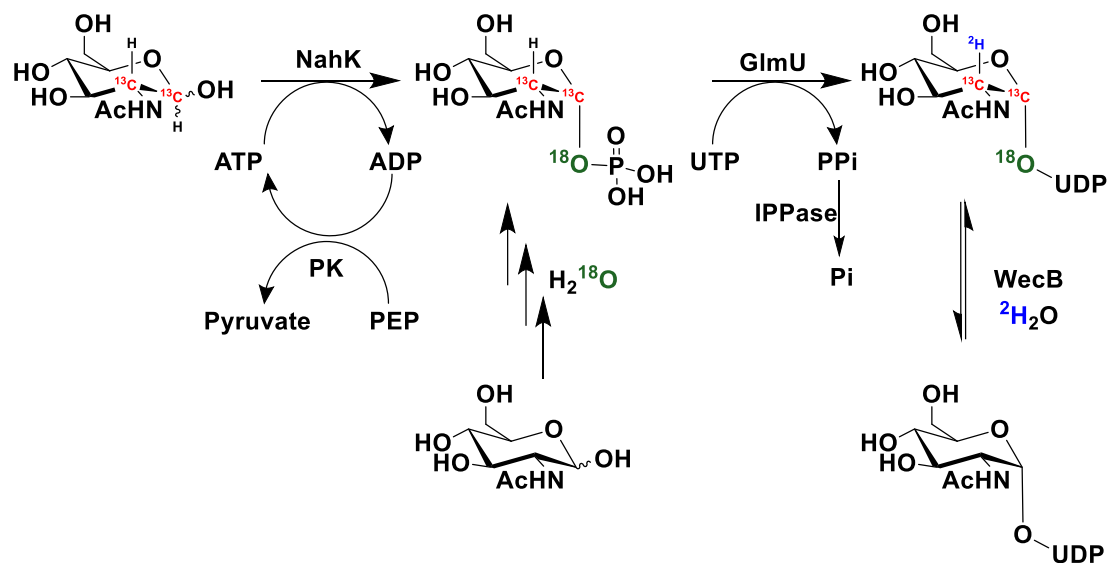
Unlike the substrates used to study β -galactosidase in Chapter 2, isotopically labeled UDP-GlcNAc substrate required to study the mechanism of BshA are not commercially available and must be synthesized from available building blocks. The specific isotopically labeled UDP-GlcNAc substrates that we require to fully characterize the mechanism of GT enzymes like BshA are summarized in Table 3.1.

Table 3.1. Summary of isotopically labeled substrates and their application.

	Isotopically Labeled Atom	Type of KIE	Information obtained
	1''- ^{13}C	Primary KIE	Extent of $\text{S}_{\text{N}}1$ vs $\text{S}_{\text{N}}2$
	2''- ^{13}C	Secondary KIE	Control (isotopically insensitive)
	1''- ^2H	Secondary KIE	Extent of oxocarbenium character
	1''- ^{18}O	Leaving group KIE	Leaving group cleavage
	$^{13}\text{C}_6$	All	Internal standard used for concentration measurements

The magnitude of the KIE resulting from isotopic substitution at 1''-C can be used to distinguish between $\text{S}_{\text{N}}1$ or $\text{S}_{\text{N}}2$ reaction manifolds. Isotopic substitution of the 2''-H position would inform us about the extent of oxocarbenium ion character at the

transition state. Isotopic substitution of the 1''-O reports directly on the extent of leaving group bond cleavage during the transition state of the rate determining step of the reaction. Whereas, isotopic substitution of the 2''-C should be relatively insensitive to the enzyme mechanism and would serve as a control for the KIE measurements.



Scheme 3.1. Overall chemoenzymatic synthesis of the isotopically labeled UDP-GlcNAc substrates.

We envisioned that most of these isotopically labeled UDP-GlcNAc substrates could be prepared using a one pot, four enzyme chemoenzymatic approach (Scheme 3.1) from an appropriately labeled GlcNAc sugar precursor. This approach is largely based on chemoenzymatic syntheses of UDP-GlcNAc first reported by PG Wang,¹⁵⁸ and later improved by the Chen lab¹³⁴ which make use of the enzyme *N*-acetylhexosamine-1-kinase from *Bifidobacterium longum* (NahK).¹³⁹ NahK catalyzes the anomeric phosphorylation of *N*-acetyl-D-glucosamine (GlcNAc) using ATP. The *N*-acetylglucosamine-1-phosphate uridylyltransferase (GlmU) enzyme of *E. coli* is then used to convert GlcNAc-1-phosphate and UTP into UDP-GlcNAc producing inorganic

pyrophosphate (iPP) as a byproduct. Two additional enzymes, pyruvate kinase (PK) and inorganic pyrophosphorylase (IPPase), are also included to regenerate ATP from ADP to prevent product inhibition of NahK, and to hydrolyze iPP to prevent inhibition of the GlmU enzyme, respectively. This approach was used to synthesize unlabeled UDP-GlcNAc, [$1''$ - ^{13}C]UDP-GlcNAc, [$2''$ - ^{13}C]UDP-GlcNAc, and [$^{13}\text{C}_6$]UDP-GlcNAc from commercially available GlcNAc, [1 - ^{13}C]GlcNAc [2 - ^{13}C]GlcNAc, and [$^{13}\text{C}_6$]GlcNAc, respectively. The resulting products were purified by anion exchange chromatography on a q-sepharose column and isolated in 40-83% yield.

Unfortunately the [2 - ^2H]GlcNAc starting material that would be required to prepare [$2''$ - ^2H]UDP-GlcNAc using the one-pot four-enzyme chemoenzymatic approach described above is not commercially available. Instead we sought to prepare [$2''$ - ^2H]UDP-GlcNAc enzymatically from unlabeled UDP-GlcNAc and D_2O taking advantage of the reaction catalyzed by the *E. coli* UDP-*N*-acetylglucosamine 2-epimerase enzyme WecB. WecB catalyzes the interconversion of UDP-GlcNAc and UDP-*N*-acetylmannosamine (UDP-ManNAc) (Figure 3.2A). The reaction of WecB involves deprotonation of the $2''$ -H of UDP-GlcNAc and elimination of UDP to generate a 1,2-glycal intermediate. Protonation of the glycal intermediate from either the top or bottom face results in the formation of UDP-GlcNAc or UDP-ManNAc, respectively, where UDP-GlcNAc is favored by a greater than 9:1 ratio at equilibrium. Carrying out the reaction in D_2O would result in the incorporation of deuterium at the $2''$ position (Figure 3.2B). As seen in Figure 3.2C and 3.2D, carrying out the WecB isomerization in D_2O enabled the synthesis of [$2''$ - ^2H]UDP-GlcNAc with greater than

75% deuterium incorporation based on MALDI-TOF MS and ^1H NMR analysis, respectively.

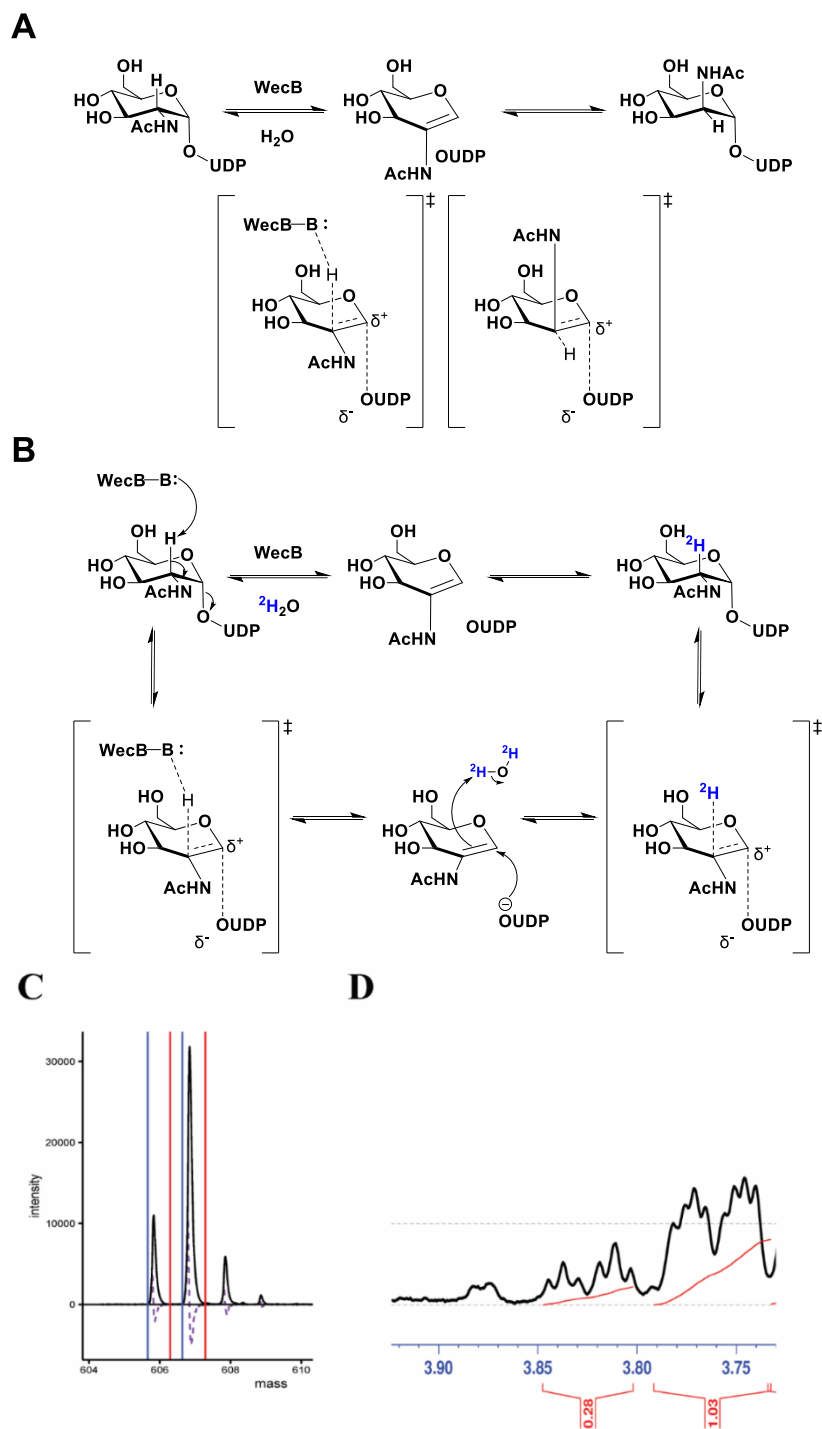
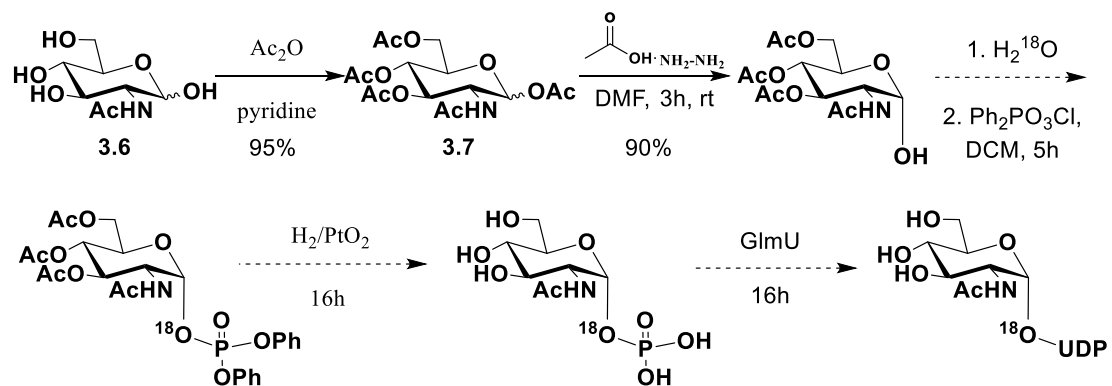


Figure 3.2: A. Proposed WecB mechanism and two potential transition states;⁹⁵ B.

Enzymatic synthesis of 2''-²H UDP-GlcNAc by WecB; **C.** MALDI-TOF MS of ²H incorporation of 75%; **D.** ¹H NMR showing ²H incorporation of 73%.

Proposed Synthesis of Uridine-Di-phosphate [1''-¹⁸O] α-D-N-Glucosamine [3-9]



Scheme 3.2: Synthesis of [1''-¹⁸O] UDP-GlcNAc from GlcNAc

Finally, we sought to synthesize [1''-¹⁸O]UDP-GlcNAc by incubating GlcNAc-2,3,4,6-tetraacetate in H₂¹⁸O followed by trapping the labeled intermediate by reacting with diphenyl-phosphoryl-chloride (Scheme 3.2). This approach has been successfully employed to synthesize [1''-¹⁸O]UDP-Glc.¹⁴⁴ Next, the ¹⁸O labelled GlcN-1-phosphate derivative can be prepared by deprotection and then enzymatically converted into UDP-GlcNAc through the action of GlmU.

We started by per-acetylating GlcNAc using Ac₂O in pyridine. Treating the per-acetate **3.1** with hydrazine acetate resulted in the formation of the tetra-acetate reducing sugar **3.2** in 90% yield. With **3.2** in hand, we explored conditions for the reaction with

diphenylphosphorylchloride. However, attempts to carry out this reaction failed. Further work is underway to complete the synthesis of [1''-¹⁸O]UDP-GlcNAc.

3.3 CONCLUSION

In this chapter, I described the use of two chemoenzymatic approaches that we have successfully employed to prepare isotopically labelled UDP-GlcNAc substrates that can be used to measure KIEs for GT enzymes (as will be described in chapter 4). The first of these methods used a modified one-pot four-enzyme reaction, modified from the Chen lab,¹³⁴ using NahK, GlmU, PK and IPPase to prepare UDP-GlcNAc, [1''-¹³C]UDP-GlcNAc, [2''-¹³C]UDP-GlcNAc, and [¹³C₆]UDP-GlcNAc in 40-83% yields from the appropriately labeled GlcNAc precursors. We then used WecB to enzymatically incorporate [2''-²H] into UDP-GlcNA by carrying out the enzymatic reaction in D₂O. Finally, we have begun to work on the synthesis of [1''-¹⁸O]UDP-GlcNAc and describe an approach to prepare this substrate that is currently underway in the lab.

3.4 EXPERIMENTAL PROCEDURES

3.4.1 General

Unless otherwise noted, all chemicals were purchased as analytical or reagent grade and used without further purification. Isotopically labeled [¹³C₆]-GlcNAc, [1'-¹³C]-GlcNAc, and [6'-¹³C]-GlcNAc were purchased from Omicron Biochemicals, Inc and prepared as described below. Inorganic pyrophosphatase (IP) and pyruvate kinase

(PK) were purchased from Millipore-Sigma as lyophilized powders and resuspended in Millipore water at a final concentration of 0.5 U/ μ l and 1 U/ μ l, respectively. ¹H NMR spectra were recorded at room temperature for solutions in CDCl₃ or D₂O with the Advance III-400 instrument (Bruker) and the chemical shifts were reported relative to residue solvent in parts per million (ppm). The following standard abbreviations are used to indicate multiplicity: s = singlet, d = doublet, t = triplet, m = multiplet, dd = doublet of doublets, dt = doublet of triplets, ddd = doublet of doublets of doublets, dddd = doublet of doublets of doublets of doublets. MALDI-TOF mass spectrometry measurements were recorded on a Bruker Autoflex Speed spectrometer equipped with a 2KHz smartbeam II laser, with a time of flight (TOF)-analyzer capable of both positive and negative ion mode as described in detail below. Matrix solution of 2-hydrazinoquinoline (2-HQ) was prepared in a 95:5 mixture of methanol and acetic acid at a final concentration of 12 mg/mL.¹⁵⁹

3.4.2 Protein preparation

Plasmid vectors for GlnU, NahK and WecB were prepared through restriction digest DNA cloning. A PET28a(+) plasmid was cut with NdeI and HindIII restriction digest enzyme and ligated with inserts containing GlnU, NahK and WecB at 37 °C. Plasmids were checked with agarose gel electrophoresis and then extracted and purified (GeneJET Gel Extraction and DNA Cleanup Micro Kit, Thermofisher Scientific). The sequences were confirmed by single pass Sanger sequencing.

GlmU Preparation

Recombinant GlmU was cloned by Merritt Scott into a pET28a:GlmU vector and expressed in BL21(DE3) *E. coli* cells. The overnight culture was grown in LB with 25 µg/mL kanamycin at 37 °C. 10 mL of the overnight culture was then used to inoculate a fresh 1L culture of LB broth containing 25 µg/mL kanamycin and grown to an OD₆₀₀ of 0.6 before inducing expression through the addition of 0.1 mM isopropyl β- D-1-thiogalactopyranoside (IPTG). The induced cells were grown at 20 °C overnight and then pelleted at 8500 rcf for 20 min, resuspended in a wash buffer of 25 mM phosphate, 300 mM NaCl, 10 mM imidazole, and lysed by sonication. The lysate was then centrifuged at 8500 rcf to remove insoluble cellular debris. Enzyme was purified from the supernatant with a Ni-NTA column through a linear gradient between 10 mM to 300 mM imidazole. Enzyme containing fractions were identified by SDS-PAGE, pooled, and dialyzed into 25 mM Tris-HCl pH 7.0. The resulting protein was concentrated to 83 µM and stored at -80 °C.

NahK Preparation

Codon optimized recombinant NahK was synthesized by Genscript and cloned into a pET28a:NahK vector. Overnight cultures grown in LB with 25 µg/mL kanamycin at 37°C, were used to inoculate fresh 1L LB cultures containin g25 µg/mL kanamycin and grown to an OD₆₀₀ of 0.6-0.8. Cells were induced with 0.1 mM IPTG and grown at 20 °C overnight. The cells were then pelleted at 8500 rcf for 20 minutes, resuspended in a wash buffer of 25 mM phosphate, 300 mM NaCl, 10 mM imidazole, and lysed by sonication. The lysate was then centrifuged at 8500 rcf to remove insoluble cellular

debris. Enzyme was purified from the supernatant with a Ni-NTA column through a linear gradient between 10 mM to 300 mM imidazole. Enzyme containing fractions were identified with SDS-PAGE, pooled, and dialyzed into 150 mM phosphate buffer pH 7.0. The resulting protein was concentrated to 165 μ M and stored at -80 °C.

WecB Preparation

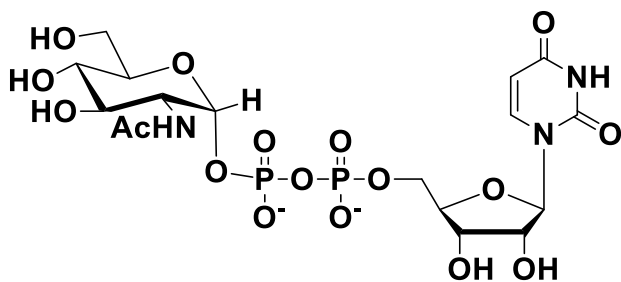
Recombinant WecB was cloned into pET28a:WecB vector and expressed in BL21(DE3) *E. coli* cells. The overnight culture was grown in LB with 25 μ g/mL kanamycin at 37 °C. Protein expression was induced with 1 mM IPTG at 17 °C overnight. The cells were then pelleted at 5500 rcf for 20 minutes, resuspended in a wash buffer of 25 mM Tris-HCl pH 7.4, 300 mM NaCl, 10 mM imidazole, 5% glycerol and lysed by sonication 3 times (30% amplitude, 1 second on, 3 seconds off for a total of 2.30 minutes on). The lysate was then centrifuged at 20000 \times g at 4 °C to remove insoluble cellular debris. Enzyme was purified from the supernatant with a HisTrap column using a linear gradient between 10 mM to 300 mM imidazole. Enzyme containing fractions were identified with SDS-PAGE, pooled, and dialyzed into 25 mM MOPS pH 7.4. The resulting protein was concentrated to 200 μ M and stored at -80 °C.

3.4.3 General procedure for Enzymatic Synthesis of UDP-GlcNAc substrates

Isotopically labeled or unlabeled UDP-GlcNAc was prepared enzymatically via a one-pot, four enzyme reaction consisting of PK, IPPase, GlmU and NahK. The reaction was adapted from a procedure developed by Xi Chen lab.¹⁶⁰ A typical reaction mixture contained 3 mM GlcNAc, 400 μ M ATP, 3.6 mM UTP, 10 mM MgCl₂, 10 mM

KCl, 100 mM TrisHCl pH 7.0, 1 U IP, 4.15 μ M NAHK, 507 nM GlmU, and 1 U PK. The reaction mixtures were incubated at 37 °C for 18 hours until the majority of the GlcNAc was consumed and no further change in reaction products was observed by analytical HPLC using a commercial C18 5 μ m Kinetex column (100 Å, 150 x 4.6 mm). The UDP-GlcNAc was then purified by strong anion exchange chromatography using three connected commercial 1ml HiTrap Q FF columns (7 x 25 mm, GE Healthcare) packed with Q Sepharose with 5 mM ammonium acetate (Buffer A) and 500 mM ammonium bicarbonate (Buffer B). Samples were eluted at 1 mL/min using a two-step gradient elution of 0% to 20% buffer B over 10 column volumes, followed by a gradient of 20% to 100% buffer B over 15 column volumes. Fractions containing UDP-GlcNAc were dried through vacuum centrifugation and re-dissolved in water. The product purity was analyzed through HPLC and MALDI-TOF MS analysis. Reaction yields were estimated based on absorbance at 262 nm of the final UDP-GlcNAc solutions ($\epsilon_{260} = 10,000 \text{ M}^{-1} \text{ cm}^{-1}$).

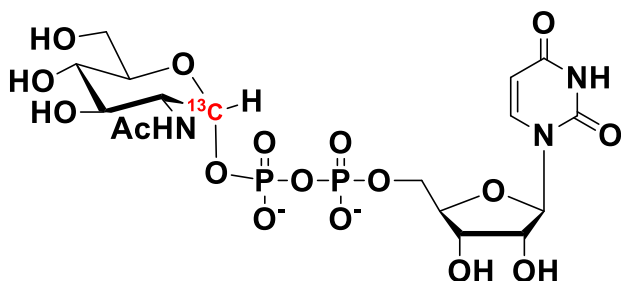
Uridine-Di-phosphate α -D-N-Glucosamine (3.1)



Instead of the commercially available UDP-GlcNAc, we decided to chemoenzymatically synthesize UDP-GlcNAc from GlcNAc because the purity of the material was crucial for the subsequent KIE measurements described in Chapter 4.

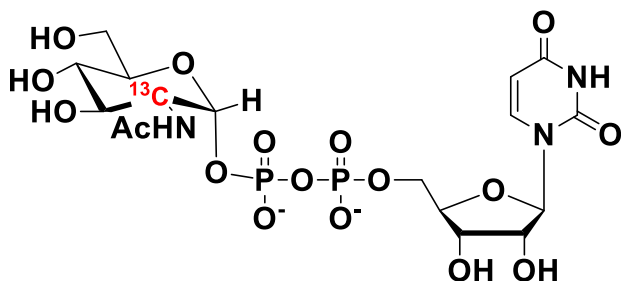
UDP-GlcNAc **3.1** was synthesized from commercially available GlcNAc and purified by ion exchange chromatography as described in General procedures (**3.4.3**) in a yield of 83%. ^1H NMR (400 MHz, D_2O) δ 7.82 (d, $J = 11.7$, 1H, H6), 5.83 – 5.8035 (m, 2H, H5/H1'), 5.37 (dd, $J = 7.4$, 3.4, 1H, H1''), 4.24 – 4.2 (m, 2H, H2'/H3'), 4.15 – 4.10 (m, 1H, H4'), 4.09 (dd, $J = 4.3$, 2.3, 1H, H5'), 4.06 – 4.00 (m, 1H, H5'), 3.85 (dt, 1H, H2''), 3.79 – 3.75 (m, 1H, H5''), 3.71 (dd, $J = 12.5$, 2.2, 1H, H6''), 3.68 – 3.63 (m, 2H, H6''), H3''), 3.39 (t, $J = 9.6$, 1H, H4'').

Uridine-Di-phosphate [$1''$ - ^{13}C] α -D-N-Glucosamine (3.2)



[$1''$ - ^{13}C]UDP-GlcNAc **3.3** was enzymatically synthesized from commercially available [1 - ^{13}C]GlcNAc. The same procedure described for UDP-GlcNAc was followed involving 4 enzymes NAHK, GlmU, PK and inorganic phosphatase, followed by ion-exchange chromatography as described in General procedures (**3.4.3**) to obtain the pure UDP-GlcNAc showing in Scheme 3.1 in 76% yield employing previously published procedures and a reference. MALDI-TOF MS calculated 606.07, found 606.5.

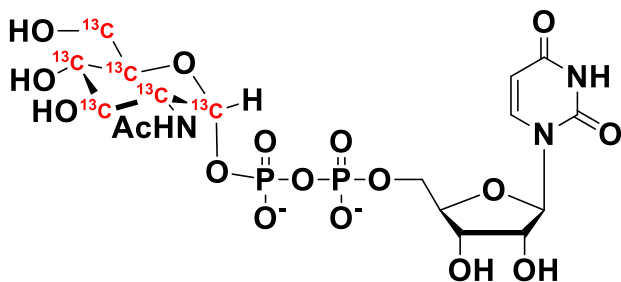
Uridine-Di-phosphate [$2''$ - ^{13}C] α -D-N-Glucosamine (3.3)



$2''$ - ^{13}C UDP-GlcNAc were enzymatically synthesized from commercially available $2''$ - ^{13}C GlcNAc. The same procedure described for UDP-GlcNAc was followed involving 4 enzymes NahK, GlmU, PK and inorganic phosphatase, followed by ion-exchange chromatography as described in General procedures (3.4.3) to obtain the pure UDP-GlcNAc showing in Scheme 3.1 in 40% yield.

^1H NMR (400 MHz, D_2O) δ 8.5 (s, 1H, HNAc), 7.8 (d, $J = 8.1$, 1H, H4), 5.82 – 5.79 (m, 2H, H5, H1'), 5.36 (d, $J_{1,2} = 7.3$ Hz, 1 H, H1), 4.22 – 4.18 (p, 2H, H2', H3'), 4.13 – 4.09 (m, 1H, H4'), 4.07 (dd, $J = 4.4, 2.4$, 1H, H5'), 4.04 – 3.97 (m, 1H, H5'), 3.78 – 3.74 (m, 1H, H5''), 3.72 (dd, $J = 12.5, 2.4$, 1H, H''), 3.66 – 3.63 (m, 2H, H6'', H3''), 3.41 – 3.36 (t, 1H, H4''). MALDI-TOF MS calculated 606.07, found 606.5.

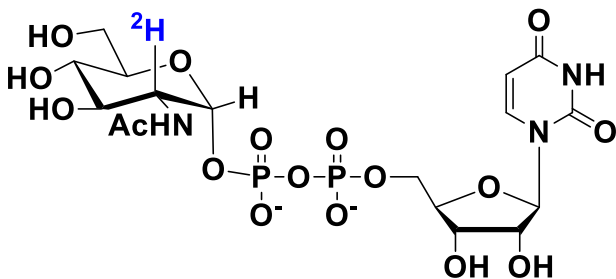
Uridine-Di-phosphate [$^{13}\text{C}_6$] α -D-N-Glucosamine (3.4)



$^{13}\text{C}_6$ UDP-GlcNAc was enzymatically synthesized from commercially available $^{13}\text{C}_6$ GlcNAc. The same procedure described for UDP-GlcNAc was followed involving 4

enzymes NAHK, GlmU, PK and inorganic phosphatase, followed by ion-exchange chromatography as described in General procedures (3.4.3) to obtain the pure UDP-GlcNAc showing in Scheme 3.1 in 77% yield. MALDI-TOF MS calculated 611.07, found 611.5.

Uridine-Di-phosphate [$2\text{-}^2\text{H}$] $\alpha\text{-D-N-Glucosamine}$ (3.5)



[$2\text{-}^2\text{H}$]UDP-GlcNAc **3.2** was obtained through enzymatic isomerization at the $2\text{-}^2\text{C}$ position using WecB in D_2O to afford incorporation of ^2H at that position. The reaction mixture contained 5 mM GlcNAc, 5 mM MgCl_2 and 25 mM MOPS pH 7.0 prepared with D_2O . The reaction mixture was incubated at room temperature for 6h with 20 μM WecB. Final product $2\text{-}^2\text{H}$ UDP-GlcNAc was purified with ion-exchange chromatography as described in General procedures (3.4.3) and confirmed with NMR. $2\text{-}^2\text{H}$ incorporation was estimated to be 90% by MALDI-TOF mass spectrometry. ^1H NMR (400 MHz, D_2O) δ 8.5 (s, 1H, HNAc), 7.8 (d, $J = 8.4$, 1H, H4), 5.82 – 5.79 (m, 2H, H5, H1'), 5.36 (d, $J = 8.0$, 1 H, H1), 4.2 (p, 2H, H2', H3'), 4.13 – 4.09 (m, 1H, H4'),

4.07 (dd, $J = 4.4, 2.4$ 1H, H5'), 4.05 – 3.99 (m, 1H, H5'), 3.78 – 3.74 (m, 1H, H5''), 3.72 (dd, $J = 12.4, 2.0$, 1H, H6''), 3.66 – 3.62 (m, 2H, H6'', H3''), 3.39 (t, $J = 9.6$, 1H, H4''). MALDI-TOF MS calculated 606.07, found 606.5.

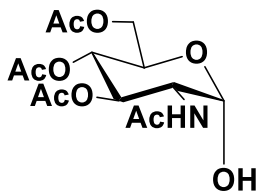
1,2,3,4,6-penta-O-acetyl D-glucosamine (3.6)



Acetic anhydride (3 ml, 29 mmol) was added to a stirring solution of glucosamine (1 g, 5.55 mmol) and pyridine (10ml). The reaction was capped and left overnight at room temperature. TLC conditions: EtOH 100%. Reaction mixture was diluted with CH_2Cl_2 and washed with 1M HCl (5x), NaHCO_3 (3x), and brine (3X). Product was dried with NaSO_4 , filtered and without further purification concentrated in vacuo in a yield of 95%. (2/1 ethyl acetate/hexane, $R_f = 0.43$)

^1H NMR (400 MHz, CDCl_3) δ 6.18 (d, $J = 3.6$, 1H, H1- α), 5.6 (d, $J = 9.0$, 1H, H1- β), 5.28 – 5.20 (m, 2H, H3, H4), 4.53 – 4.47 (m, 1H, H2), 4.28 (dd, $J = 12.5, 4.0$, 1H, H5), 4.09 (dd, $J = 12.3, 2.2$, 1H, H6), 4.02 – 3.98 (m, 1H, H7), 2.2 (s, 3H, OAc), 2.1 (s, 3H, OAc), 2.07 (s, 3H, OAc), 2.06 (s, 3H, OAc), 1.95 (s, 3H, OAc).

2,3,4,6-tetra-O-acetyl- N-acetyl- D-glucosamine (3.7)



Following a previously published procedure for partial deprotection, we obtained 2,3,4,6-Tetra-*O*-acetyl-D-glucosamine.⁵⁵ D-glucosamine pentaacetate (500 mg, 1.28 mmol, 1 equiv.) was dissolved in DMF (10 mL). Hydrazine acetate (143 mg, 1.54 mmol, 1.2 equiv.) was added, and was stirred at 50°C for 1 h. The reaction was monitored by TLC (hexane:EtOAc, 1:1). The mixture was diluted with ethyl acetate (10 mL) and washed with brine. The organic layer was dried over anhydride sodium sulfate, filtered and concentrated. Reaction mixture was purified manually on silica gel in a 1 in diameter column with a gradient solvent system starting with 1/2 ethyl acetate/hexane and ending in 2/1 ethyl acetate/hexane to give **3.7** as a white solid in a 90% yield. (2/1 ethyl acetate/hexane, R_f = 0.29)

¹H NMR (400 MHz, CDCl₃) δ 6.21 (d, *J* = 9.4, 1H, NH), 5.29 – 5.24 (m, 1H, H3), 5.19 (d, *J* = 3.5, 1H, H1- α), 5.11 (t, *J* = 9.6, 1H, H4), 4.27 – 4.21 (m, 1H, H5), 4.21 (d, *J* = 4.4, 1H, H6), 4.18 (d, *J* = 3.2, 1H, H7), 4.09 (dd, *J* = 13.6, 3.8, 1H, H2), 2.06 (s, 3H, OAc), 2.00 (s, 3H, OAc), 1.99 (s, 3H, OAc), 1.94 (s, 3H, OAc).

3.5 BIBLIOGRAPHY

- (1) Na, L.; Li, R.; Chen, X. Recent Progress in Synthesis of Carbohydrates with Sugar Nucleotide-Dependent Glycosyltransferases. *Curr. Opin. Chem. Biol.* **2021**, 61, 81–95. <https://doi.org/10.1016/j.cbpa.2020.10.007>.
- (2) Lairson, L. L.; Henrissat, B.; Davies, G. J.; Withers, S. G. Glycosyl Transferases: Structures, Functions, and Mechanisms. *Annu. Rev. Biochem.* 2008, pp 521–555. <https://doi.org/10.1146/annurev.biochem.76.061005.092322>.
- (3) Mikkola, S. Nucleotide Sugars in Chemistry and Biology. *Molecules*. MDPI AG December 1, 2020. <https://doi.org/10.3390/molecules25235755>.
- (4) Ahmadipour, S.; Miller, G. J. Recent Advances in the Chemical Synthesis of Sugar-Nucleotides. *Carbohydr. Res.* **2017**, pp 95–109. <https://doi.org/10.1016/j.carres.2017.08.014>.

- (5) Miyagawa, A.; Toyama, S.; Ohmura, I.; Miyazaki, S.; Kamiya, T.; Yamamura, H. One-Step Synthesis of Sugar Nucleotides. *J. Org. Chem.* American Chemical Society December 4, 2020, pp 15645–15651. <https://doi.org/10.1021/acs.joc.0c01943>.
- (6) Wagner, G. K.; Pesnot, T.; Field, R. A. A Survey of Chemical Methods for Sugar-Nucleotide Synthesis. *Nat. Prod. Rep.* Royal Society of Chemistry 2009, pp 1172–1194. <https://doi.org/10.1039/b909621n>.
- (7) Cai, L. Recent Progress in Enzymatic Synthesis of Sugar Nucleotides. *J Carbohydr. Chem.* **2012**, *31* (7), 535–552. <https://doi.org/10.1080/07328303.2012.687059>.
- (8) Wen, L.; Gadi, M. R.; Zheng, Y.; Gibbons, C.; Kondengaden, S. M.; Zhang, J.; Wang, P. G. Chemoenzymatic Synthesis of Unnatural Nucleotide Sugars for Enzymatic Bioorthogonal Labeling. *ACS Catal.* **2018**, *8* (8), 7659–7666. <https://doi.org/10.1021/acscatal.8b02081>.
- (9) Matthies, S.; Stallforth, P.; Seeberger, P. H. Total Synthesis of Legionaminic Acid as Basis for Serological Studies. *J. Am. Chem. Soc.* **2015**, *137* (8), 2848–2851. <https://doi.org/10.1021/jacs.5b00455>.
- (10) Wang, Y.; Carder, H. M.; Wendlandt, A. E. Synthesis of Rare Sugar Isomers through Site-Selective Epimerization. *Nature* **2020**, *578* (7795), 403–408. <https://doi.org/10.1038/s41586-020-1937-1>.
- (11) Li, X.; Wu, J.; Tang, W. General Strategy for the Synthesis of Rare Sugars via Ru(II)-Catalyzed and Boron-Mediated Selective Epimerization of 1,2- Trans-Diols to 1,2-

Cis-Diols. *J. Am. Chem. Soc.* **2022**, *144* (8), 3727–3736.

<https://doi.org/10.1021/jacs.1c13399>.

- (12) Samuel, G.; Reeves, P. Biosynthesis of O-Antigens: Genes and Pathways Involved in Nucleotide Sugar Precursor Synthesis and O-Antigen Assembly. *Carbohydr. Res.* **2003**, pp 2503–2519. <https://doi.org/10.1016/j.carres.2003.07.009>.
- (13) Singh, S.; Phillips, G. N.; Thorson, J. S. The Structural Biology of Enzymes Involved in Natural Product Glycosylation. *Nat. Prod. Rep.*. Royal Society of Chemistry 2012, pp 1201–1237. <https://doi.org/10.1039/c2np20039b>.
- (14) Liu, B.; Furevi, A.; Perepelov, A. V.; Guo, X.; Cao, H.; Wang, Q.; Reeves, P. R.; Knirel, Y. A.; Wang, L.; Widmalm, G. Structure and Genetics of Escherichia Coli O Antigens. *FEMS Microbiol. Rev.* Oxford University Press November 1, 2020, pp 655–683. <https://doi.org/10.1093/femsre/fuz028>.
- (15) Liu, B.; Knirel, Y. A.; Feng, L.; Perepelov, A. V.; Senchenkova, S. N.; Reeves, P. R.; Wang, L. Structural Diversity in Salmonella O Antigens and Its Genetic Basis. *FEMS Microbiol. Rev.*. January 2014, pp 56–89. <https://doi.org/10.1111/1574-6976.12034>.
- (16) Wang, S.; Zhang, J.; Wei, F.; Li, W.; Wen, L. Facile Synthesis of Sugar Nucleotides from Common Sugars by the Cascade Conversion Strategy. *J. Am. Chem. Soc.* **2022**, *144* (22), 9980–9989. <https://doi.org/10.1021/jacs.2c03138>.
- (17) Mengin-Lecreulx, D. and Van Heijenoort, J., Copurification of glucosamine-1-phosphate acetyltransferase and N-acetylglucosamine-1-phosphate uridyltransferase activities of Escherichia coli: characterization of the glmU gene product as a

- bifunctional enzyme catalyzing two subsequent steps in the pathway for UDP-N-acetylglucosamine synthesis. *J. Bacteriol.*, **1994**, 176(18), pp.5788-5795.
- (18) Höltje, J.-V.; Schwarz, U. Biosynthesis and Growth of the Murein Sacculus. 1985.
- (19) Neidhardt, F. C.; Ingraham, J. L. Escherichia Coli and Salmonella Typhimurium: Cellular and Molecular Biology. 1987.
- (20) Dobrogosz, W.J., 1968. Effect of amino sugars on catabolite repression in Escherichia coli. *Am. Soc. Microbiol.*, **1968**, 95(2), pp.578-584.
- (21) Freese, E. B.; Cole, R. M.; Klofat, W.; Freese, E. Growth, Sporulation, and Enzyme Defects of Glucosamine Mutants of Bacillus Subtilis; *Am. Soc. Microbiol.* **1970**, 101(3), 1046-1062.
- (22) White, R., 1968. Control of amino sugar metabolism in Escherichia coli and isolation of mutants unable to degrade amino sugars. *Biochem. J.*, **1968**, 106(4), pp.847-858.
- (23) Dutka-Malen, S.; Mazodier, P.; Badet, B. Molecular Cloning and Overexpression of the Glucosamine Synthetase Gene from Escherichia Coli. *Biochim.* **1988**, 70 (2), 287–290.
- (24) Strominger, J.L. and Smith, M.S., Uridine diphosphoacetylglucosamine pyrophosphorylase. *J. Biol. Chem.*, **1959**, 234(7), pp.1822-1827.
- (25) Fischöder, T.; Wahl, C.; Zerhusen, C.; Elling, L. Repetitive Batch Mode Facilitates Enzymatic Synthesis of the Nucleotide Sugars UDP-Gal, UDP-GlcNAc, and UDP-GalNAc on a Multi-Gram Scale. *Biotechnol. J.* **2019**, 14 (4).
<https://doi.org/10.1002/biot.201800386>.

- (26) Zhao, G.; Guan, W.; Cai, L.; Wang, P. G. Enzymatic Route to Preparative-Scale Synthesis of UDP-GlcNAc/GalNAc, Their Analogues and GDP-Fucose. *Nat. Protoc.* **2010**, *5* (4), 636–646. <https://doi.org/10.1038/nprot.2010.3>.
- (27) Chen, Y.; Thon, V.; Li, Y.; Yu, H.; Ding, L.; Lau, K.; Qu, J.; Hie, L.; Chen, X. One-Pot Three-Enzyme Synthesis of UDP-GlcNAc Derivatives. *Chem. Comm.* **2011**, *47* (38), 10815–10817. <https://doi.org/10.1039/c1cc14034e>.
- (28) Guan, W.; Cai, L.; Wang, P. G. Highly Efficient Synthesis of UDP-GalNAc/GlcNAc Analogues with Promiscuous Recombinant Human UDP-GalNAc Pyrophosphorylase AGX1. *Chem. Eur. J.* **2010**, *16* (45), 13343–13345. <https://doi.org/10.1002/chem.201002315>.
- (29) Wahl, C.; Hirtz, D.; Elling, L. Multiplexed Capillary Electrophoresis as Analytical Tool for Fast Optimization of Multi-Enzyme Cascade Reactions – Synthesis of Nucleotide Sugars: Dedicated to Prof. Dr. Vladimír Křen on the Occasion of His 60th Birthday. *J. Biotechnol.* **2016**, *11* (10), 1298–1308. <https://doi.org/10.1002/biot.201600265>.
- (30) Wahl, C.; Spiertz, M.; Elling, L. Characterization of a New UDP-Sugar Pyrophosphorylase from *Hordeum Vulgare* (Barley). *J. Biotechnol.* **2017**, *258*, 51–55. <https://doi.org/10.1016/j.jbiotec.2017.03.025>.
- (31) Zou, Y.; Xue, M.; Wang, W.; Cai, L.; Chen, L.; Liu, J.; Wang, P. G.; Shen, J.; Chen, M. One-Pot Three-Enzyme Synthesis of UDP-Glc, UDP-Gal, and Their Derivatives. *Carbohydr. Res.* **2013**, *373*, 76–81. <https://doi.org/10.1016/j.carres.2013.03.005>.

- (32) Zhao, Y.; She, N.; Ma, Y.; Wang, C.; Cao, Z. A Description of Enzymatic Catalysis in N-Acetylhexosamine 1-Kinase: Concerted Mechanism of Two-Magnesium-Ion-Assisted GlcNAc Phosphorylation, Flexibility Behavior of Lid Motif upon Substrate Recognition, and Water-Assisted GlcNAc-1-P Release. *ACS Catal.* **2018**, *8* (5), 4143–4159. <https://doi.org/10.1021/acscatal.8b00006>.
- (33) Nishimoto, M.; Kitaoka, M. The Complete Lacto-N-Biose I/Galacto-N-Biose Metabolic Pathway in *Bifidobacterium Longum*: Identification of N-Acetylhexosamine 1-Kinase. *Appl. Environ. Microbiol.* **2007**, *73*, 6444–6449.
- (34) Bourgeaux, V.; Piller, F.; Piller, V. Two-Step Enzymatic Synthesis of UDP-N-Acetylgalactosamine. *Bioorg. Med. Chem. Lett.* **2005**, *15* (24), 5459–5462. <https://doi.org/10.1016/j.bmcl.2005.08.088>.
- (35) Peneff, C.; Ferrari, P.; Charrier, V.; Taburet, Y.; Monnier, C.; Zamboni, V.; Winter, J.; Harnois, M.; Fassy, F.; Bourne, Y. Crystal Structures of Two Human Pyrophosphorylase Isoforms in Complexes with UDPGlc(Gal)NAc: Role of the Alternatively Spliced Insert in the Enzyme Oligomeric Assembly and Active Site Architecture. *EMBO J.* **2001**, *20* (22), 6191–6202. <https://doi.org/10.1093/emboj/20.22.6191>.
- (36) Guan, W.; Cai, L.; Fang, J.; Wu, B.; George Wang, P. Enzymatic Synthesis of UDP-GlcNAc/UDP-GalNAc Analogs Using N-Acetylglucosamine 1-Phosphate Uridyltransferase (GlmU). *Chem. Comm*, **2009**, No. 45, 6976–6978. <https://doi.org/10.1039/b917573c>.

- (37) Lee, S. S.; Hong, S. Y.; Errey, J. C.; Izumi, A.; Davies, G. J.; Davis, B. G. Mechanistic Evidence for a Front-Side, S_{Ni} -Type Reaction in a Retaining Glycosyltransferase. *Nat. Chem. Biol.* **2011**, 7 (9), 631–638.
<https://doi.org/10.1038/nchembio.628>.
- (38) Sala, R. F.; Morgan, P. M.; Tanner, M. E. *Enzymatic Formation and Release of a Stable Glycal Intermediate: The Mechanism of the Reaction Catalyzed by UDP-N-Acetylglucosamine 2-Epimerase*; 1996.
- (39) Morgan, P. M.; Sala, R. F.; Tanner, M. E. *Eliminations in the Reactions Catalyzed by UDP-N-Acetylglucosamine 2-Epimerase*; 1997.
- (40) Kawamura, T.; Ishimoto, N.; Ito, E. Enzymatic Synthesis of Uridine Diphosphate N-Acetyl-D-Mannosaminuronic Acid. *J Biol Chem* **1979**, 254 (17), 8457–8465.
- (41) Kawamura, T.; Ishimoto, N.; Ito, E. [42] UDP-N-Acetyl-d-Glucosamine 2'-Epimerase from Escherichia Coli. In *Meth. Enzym.* **1982**; Vol. 83, pp 515–519.
- (42) Kawamura, T.; Kimura, M.; Yamamori, S.; Ito, E. Enzymatic Formation of Uridine Diphosphate N-Acetyl-D-Mannosamine. *J. Biol. Chem.* **1978**, 253 (10), 3595–3601.
[https://doi.org/10.1016/s0021-9258\(17\)34843-3](https://doi.org/10.1016/s0021-9258(17)34843-3).
- (43) Yoneyama, T.; Koike, Y.; Arakawa, H.; Yokoyama, K.; Sasaki, Y.; Kawamura, T.; Araki, Y.; Ito, E.; Takao, S. *Distribution of Mannosamine and Mannosaminuronic Acid Among Cell Walls of Bacillus Species*; **1982**, 149 (1), 15-21.
- (44) HARRINGTON, C. R.; BADDILEY, J. Biosynthesis of Wall Tiechoic Acids in Staphylococcus Aureus H, Micrococcus Varians and Bacillus Subtilis W23:

- Involvement of Lipid Intermediates Containing the Disaccharide N-acetylmannosaminyl N-acetylglucosamine. *Eur. J. Biochem.* **1985**, *153* (3), 639–645.
<https://doi.org/10.1111/j.1432-1033.1985.tb09348.x>.
- (45) Kuhn, H.-M.; Meier-Dieter, U.; Mayer, H. ECA, the Enterobacterial Common Antigen. *FEMS Microbiol. Lett.* **1988**, *54* (3), 195–222.
<https://doi.org/10.1111/j.1574-6968.1988.tb02743.x>.
- (46) Meier-Dieter, U.; Starman, R.; Barr, K.; Mayer, H.; Rick, P. D. Biosynthesis of Enterobacterial Common Antigen in Escherichia Coli. Biochemical Characterization of Tn10 Insertion Mutants Defective in Enterobacterial Common Antigen Synthesis. *J. Biol. Chem.* **1990**, *265* (23), 13490–13497. [https://doi.org/10.1016/s0021-9258\(18\)77373-0](https://doi.org/10.1016/s0021-9258(18)77373-0).
- (47) Adams, E. Catalytic Aspects of Enzymatic Racemization. *Adv. Enzymol. Relat. Areas Mol. Biol.* **1976**, *44*, 69–138.
- (48) Salo, W.L., The incorporation of tritium from tritium-enriched water into UDP-N-Acetylglucosamine and UDP-N-Acetyl Mannosamine catalyzed by UDP-N-Acetylglucosamine 2-Epimerase from Escherichia coli. *Biochim. Biophys. Acta Enzymol.* **1976**, *452*(2), pp.625-628.
- (49) Palmer, J.L. and Abeles, R.H., The mechanism of action of S-adenosylhomocysteinase. *J. Biol. Chem.*, **1979**, *254*(4), pp.1217-1226.

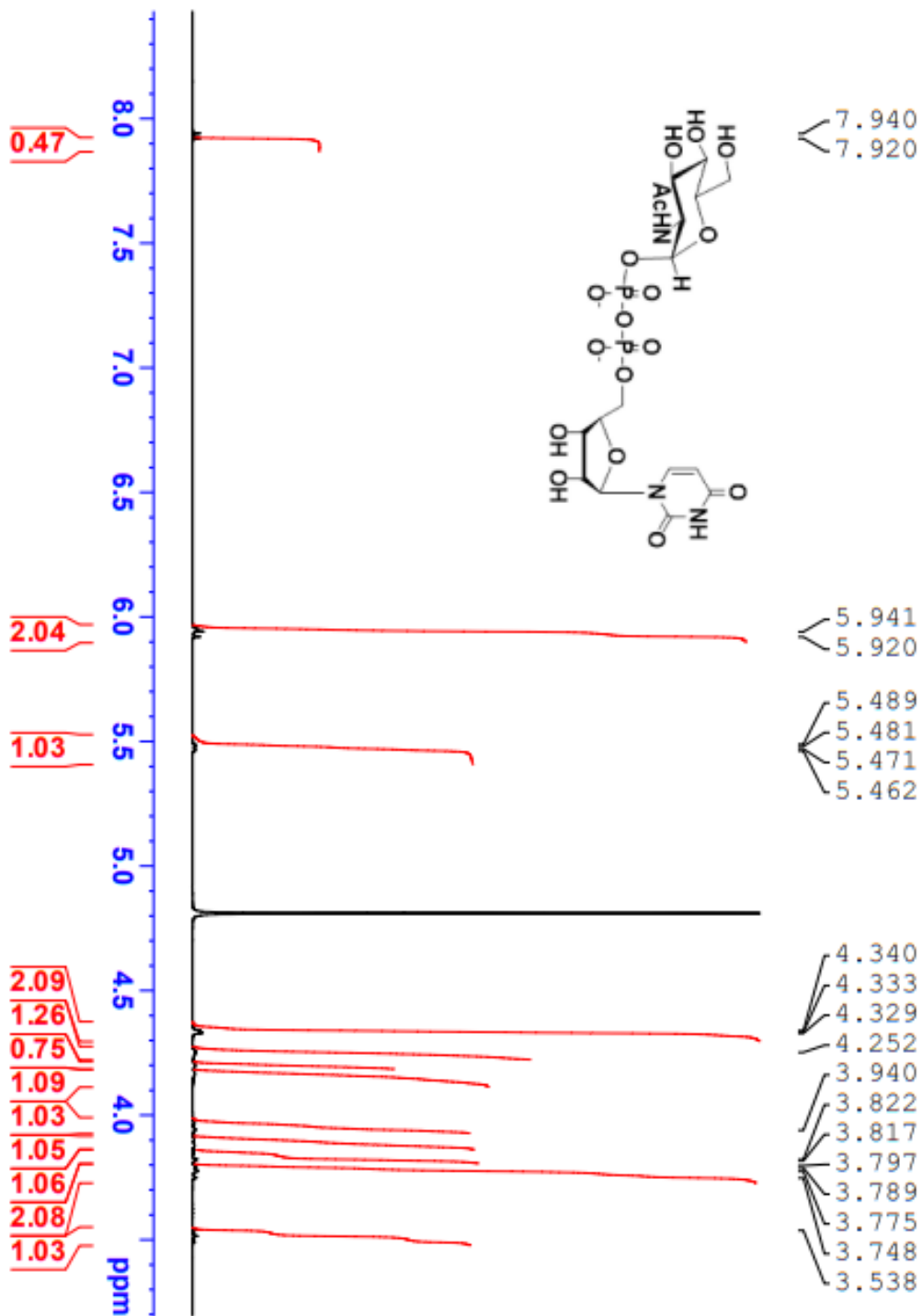
- (50) Sommar, K.M. and Ellis, D.B., Uridine diphosphate N-acetyl-d-glucosamine 2-epimerase from rat liver: I. Catalytic and regulatory properties. *Biochim. Biophys. Acta Enzymol.* **1972**, 268(2), pp.581-589.
- (51) Campbell, R. E.; Mosimann, S. C.; Tanner, M. E.; Strynadka, N. C. J. The Structure of UDP-N-Acetylglucosamine 2-Epimerase Reveals Homology to Phosphoglycosyl Transferases. *J. Biochem.* **2000**, 39 (49), 14993–15001.
<https://doi.org/10.1021/bi001627x>.
- (52) Cai, L.; Guan, W.; Wang, W.; Zhao, W.; Kitaoka, M.; Shen, J.; O’Neil, C.; Wang, P. G. Substrate Specificity of N-Acetylhexosamine Kinase towards N-Acetylgalactosamine Derivatives. *Bioorg. Med. Chem. Lett.* **2009**, 19 (18), 5433–5435. <https://doi.org/10.1016/j.bmcl.2009.07.104>.
- (53) Lin, X.; Xiao, C.; Ling, L.; Guo, L.; Guo, X. A Dual-Mode Reactive Matrix for Sensitive and Quantitative Analysis of Carbohydrates by MALDI-TOF MS. *Talanta* **2021**, 235. <https://doi.org/10.1016/j.talanta.2021.122792>.
- (54) Li, Y.; Xue, M.; Sheng, X.; Yu, H.; Zeng, J.; Thon, V.; Chen, Y.; Muthana, M. M.; Wang, P. G.; Chen, X. Donor Substrate Promiscuity of Bacterial B1-3-N-Acetylglucosaminyltransferases and Acceptor Substrate Flexibility of B1-4-Galactosyltransferases. *Bioorg. Med. Chem.* **2016**, 24 (8), 1696–1705.
<https://doi.org/10.1016/j.bmc.2016.02.043>.
- (55) Lee, S. S.; Hong, S. Y.; Errey, J. C.; Izumi, A.; Davies, G. J.; Davis, B. G. Mechanistic Evidence for a Front-Side, S_Ni-Type Reaction in a Retaining

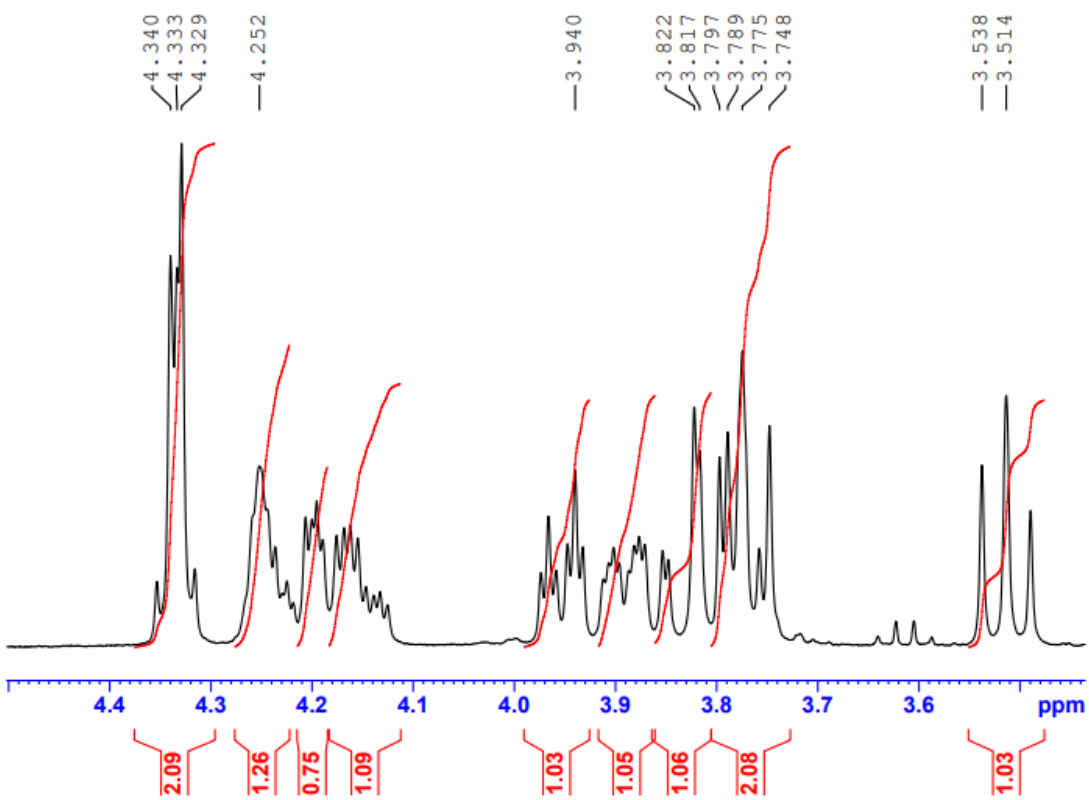
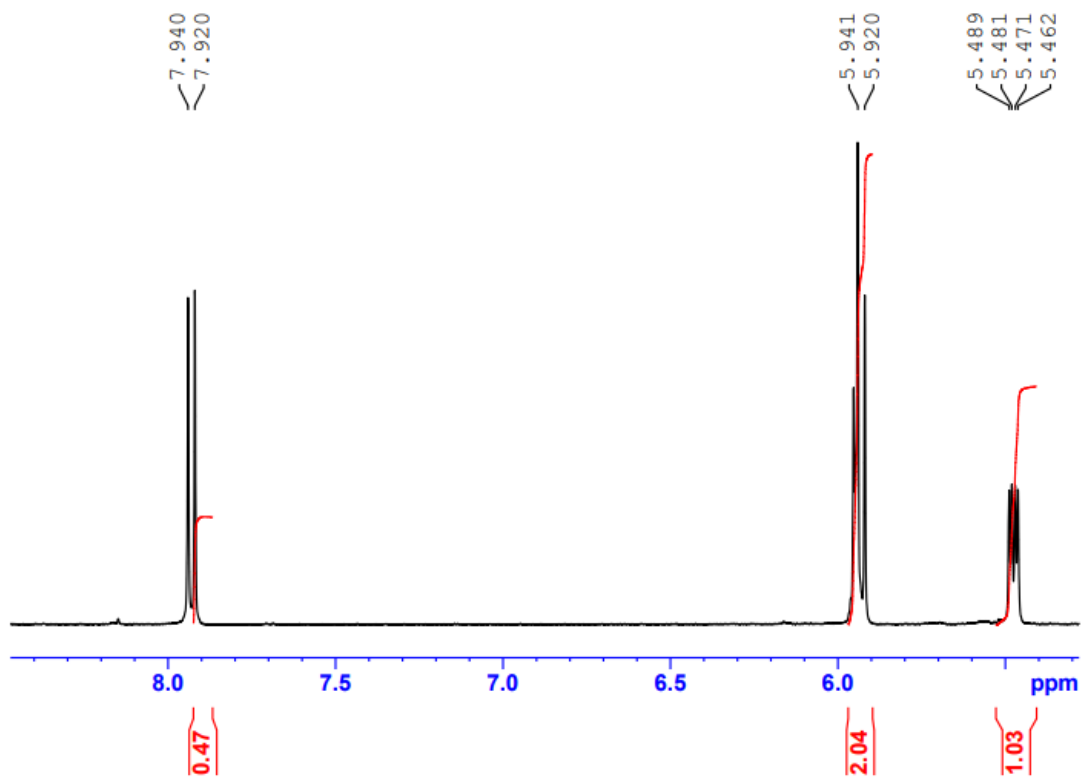
Glycosyltransferase. *Nat Chem Biol* **2011**, 7 (9), 631–638.

<https://doi.org/10.1038/nchembio.628>.

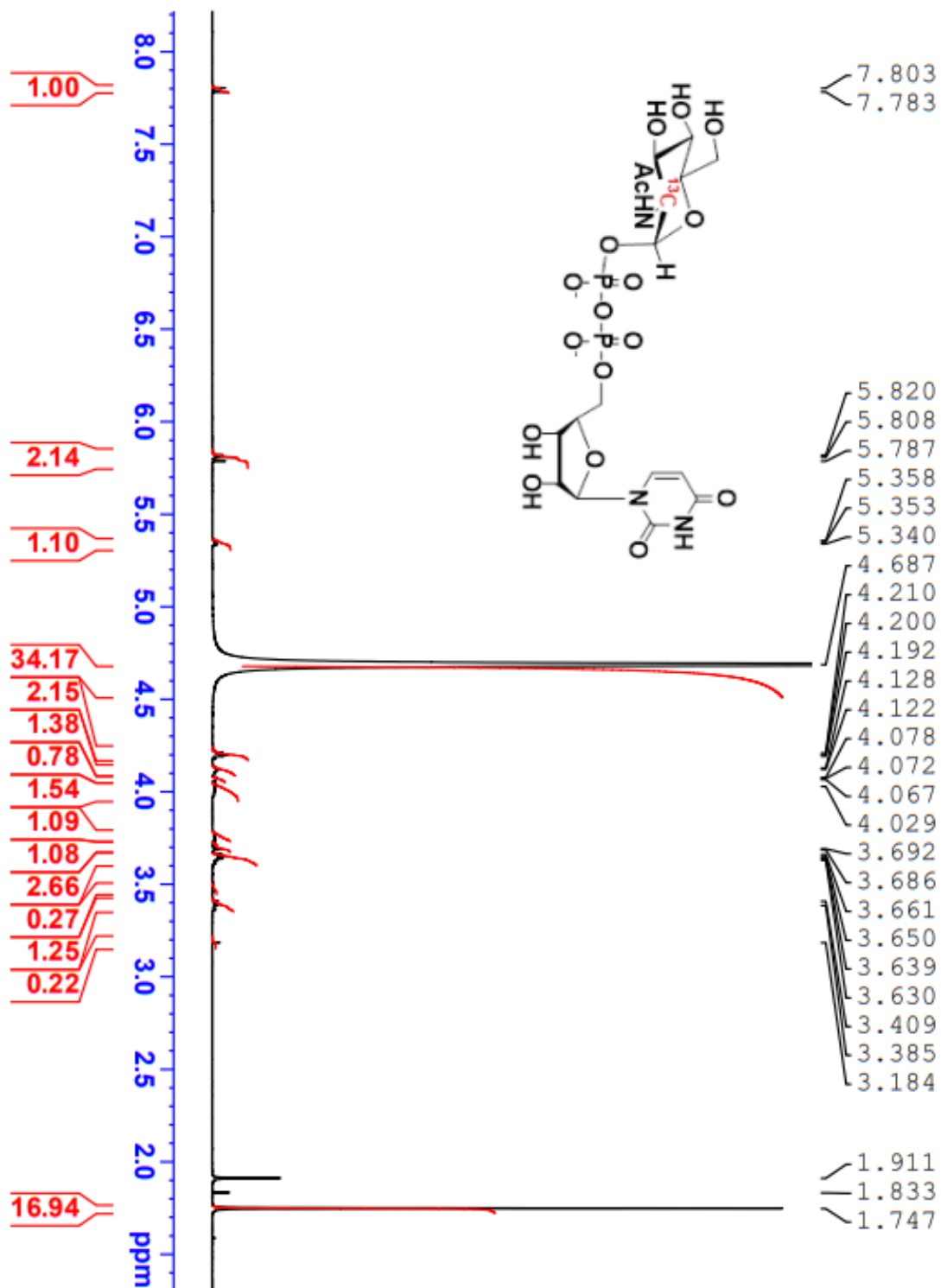
3.6 APPENDIX

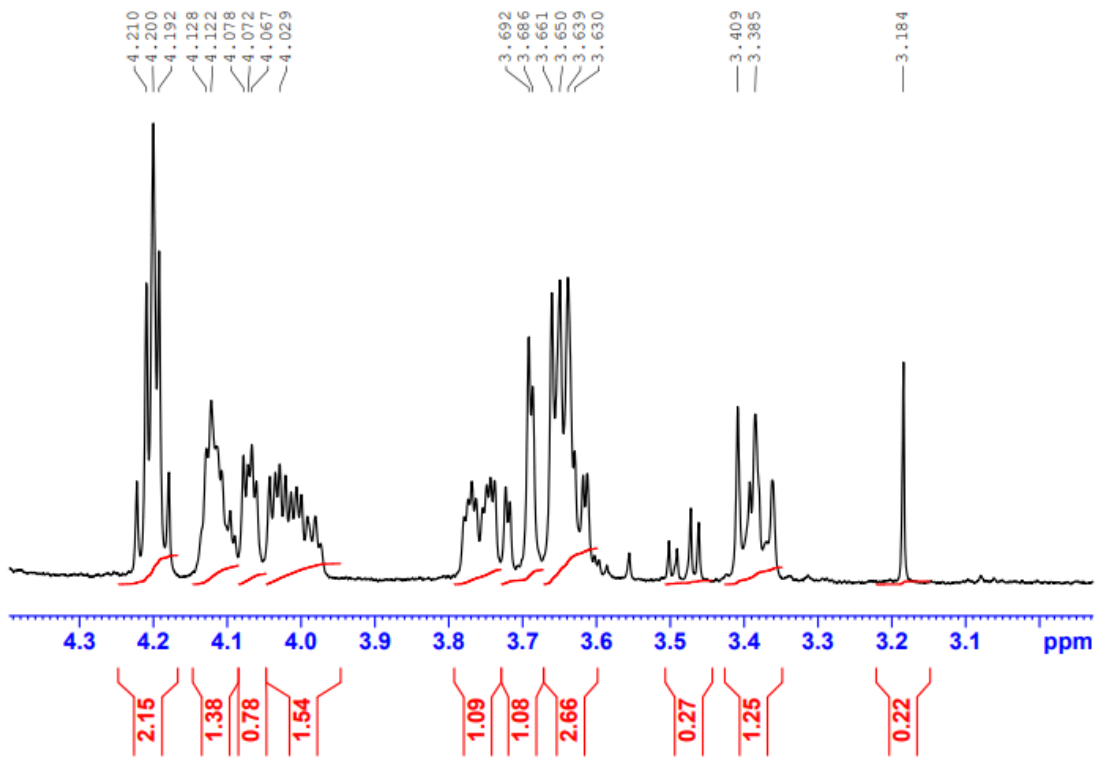
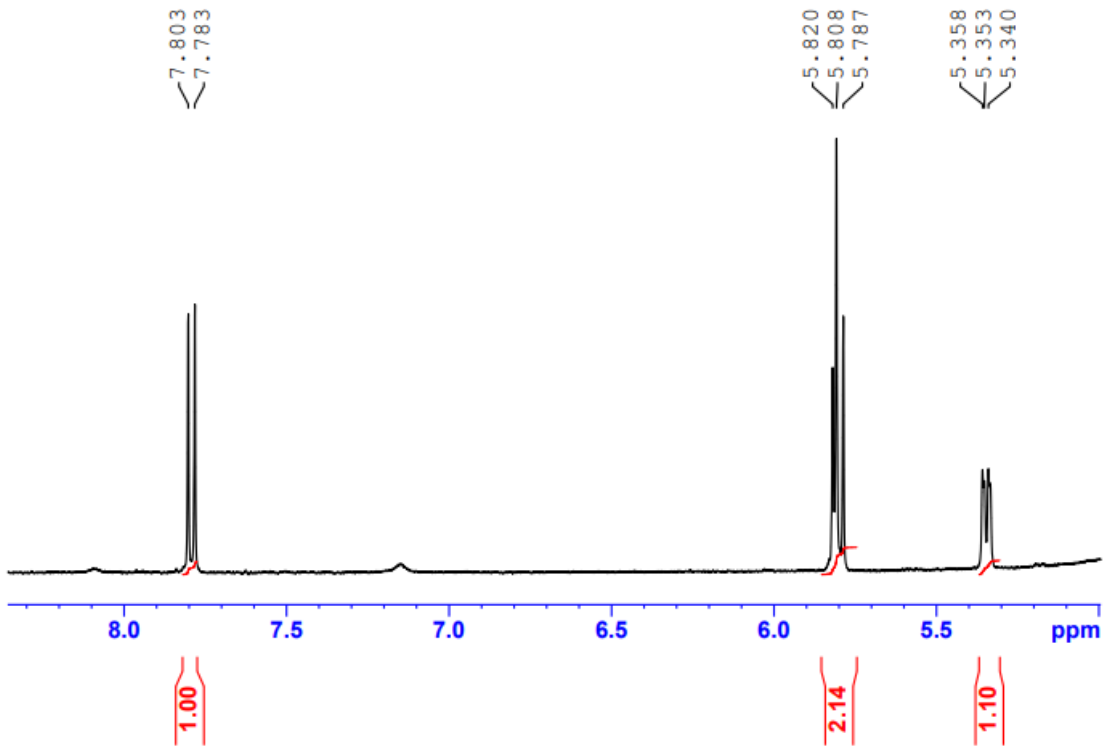
UDP-GlcNAc (3.1)



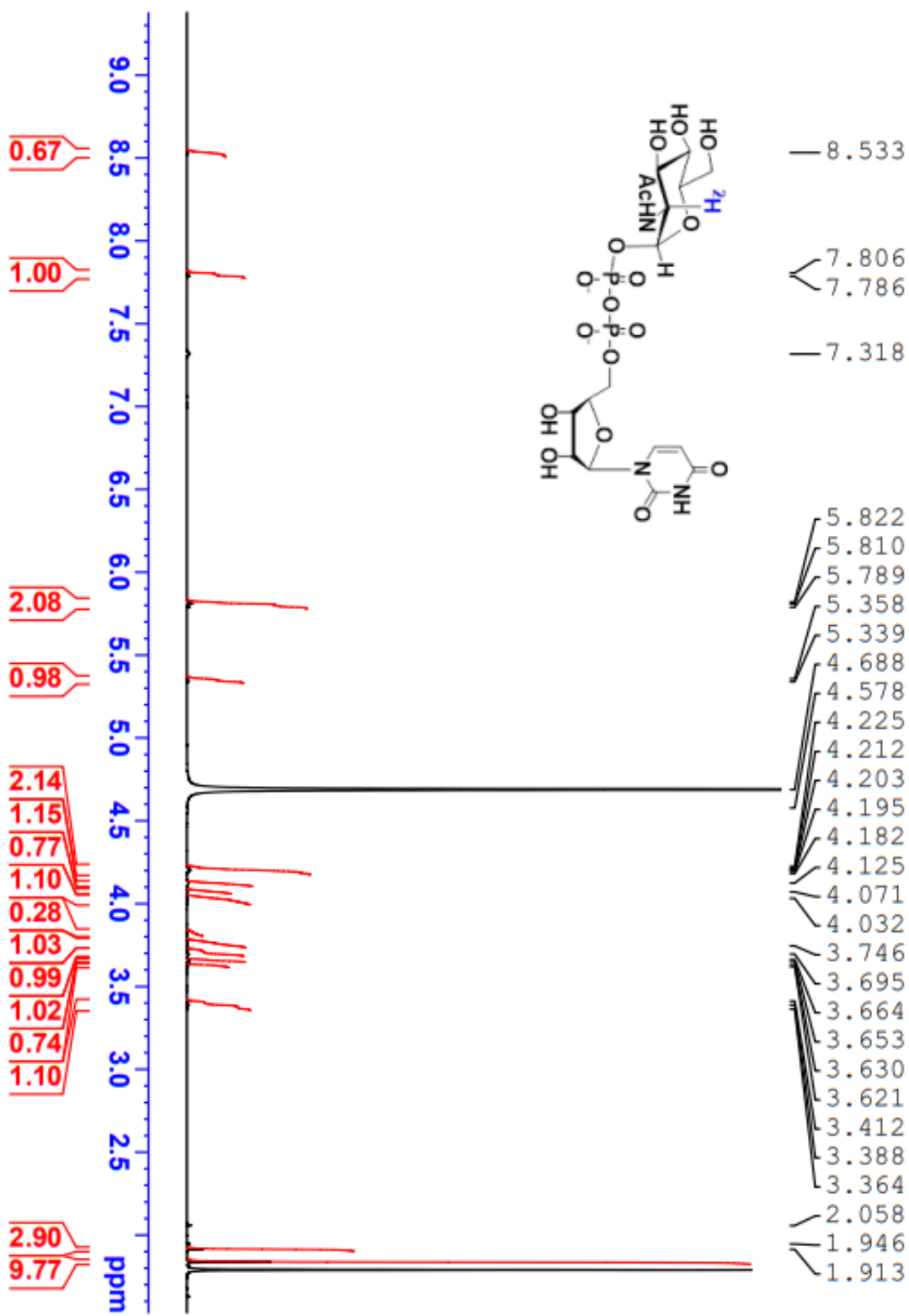


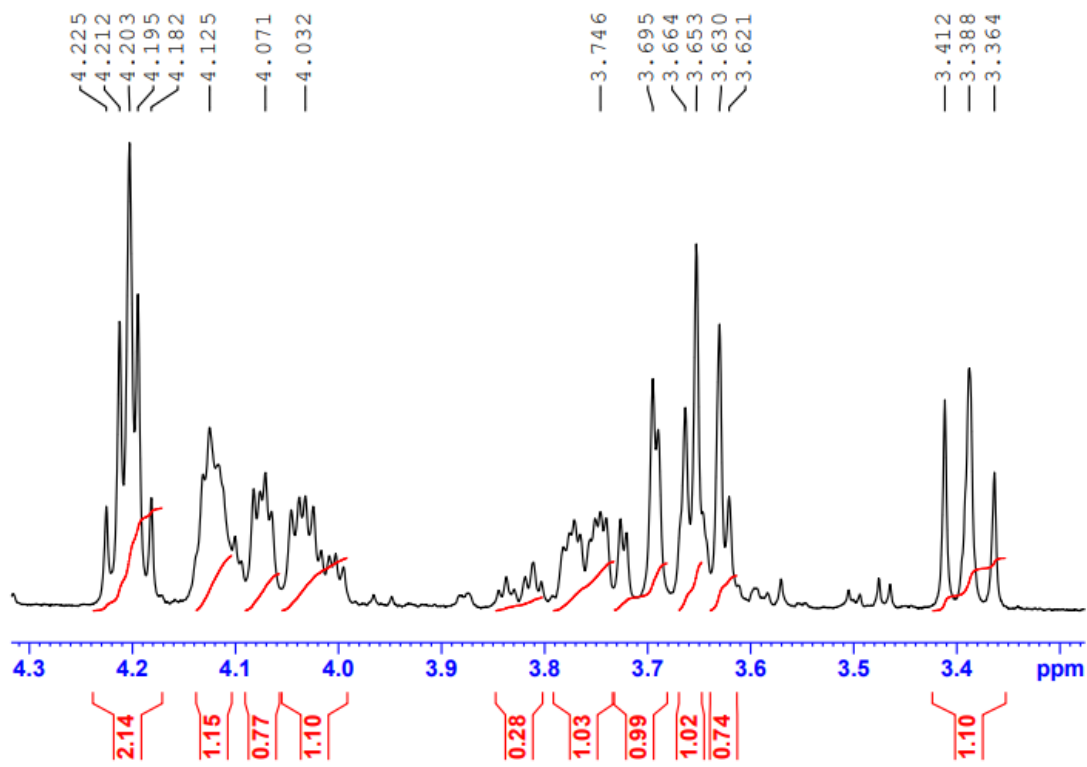
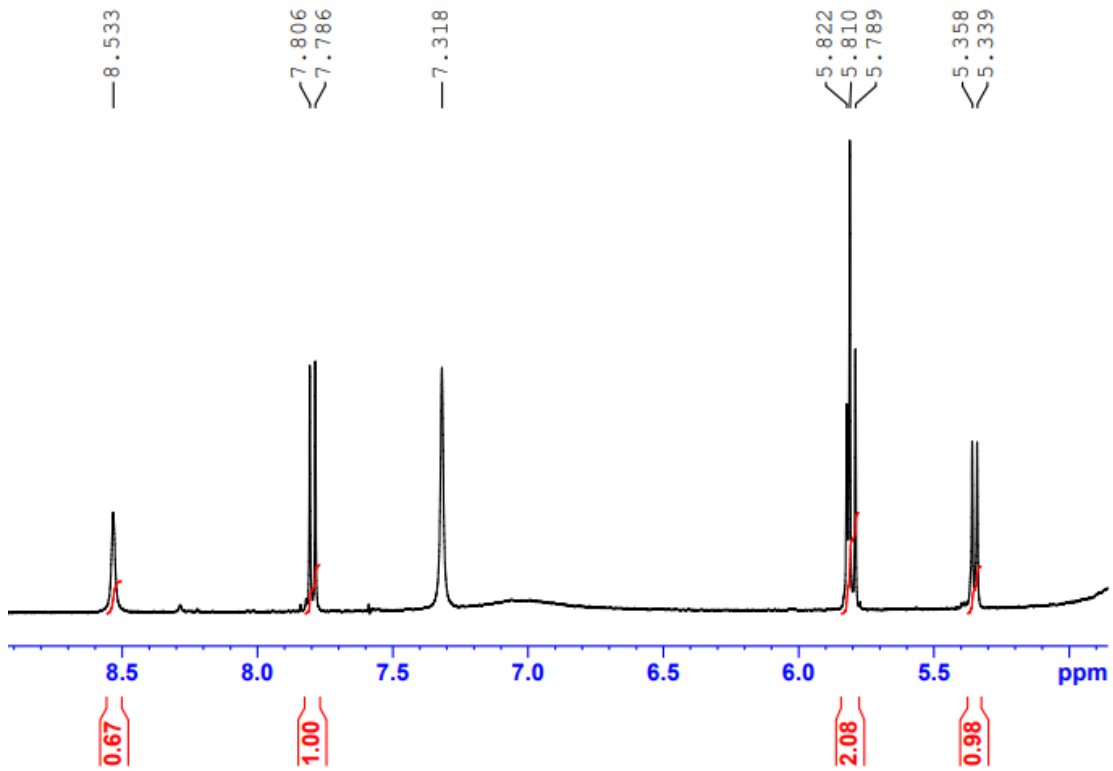
[2-¹³C]UDP-GlcNAc (3.3)



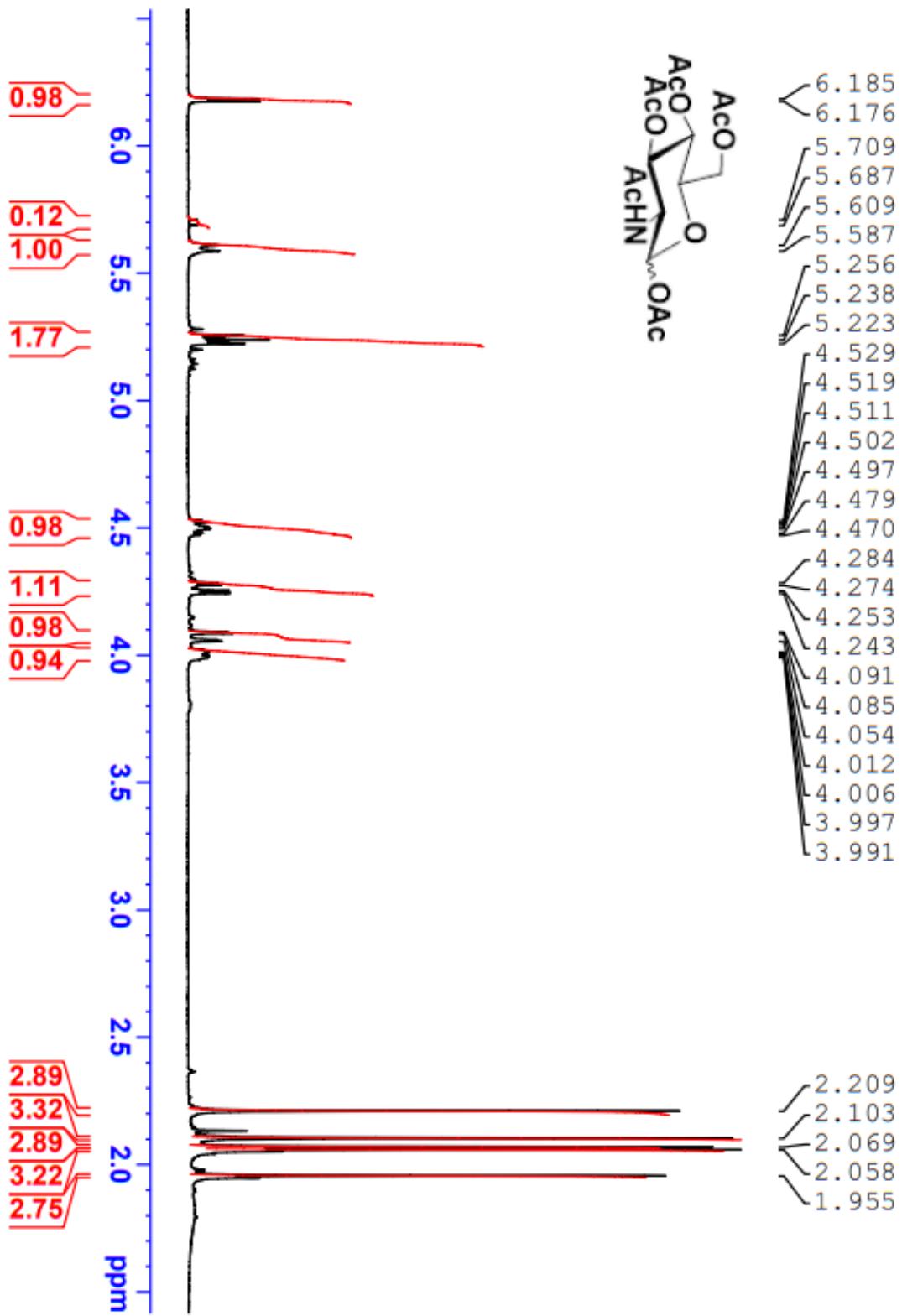


[2-²H]UDP-GlcNAc (3.5)

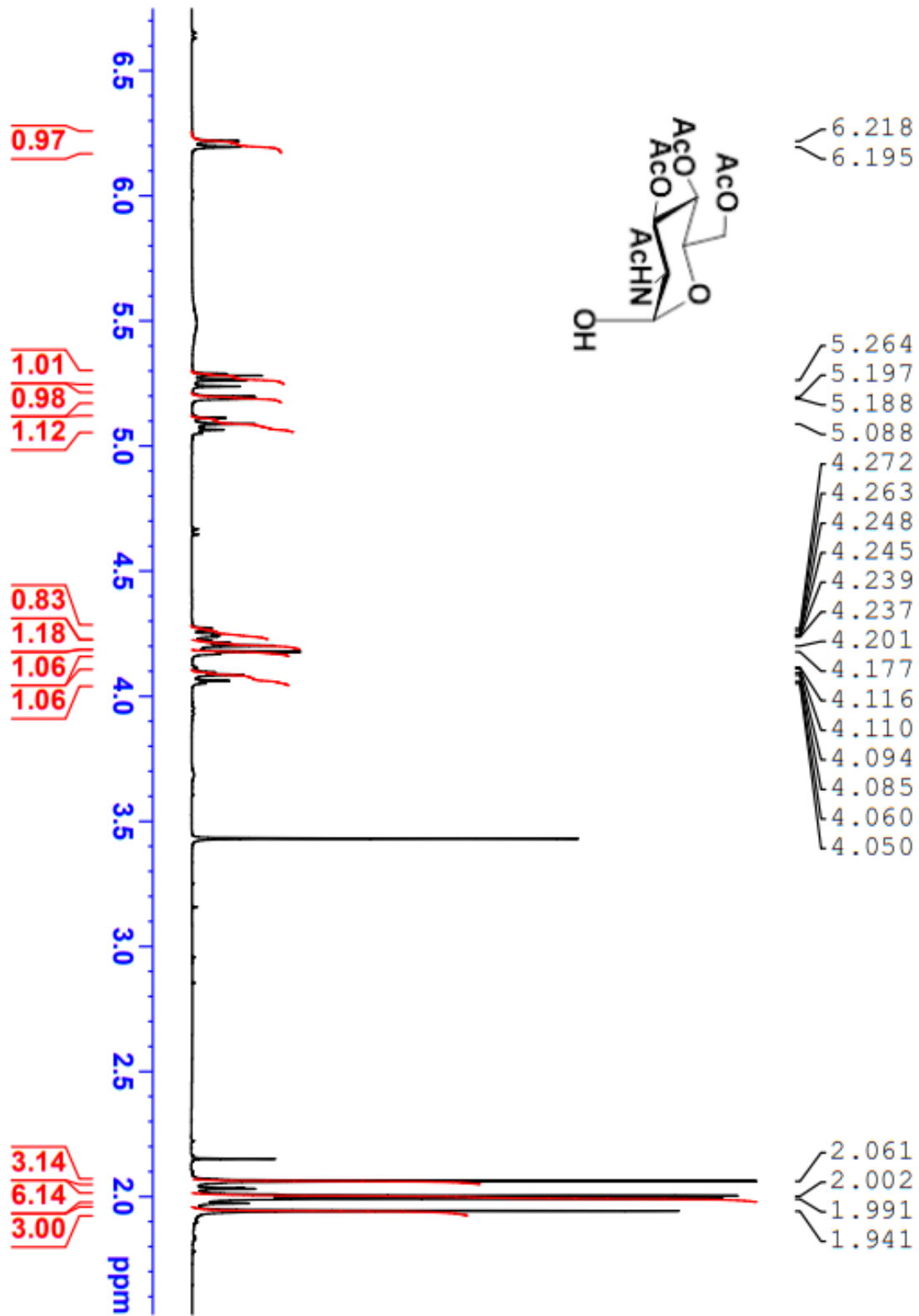




Ac-GlcNAc (3.6)



Ac-GlcNAc-OH (3.7)



Chapter 4: Direct Competitive Kinetic Isotope Effect Measurements of BshA Using Quantitative Whole Molecule MALDI-TOF Mass Spectrometry

Contributions of other authors:

Veronica Guirguis ran initial KIE measurements on BshA system with a different matrix and quenching procedure. Her data collections were not reported in this thesis.

Michael Tyrlic designed MALDI-TOF MS peak data analysis in RStudio for all samples analyzed in this chapter.

4.1 INTRODUCTION

Complex carbohydrates and polysaccharides play crucial roles in a diverse range of cellular functions, including energy storage, cell-wall structure, cell-cell recognition and signaling, pathogenesis, and protein glycosylation^{161–163}. The enzymes predominantly responsible for the biosynthesis of glycans and glycoconjugates are glycosyltransferases (GTs). They catalyze the transfer of a sugar moiety through formation of regio- and stereo-specific glycosidic bond between an activated sugar donor and saccharide or non-saccharide acceptors. The diversity in their donor, acceptor and product specificity results in a large number of glycoconjugates, oligo- and polysaccharides.

Classification of the GT family system is mainly based on sequence similarity collected in the Carbohydrate Active Enzyme database (CAZy, <http://www.cazy.org/>). CAZy differentiates GTs based on function, 3D architecture (ie. GT-A, GT-B and GT-C folds) and the chemical catalysis mechanisms. Catalysis occurs with two possible outcomes: inversion or retention of the anomeric configuration of the donor. Based on the outcomes, the glycosyltransferases are categorized to inverting and retaining glycosyltransferases.

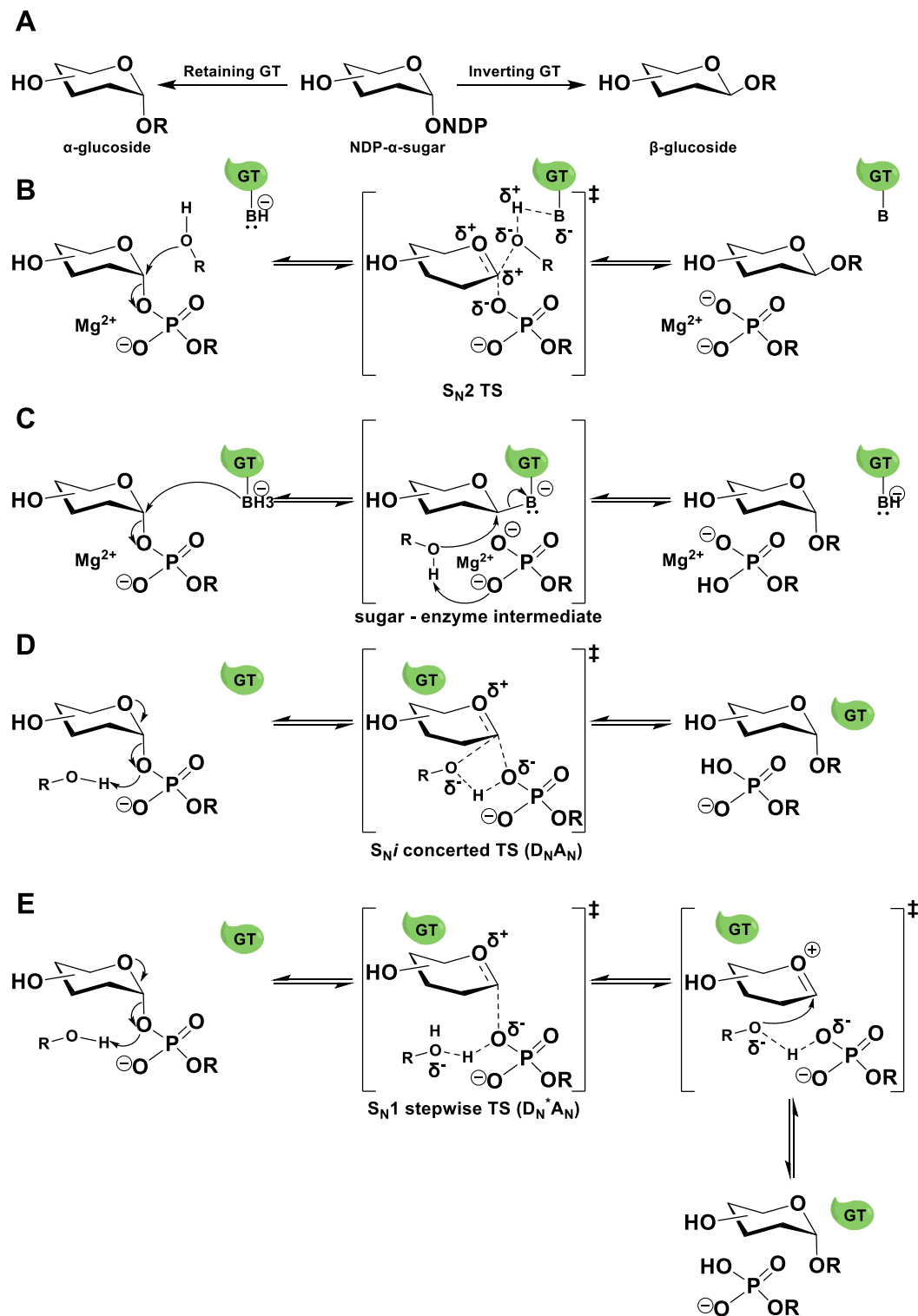


Figure 4.1 The basic chemical reaction mechanisms of glycosylation. (A) Reaction schemes of inverting and retaining GTs (B) Classical S_N2 -like mechanism for inverting glycosylation. “B” represents the catalytic base provided by GTs

- (C) Double-displacement mechanism for retaining GTs. (D) Proposed internal return (S_{Ni} -like) mechanism for retaining GTs with concerted transition state (D_NA_N)
(E) Proposed mechanism for retaining GTs with stepwise transition state ($D_N^*A_N$)

Inverting GTs are generally accepted to undergo a direct displacement S_N2 -like mechanism, according to both the theoretical^{164–166} and experimental studies, including mechanistic studies and kinetic isotope measurements^{91,167,168}. When the catalytic base from the active site side chain (typically Asp, Glu or His)^{169–171} of the GT abstracts a proton from a hydroxy group of the acceptor, facilitating the subsequent nucleophilic attack at the anomeric position of the donor (general base catalysis), resulting in formation of the glycosidic bond with inversion of stereochemistry at C1 position^{107,172,173}. Information from theoretical studies suggests that the nucleophilic attack and glycosidic bond cleavage happen nearly simultaneously, accompanied by the proton transfer^{164,165}. During the formation of the transition state (TS), the anomeric carbon migrates towards the nucleophilic oxygen accompanied by the rotation of the diphosphate group, which is conducive to the glycosylation reaction (Figure 4.1B).¹⁰⁷ The catalytic base is usually located near the acceptor OH-group, based on structural studies.^{164–166} The existence of hydrogen bonding between catalytic His and Asp residues in some GTs and divalent metal ions (Mn^{2+} or Mg^{2+}) in most other GTs usually stabilizes the developing anionic charge on the leaving group. It is also frequently observed that cationic AA like Arg or Lys can serve to stabilize the anionic leaving group.

Unlike inverting glycosyltransferases, the mechanism of retaining glycosyltransferases is still poorly understood and heavily debated. Two main explanations of the mechanisms are the double-displacement mechanism (Figure 4.1C)

or the “internal return–like” S_{Ni} -like mechanism (Figure 4.1C). Another alternative mechanism would be S_{N1} , a more dissociative mechanism with a discrete oxocarbenium ion intermediate (Figure 4.1D). The double displacement mechanism involves the formation of covalent glycosyl-enzyme intermediate with configuration inversion at the anomeric position of the donor^{174–176}. The donor is then transferred to the acceptor reverting to the original anomeric configuration. Using mutant enzymes some experiments were able to provide evidence for such covalent intermediates by mass spectrometry.^{175,177} However, efforts to capture the covalent glycosyl-enzyme intermediate in wild type enzymes were unsuccessful.^{175,178} Structural studies on retaining glycosyltransferases suggest that amino acid side chains are rarely positioned to act as a nucleophile in the active site, making a double-displacement mechanism hard to support.^{179–186}

Being that a suitable nucleophile or catalytic base could not be identified in the catalytic site of most retaining GTs, the alternative internal return-like (S_{Ni} -like) mechanism was proposed.^{91,181,186,187} In this mechanism, the hydroxy group of the acceptor participates in a nucleophilic attack on the anomeric center from the same face of the sugar as the leaving group. The reaction involves the formation of an oxocarbenium ion-like TS that is shielded on one face of the reaction center by the GT, consequently protecting against nucleophilic attack from the opposite face and resulting in retention of C1 configuration.^{179,188–190} Theoretical studies¹⁴⁴ indicate that the cleavage of the UDP–sugar bond takes UDP-GlcNAc first, followed by the formation of the glycosidic bond, allowing the formation of an intimate ion-pair intermediate. Both experimental^{190,191} and theoretical¹⁸⁸ studies suggested that the

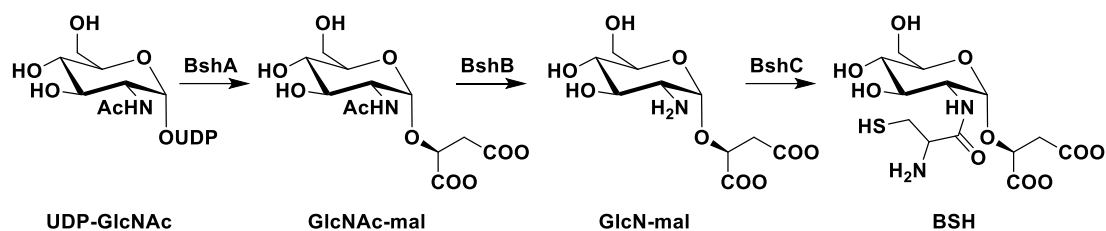
leaving phosphate group could function as the catalytic base to deprotonate the acceptor OH-group. Since the S_{Ni} -like mechanism involves a front-face nucleophilic attack, it leads to an open transition state with a net retention of the anomeric stereochemistry. This open transition state is expected to be highly dissociative,¹⁷⁹ with a considerable oxocarbenium ion character.¹⁹² Structural studies indicate a possible formation of hydrogen bonds between the leaving group and the incoming nucleophile, resulting in the front-face nucleophilic attack while assisting leaving group dissociation.^{91,179,193}

The concept of S_{Ni} mechanism was first introduced to explain unusual stereochemical outcomes of simple alkyl halide.¹⁹⁴ When the nucleophile and leaving group are constrained on the same face, reaction with secondary alkyl chlorosulfites results in retention of stereochemistry. In carbohydrate chemistry, S_{Ni} mechanism was first proposed to explain the retention of anomeric stereochemistry in the solvolysis of α -glucosyl fluoride by mixtures of ethanol and trifluoroethanol¹⁹⁵. Theoretical studies suggest that an internal return mechanism provides an energetically plausible pathway inside enzymes because of active site geometrical constraints^{179,192}. Although direct experimental support for the S_{Ni} mechanism over a S_{N1} mechanism are limited, one way to distinguish between these two mechanistic manifolds would be through the measurement of experiment KIEs for the reaction catalyzed by a retaining GT enzyme. One such enzyme is the GT4 enzyme BshA that catalyzes the first step in the biosynthesis bacillthiol (BSH) biosynthesis in Gram-positive bacteria like *Bacillus subtilis*.

Low-molecular weight thiols, like BSH, are prevalent in eukaryotes, Gram-negative and Gram-positive bacteria, where they are involved in the maintenance of

redox homeostasis and detoxification of reactive oxygen species and electrophilic reagents.¹⁹⁶ Gram-positive bacteria, including *B. subtilis*, *Staphylococcus aureus*, and *Deinococcus radiodurans*, utilize bacillithiol (BSH) as the major low-molecular weight thiol.^{196–204} BSH reacts rapidly with some alkylating agents (e.g., N-ethylmaleimide, iodoacetamide) and with electrophiles (formaldehyde, methylglyoxal, S-nitrosocompounds), but most importantly BSH is the preferred co-substrate for FosB, an enzyme produced by certain species of Gram-positive bacteria that permits resistance to the FDA-approved antibiotic Fosfomycin.^{205–207} Monurol-fosfomycin is the only clinically used drug that inhibits MurA, the enzyme that catalyzes the committed step in bacterial cell wall biogenesis²⁰⁸. Hence, inhibition of enzymes involved in BSH biosynthesis could be an effective therapeutic avenue for the treatment of infections caused by fosfomycin-resistant Gram-positive organisms.¹⁹⁸

BSH consists of a glucosamine core with a cysteinyl moiety attached via an amide linkage at position 2, and with an L-malyl group at the sugar's anomeric carbon. These moieties are produced through the BSH biosynthesis pathway, which consists of the retaining glycosyltransferase BshA, the zinc-dependent deacetylase BshB, and a putative cysteine ligase BshC (Scheme 4-1).¹⁹⁶ BshA catalyzes the first committed step in BSH production, utilizing UDP-*N*-acetylglucosamine (UDP-GlcNAc) as an activated sugar donor and L-malate as an acceptor to form *N*-acetylglucosaminyl-malate (GlcNAc-mal) and the byproduct UDP.



Scheme 4.1. Bacillithiol biosynthesis pathway.

BshA is a family 4 retaining GT of the GT-B fold^{196,209,210}. GT-4 family enzymes are typically retaining GTs that are hypothesized to utilize an S_Ni -like reaction mechanism in which the departure of the UDP leaving group and attack by the malate hydroxyl group at the anomeric position occur at the same face of the sugar in a concerted fashion, with a single TS with simultaneous bond formation and bond breaking.¹⁹⁶ Deprotonation of the malate hydroxyl group and protonation of the UDP leaving group are hypothesized to proceed via substrate-assisted catalysis. The features within the active site of BshA that accommodate the substrates are currently not well understood, and it is unclear if the substrates bind the enzyme in the manner required for a substrate-assisted S_Ni -like mechanism. Apo and ligand-bound structures of BshA from *Bacillus anthracis* have been previously determined at low resolution (3.1 Å).^{210,211} Additionally, X-ray crystallographic structures of BshA from *B. subtilis* strain 168 complexed with UMP and product GlcNAc-mal were determined at higher resolution of 2.15 and 2.02 Å.¹⁹⁶ These structures provide some insight into the active site features critical for catalysis, however, there is limited information about the dynamic mechanistic details of BshA which would determine more conclusively whether it goes through the S_Ni -like reaction mechanism.

Here we use the MALDI-TOF MS KIE approach developed in Chapter 2 to probe the TS structure of BshA using the specific isotope labeled UDP-GlcNAc substrates synthesized in Chapter 3.

4.2 RESULTS AND DISCUSSION

Using the quantitative whole molecule matrix assisted laser desorption/ionization (MALDI) time of flight (TOF) MS approach described in Chapter 2, we determined multiple competitive KIEs for the enzymatic reaction catalyzed by BshA. KIEs were measured using UDP-GlcNAc donor substrates containing specific isotope labels surrounding the reaction center (ie. [1''-¹³C]UDP-GlcNAc, [2''-²H]UDP-GlcNAc and [2''-¹³C]UDP-GlcNAc), and the results are summarized in Table 4.1. The substrates were synthesized and characterized as described in Chapter 3. As the 2''-¹³C position is not involved in the mechanism of BshA, it was used as a reference. Competitive KIEs for both [1''-¹³C]UDP-GlcNAc, and [2''-²H]UDP-GlcNAc were measured relative to light [¹²C₁₂]UDP-GlcNAc by introducing a fixed concentration of [¹³C₆]UDP-GlcNAc internal standard to the reaction mixture after quenching. A reaction mixture containing only “light” UDP-GlcNAc was analyzed in the same fashion to account for concentration of natural abundance ¹³C present in the “light” UDP-GlcNAc sample. Competitive KIEs are calculated using eq. 1:

$$(R_F/R_o) = (1 - F)^{(1/kie-1)}$$

where R_F is the heavy/light isotope ratio measured for the unreacted substrate at F , R_o is the initial heavy/light isotope ratio for the substrate at time zero, F is the fraction of

substrate that has been converted to product (ie. fractional conversion), and *kie* is the isotope effect.

Table 4.1. Summary of experimental KIEs for BshA.

“Heavy” substrate	KIE	Type of KIE	Experimental KIE ^a
[1''- ¹³ C]UDP-GlcNAc	1''- ¹³ C	primary	1.010 ± 0.011
[2''- ² H]UDP-GlcNAc	2''- ² H	β-secondary	1.111 ± 0.003
[2''- ¹³ C]UDP-GlcNAc	2''- ¹³ C	remote label	1.001 ± 0.001

^a Errors are the standard error for the nonlinear regression fit for a single run.

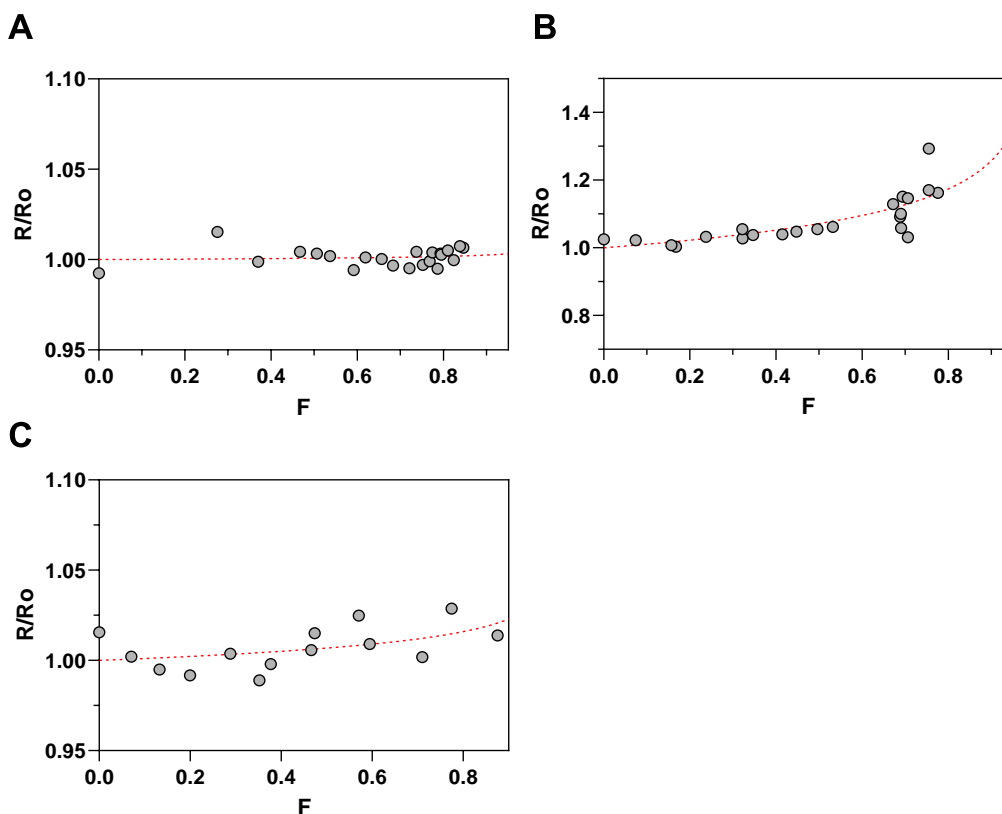


Figure 4.2. Experimental KIEs for BshA glycosyltransferase. (A) Plot of R/R_0 vs. F fit to eq. 1 using 22 time points derived from a single BshA reaction for [2''-¹³C]UDP-GlcNAc resulting in a KIE of 1.01 ± 0.001 . (B) Plot of R/R_0 vs. F fit to eq. 1 using 22 time points derived from a single BshA reaction with [2''-²H]UDP-GlcNAc with a KIE

value of 1.111 ± 0.003 . (C) Plot of R/R_o vs. F fit to eq. 1 using 14 time points derived from a single BshA reaction with $[1''\text{-}^{13}\text{C}]\text{UDP-GlcNAc}$ with a KIE value of 1.010 ± 0.011 .

The experimental KIE measured using $[2''\text{-}^{13}\text{C}]\text{UDP-GlcNAc}$, shown in Figure 4.2A, resulted in a KIE value of 1.001 ± 0.001 that is not statistically different than unity (KIE = 1). This result indicates that there is no isotope effect for $2''\text{-}^{13}\text{C}$ and corroborates that C2'' position does not undergo a significant change in bonding at the TS of BshA.

For the TS with high oxocarbenium ion-like character and hyperconjugation, β -secondary kinetic effect is larger than 1.07.^{10,12,14-24,26-28} For the TS with low oxocarbenium ion character or lack of hyperconjugation, β -secondary kinetic effect is smaller than 1.035.^{9,23-25} We measured a β -secondary $2''\text{-}^2\text{H}$ KIE of 1.111 ± 0.003 as seen in Figure 4.2B. This β -secondary KIE results from hyperconjugation between H2'' and the electron-deficient C1'' of the oxocarbenium, which stabilizes the TS.²¹² The normal KIE (>1) indicates that the C2''-H2'' bond is weakened at the rate determining TS due to electron donation from the sigma bond between H2'' and C2'' to the empty p-orbital of C1''. This hyperconjugation will lead to flattening of C5''-O5''-C1''-C2'' of the pyranose ring. The β -secondary deuterium KIE also suggests a considerably dissociative transition state, with a substantial oxocarbenium ion-like character, as shown in Figure 4.2.C.

Using $[1''\text{-}^{13}\text{C}]\text{UDP-GlcNAc}$ we measured a primary KIE of 1.010 ± 0.011 (Figure 4.2C), which is consistent with our observed β -secondary $[2''\text{-}^2\text{H}]$ KIE. Primary carbon KIEs normally ranges in magnitude between 0.995 and 1.08. For the TS forming through a synchronous A_ND_N , primary C kinetic effect ranges between 1.07

and 1.08.⁹ For the transition state forming a dissociative $A_N D_N$, primary C kinetic effect ranges between 1.013 and 1.03.¹⁰⁻²¹ For the transition state forming through a stepwise $D_N^* A_N$ with discrete oxocarbenium ion intermediate, primary C kinetic effect ranges between 1.005–1.01.^{20,22,23} For the transition state forming through a stepwise $D_N^* A_N$, primary C kinetic effect ranges between 0.995 and 1.0.²³⁻²⁵ Thus, the $1''\text{-}^{13}\text{C}$ KIE observed for BshA is consistent with a stepwise $D_N^* A_N$ with discrete oxocarbenium ion-like intermediate Figure 4.3.

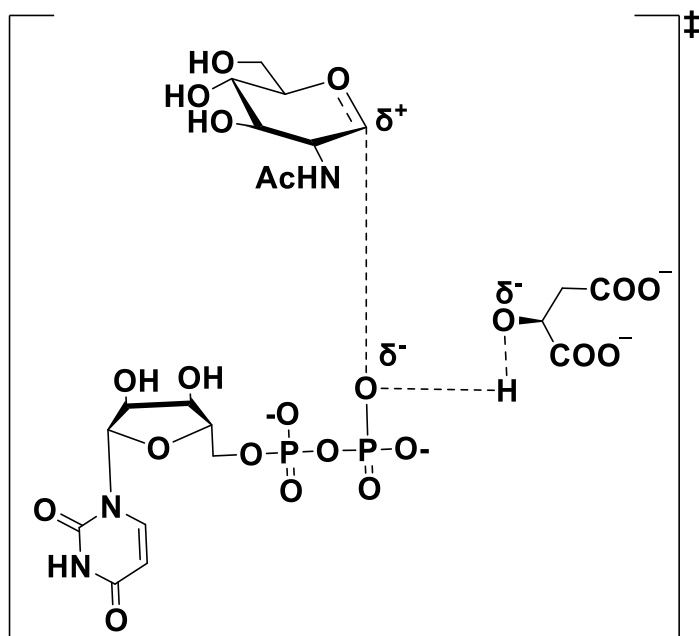


Figure 4.3. Proposed front-face transition state for BshA-catalyzed conjugation of UDP-GlcNAc and L-malate.

4.3 CONCLUSION

Using the isotopically labeled donor substrates $[1''\text{-}^{13}\text{C}]\text{UDP-GlcNAc}$, $[2''\text{-}^2\text{H}]\text{UDP-GlcNAc}$ and $[2''\text{-}^{13}\text{C}]\text{UDP-GlcNAc}$, we determined three experimental KIEs using a whole molecule MALDI-TOF MS approach. The experimentally measured $2''\text{-}^{13}\text{C}$

KIE of 1.001 ± 0.001 show that C2'' position does not undergo a significant change in bonding at the TS of BshA. The primary $1''\text{-}^{13}\text{C}$ KIE of 1.010 ± 0.011 is consistent with a rate determining TS that leads to formation of a stepwise $\text{D}_\text{N}^*\text{A}_\text{N}$ with discrete oxocarbenium ion intermediate. The β -secondary KIE $2''\text{-}^2\text{H}$ KIE of 1.111 ± 0.003 , suggests there is significant oxocarbenium ion-like character at the rate determining TS, again consistent with a $\text{D}_\text{N}^*\text{A}_\text{N}$ reaction manifold. Previous studies have suggested a front-face S_{Ni} ($\text{A}_\text{N}\text{D}_\text{N}$) TS for the conjugation of UDP-GlcNAc and L-malate based on structural characterization of BshA. Our KIE results, however, are more consistent with a stepwise mechanism resulting in the formation of a discrete, though likely short lived, oxocarbenium ion intermediate.

4.4 EXPERIMENTAL PROCEDURES

4.4.1 General

Unless otherwise noted, all chemicals were purchased as analytical or reagent grade and used without further purification. MALDI-TOF mass spectrometry measurements were recorded on a Bruker Autoflex Speed spectrometer equipped with a 2KHz smartbeam II laser, with a time of flight (TOF)-analyzer capable of both positive and negative ion mode as described in detail below. Matrix solution of 2-hydrazinoquinoline (2-HQ) was prepared in a 95:5 mixture of methanol and acetic acid at a final concentration of 12 mg/mL.¹⁵⁹

4.4.2 Protein preparation

A plasmid for the recombinant expression of BshA was obtained as a generous gift from Prof. Paul Cook (Grand Valley State University) and expressed in BL21(DE3) *E. coli* cells as described previously.²¹³ The overnight culture was grown in LB with 25 $\mu\text{g}/\text{mL}$ kanamycin at 37 °C. Protein expression was induced with 0.1 mM IPTG at 18°C overnight. The cells were then pelleted at 8500 rcf for 20 minutes, resuspended in a wash buffer of 25 mM Tris-HCl, pH 7.4 containing 10 mM imidazole, and lysed by sonication. The lysate was then centrifuged at 8500 rcf to remove insoluble cellular debris. Enzyme was purified from the supernatant with a Ni-NTA column using a linear gradient between 10 mM to 300 mM imidazole. Enzyme containing fractions were identified using SDS-PAGE, pooled, and dialyzed into 25 mM Tris-HCl pH 7.4. Individual aliquots of enzyme were flash frozen and stored at -80 °C until use.

4.4.3 Sample quenching

Quenching of enzyme activity was accomplished by thermally inactivating BshA containing samples at 95 °C. Thermal inactivation was tested for efficient quenching by monitoring UDP-GlcNAc consumption with BshA pre-incubated at 95 °C. Two 50 μL reaction mixtures were prepared containing 1 mM UDP-GlcNAc, 10 mM L-malate and 1 mM MgCl_2 in 20 mM Tris-HCl buffer pH 7.4. A 10 μL fraction from each reaction mixture was removed prior to initiating the reaction to allow for measurement of initial UDP-GlcNAc concentration at time zero. The first reaction was initiated through the addition of 2 μL of 6 μM of BshA, and the second reaction was initiated through the addition of 2 μL of 6 μM BshA which had been pre-incubated at

95 °C for 10 min. Each reaction mixture was allowed to proceed at 22 °C. At 10 min time intervals, 10 µL aliquots were removed from each reaction mixture and incubated at 95 °C for 10 min. The time zero time points were diluted with 1 µL of 20 mM Tris-HCl pH 7.4. All time points were diluted with water to a total volume of 100 µL, and 20 µL of each time point was injected on HPLC to monitor UDP-GlcNAc consumption. Reactions were repeated in triplicate. Samples were separated by HPLC using reversed phase ion pairing chromatography approach using phosphate buffer pH 6.0 containing tetra butyl ammonium bisulfate. The column was washed with buffer B for 4 min and then re-equilibrated with buffer A for 4 min before subsequent injections. Analytes were observed using the absorbance at 254 nm. Concentrations were determined from their relative peak areas, which were plotted as a function of time to obtain the reaction time course. Analyte concentrations from three independent experiments were averaged to obtain reaction progress curve.

4.4.4 MALDI-TOF MS Sample Preparation and Acquisition

For MALDI-TOF measurements using 2-HQ as the matrix, 10 µL of analyte sample was directly mixed with 10 µL of 2-HQ suspension and subsequently incubated at 37 °C for 10 minutes as previously described.¹⁵⁹ 1 µL samples of the 2-HQ–analyte mixture were spotted on the target plate and allowed to dry for 10 minutes at room temperature and humidity of 45-50%.

Mass spectra were recorded in negative-ion reflectron mode to achieve optimal baseline peak resolution. A spectral window from 300 to 800 m/z was used for analyzing UDP-GlcNAc samples. A total of five technical replicate spots were

analyzed for each analyte sample to minimize variability in sample concentration or isotope composition resulting from sample spotting. Summed spectrum from a minimum of 3000 shots for each sample spot were recorded and exported in mzXML format and further processed in R using the MaldiQuant package,^{214,215} as described in Chapter 2.

4.4.5 KIE measurements

UDP-GlcNAc substrate samples, both isotopically labeled and unlabeled, were prepared by dissolving the solid to a concentration of 10 mM. Concentrations were verified by measuring the absorption at 262 nm ($\epsilon_{262} = 10,000 \text{ M}^{-1}\text{cm}^{-1}$).

Reaction mixtures for BshA KIE measurements were prepared containing 2 mM total UDP-GlcNAc substrate (in a ~ 1:1 ratio of “heavy” to “light” sample) in 20 mM Tris-HCl pH 7.4 with 10 mM L-malate and 1 mM MgCl_2 in a final volume of 120 μL . Prior to initiation of the reaction, a time zero time point consisting of 20 μL of the reaction mixture was removed and diluted to a final volume of 22 μL to measure initial UDP-GlcNAc concentrations and isotope ratios (R_0). Reactions were carried out at 22 °C and initiated through the addition of 10 μL of 6 μM BshA. At regular time intervals 5 μL aliquots of the reaction mixture were removed and the BshA activity was quenched by incubation at 95 °C. Thermal inactivation was found to rapidly inactivate BshA without any degradation of the UDP-GlcNAc substrate. Subsequently, aliquots of the reaction mixture were mixed with an equal volume of solution consisting of 0.5 mM $[\text{Glc-}^{13}\text{C}_6]\text{UDP-GlcNAc}$ standard. Quenched fractions were centrifuged at 17,000

× g for 2 min to remove any solid precipitates and stored at $-20\text{ }^{\circ}\text{C}$ prior to MALDI-TOF analysis as described above.

4.4.6 Peak integration and data analysis

Relative peak areas for the $[^{12}\text{C}_{12}]\text{UDP-GlcNAc}$ (light, $m/z = 605.7$), $[1\text{-}^{13}\text{C}_1]\text{UDP-GlcNAc}$ (heavy, $m/z = 606.7$) and $[^{13}\text{C}_6]\text{UDP-GlcNAc}$ (standard, $m/z = 611.7$) were determined for each mass spectrum using a numerical peak integration script developed in R. Briefly, mass spectral mzXML files were imported in R using the MALDIquant package.^{214,215} A 10 m/z window containing the peaks of interest was selected for further analysis. The 25th percentile of all intensity values within this segment was used as a baseline and subtracted from all intensities within the segment. Subsequently, the boundaries of each relevant peak were identified. Initial guesses of outer integration boundaries were provided by the user and were identical for all mass spectra analyzed from the same enzyme-substrate combination. Subsequently, an approximate first derivative was calculated for the entire spectrum segment and smoothed using an “SMA” moving average calculation. A difference in treatment of the left and right boundaries was necessitated by the peak asymmetry. The left boundary was selected as the highest mass number lower than the 20th percentile of smoothed derivatives within the segment bound by the initial guess and the peak maximum. The right boundary was selected as the lowest mass number lower than the 5th percentile of smoothed derivatives within the segment bound by the peak maximum and the initial guess. The total peak intensity was determined after boundary selection from the sum of all intensities within these boundaries. A plot of spectra with overlaid final integration boundaries was manually examined for each measurement to verify

accurate boundary detection. An integration was considered successful if the boundaries included the entire target peak, excluded all other peaks, and divided overlapping peaks at a local minimum between them.

4.5 BIBLIOGRAPHY

- (1) Coutinho, P. M.; Deleury, E.; Davies, G. J.; Henrissat, B. An Evolving Hierarchical Family Classification for Glycosyltransferases. *J. Mol. Biol.* **2003**, *328* (2), 307–317. [https://doi.org/10.1016/S0022-2836\(03\)00307-3](https://doi.org/10.1016/S0022-2836(03)00307-3).
- (2) Gao, Y.; Wells, L.; Comer, F. I.; Parker, G. J.; Hart, G. W. Dynamic O-Glycosylation of Nuclear and Cytosolic Proteins: Cloning and Characterization of a Neutral, Cytosolic β -N-Acetylglucosaminidase from Human Brain. *J. Biol. Chem.* **2001**, *276* (13), 9838–9845. <https://doi.org/10.1074/jbc.M010420200>.
- (3) Bertozzi, C.R. and Kiessling, A.L.L., Chemical glycobiology. *Science*, **2001**, *291*(5512), 2357-2364.
- (4) Krupička, M.; Tvaroška, I. Hybrid Quantum Mechanical/Molecular Mechanical Investigation of the β -1,4-Galactosyltransferase-I Mechanism. *J. Phys. Chem.* **2009**, *113* (32), 11314–11319. <https://doi.org/10.1021/jp904716t>.
- (5) Tvaroška, I.; Kozmon, S.; Wimmerová, M.; Koča, J. Substrate-Assisted Catalytic Mechanism of O-GlcNAc Transferase Discovered by Quantum Mechanics/Molecular Mechanics Investigation. *J. Am. Chem. Soc.* **2012**, *134* (37), 15563–15571. <https://doi.org/10.1021/ja307040m>.

- (6) Tvaroška, I.; Kozmon, S.; Wimmerová, M.; Koča, J. A QM/MM Investigation of the Catalytic Mechanism of Metal-Ion-Independent Core 2 B1,6-N-Acetylglucosaminyltransferase. *Chem. Eur. J.* **2013**, *19* (25), 8153–8162.
<https://doi.org/10.1002/chem.201300383>.
- (7) Lairson, L. L.; Henrissat, B.; Davies, G. J.; Withers, S. G. Glycosyl Transferases: Structures, Functions, and Mechanisms. *Annu. Rev. Biochem.* **2008**, pp 521–555.
<https://doi.org/10.1146/annurev.biochem.76.061005.092322>.
- (8) Kim, S.C., Singh, A.N. and Raushel, F.M., Analysis of the galactosyltransferase reaction by positional isotope exchange and secondary deuterium isotope effects. *Arch.Biochem. Biophys.* **1988**, *267*(1), 54-59.
- (9) Bruner, M. and Horenstein, B.A., Isotope trapping and kinetic isotope effect studies of rat liver α -(2 \rightarrow 6)-sialyltransferase. *J. Biochem.* **1988**, *37*(1), pp.289-297.
- (10) Chiu, C. P. C.; Watts, A. G.; Lairson, L. L.; Gilbert, M.; Lim, D.; Wakarchuk, W. W.; Withers, S. G.; Strynadka, N. C. J. Structural Analysis of the Sialyltransferase CstII from *Campylobacter Jejuni* in Complex with a Substrate Analog. *Nat. Struct. Mol. Biol.* **2004**, *11* (2), 163–170.
- (11) Chiu, C. P. C.; Lairson, L. L.; Gilbert, M.; Wakarchuk, W. W.; Withers, S. G.; Strynadka, N. C. J. Structural Analysis of the α -2, 3-Sialyltransferase Cst-I from *Campylobacter Jejuni* in Apo and Substrate-Analogue Bound Forms. *Biochem.* **2007**, *46* (24), 7196–7204.

- (12) Pak, J. E.; Arnoux, P.; Zhou, S.; Sivarajah, P.; Satkunarajah, M.; Xing, X.; Rini, J. M. X-Ray Crystal Structure of Leukocyte Type Core 2 B1, 6-N-Acetylglucosaminyltransferase: Evidence for a Convergence of Metal Ion-Independent Glycosyltransferase Mechanism. *J. Biol. Chem.* **2006**, *281* (36), 26693–26701.
- (13) Liang, D. M.; Liu, J. H.; Wu, H.; Wang, B. Bin; Zhu, H. J.; Qiao, J. J. Glycosyltransferases: Mechanisms and Applications in Natural Product Development. *Chem. Soc. Rev.* Royal Society of Chemistry November 21, **2015**, pp 8350–8374. <https://doi.org/10.1039/c5cs00600g>.
- (14) Ruan, X.; Loyola, D. E.; Marolda, C. L.; Perez-Donoso, J. M.; Valvano, M. A. The WaaL O-Antigen Lipopolysaccharide Ligase Has Features in Common with Metal Ion-Independent Inverting Glycosyltransferases. *J. Glycobiol.* **2012**, *22* (2), 288–299. <https://doi.org/10.1093/glycob/cwr150>.
- (15) Lee, S. S.; Hong, S. Y.; Errey, J. C.; Izumi, A.; Davies, G. J.; Davis, B. G. Mechanistic Evidence for a Front-Side, S_Ni-Type Reaction in a Retaining Glycosyltransferase. *Nat. Chem. Biol.* **2011**, *7* (9), 631–638. <https://doi.org/10.1038/nchembio.628>.
- (16) Rojas-Cervellera, V.; Ardèvol, A.; Boero, M.; Planas, A.; Rovira, C. Formation of a Covalent Glycosyl-Enzyme Species in a Retaining Glycosyltransferase. *Chem. Eur. J.* **2013**, *19* (42), 14018–14023. <https://doi.org/10.1002/chem.201302898>.

- (17) Soya, N.; Fang, Y.; Palcic, M. M.; Klassen, J. S. Trapping and Characterization of Covalent Intermediates of Mutant Retaining Glycosyltransferases. *J. Glycobiol.* **2011**, *21* (5), 547–552. <https://doi.org/10.1093/glycob/cwq190>.
- (18) Monegal, A.; Planas, A. Chemical Rescue of A3-Galactosyltransferase. Implications in the Mechanism of Retaining Glycosyltransferases. *J. Am. Chem. Soc.* **2006**, *128* (50), 16030–16031. <https://doi.org/10.1021/ja0659931>.
- (19) Ly, H. D.; Loughheed, B.; Wakarchuk, W. W.; Withers, S. G. Mechanistic Studies of a Retaining α -Galactosyltransferase from *Neisseria Meningitidis*. *J. Biochem.* **2002**, *41* (16), 5075–5085. <https://doi.org/10.1021/bi012031s>.
- (20) Lairson, L. L.; Chiu, C. P. C.; Ly, H. D.; He, S.; Wakarchuk, W. W.; Strynadka, N. C. J.; Withers, S. G. Intermediate Trapping on a Mutant Retaining α -Galactosyltransferase Identifies an Unexpected Aspartate Residue. *J. Biol. Chem.* **2004**, *279* (27), 28339–28344. <https://doi.org/10.1074/jbc.M400451200>.
- (21) Lee, S. S.; Hong, S. Y.; Errey, J. C.; Izumi, A.; Davies, G. J.; Davis, B. G. Mechanistic Evidence for a Front-Side, S_Ni-Type Reaction in a Retaining Glycosyltransferase. *Nat. Chem. Biol.* **2011**, *7* (9), 631–638. <https://doi.org/10.1038/nchembio.628>.
- (22) Gibson, R. P.; Turkenburg, J. P.; Charnock, S. J.; Lloyd, R.; Davies, G. J. Insights into Trehalose Synthesis Provided by the Structure of the Retaining Glucosyltransferase OtsA. *Chem. Biol.* **2002**, *9* (12), 1337–1346.

- (23) Persson, K.; Ly, H. D.; Dieckelmann, M.; Wakarchuk, W. W.; Withers, S. G.; Strynadka, N. C. J. Crystal Structure of the Retaining Galactosyltransferase LgtC from *Neisseria Meningitidis* in Complex with Donor and Acceptor Sugar Analogs. *Nat. Struct. Biol.* **2001**, *8* (2), 166–175. <https://doi.org/10.1038/84168>.
- (24) Gastinel, L. N.; Bignon, C.; Misra, A. K.; Hindsgaul, O.; Shaper, J. H.; Joziase, D. H. Bovine A1, 3-Galactosyltransferase Catalytic Domain Structure and Its Relationship with ABO Histo-Blood Group and Glycosphingolipid Glycosyltransferases. *EMBO J.* **2001**, *20* (4), 638–649.
- (25) Patenaude, S. I.; Seto, N. O. L.; Borisova, S. N.; Szpacenko, A.; Marcus, S. L.; Palcic, M. M.; Evans, S. V. The Structural Basis for Specificity in Human ABO (H) Blood Group Biosynthesis. *Nat. Struct. Biol.* **2002**, *9* (9), 685–690.
- (26) Martinez-Fleites, C.; Proctor, M.; Roberts, S.; Bolam, D. N.; Gilbert, H. J.; Davies, G. J. Insights into the Synthesis of Lipopolysaccharide and Antibiotics through the Structures of Two Retaining Glycosyltransferases from Family GT4. *Chem. Biol.* **2006**, *13* (11), 1143–1152.
- (27) Jamaluddin, H.; Tumbale, P.; Withers, S. G.; Acharya, K. R.; Brew, K. Conformational Changes Induced by Binding UDP-2F-Galactose to α -1, 3 Galactosyltransferase-Implications for Catalysis. *J. Mol. Biol.* **2007**, *369* (5), 1270–1281.
- (28) Vetting, M. W.; Frantom, P. A.; Blanchard, J. S. Structural and Enzymatic Analysis of MshA from *Corynebacterium Glutamicum*: Substrate-Assisted Catalysis. *J. Bio. Chem.* **2008**, *283* (23), 15834–15844. <https://doi.org/10.1074/jbc.M801017200>.

- (29) Liang, D. M.; Liu, J. H.; Wu, H.; Wang, B. Bin; Zhu, H. J.; Qiao, J. J. Glycosyltransferases: Mechanisms and Applications in Natural Product Development. *Chem. Soc. Rev.* Royal Society of Chemistry November 21, 2015, pp 8350–8374. <https://doi.org/10.1039/c5cs00600g>.
- (30) Gómez, H.; Polyak, I.; Thiel, W.; Lluch, J. M.; Masgrau, L. Retaining Glycosyltransferase Mechanism Studied by QM/MM Methods: Lipopolysaccharyl- α -1,4-Galactosyltransferase C Transfers α -Galactose via an Oxocarbenium Ion-like Transition State. *J. Am. Chem. Soc.* **2012**, *134* (10), 4743–4752. <https://doi.org/10.1021/ja210490f>.
- (31) Ardèvol, A.; Rovira, C. The Molecular Mechanism of Enzymatic Glycosyl Transfer with Retention of Configuration: Evidence for a Short-Lived Oxocarbenium-like Species. *Angew. Chem., Int. Ed.* **2011**, *50* (46), 10897–10901. <https://doi.org/10.1002/anie.201104623>.
- (32) Fernández-González, M.; Boutureira, O.; Bernardes, G. J. L.; Chalker, J. M.; Young, M. A.; Errey, J. C.; Davis, B. G. Site-Selective Chemoenzymatic Construction of Synthetic Glycoproteins Using Endoglycosidases. *Chem. Sci.* **2010**, *1* (6), 709–715. <https://doi.org/10.1039/c0sc00265h>.
- (33) Lee, S. S.; Hong, S. Y.; Errey, J. C.; Izumi, A.; Davies, G. J.; Davis, B. G. Mechanistic Evidence for a Front-Side, S_Ni-Type Reaction in a Retaining Glycosyltransferase. *Nat. Chem. Biol.* **2011**, *7* (9), 631–638. <https://doi.org/10.1038/nchembio.628>.

- (34) Ziegler, M. O. P.; Jank, T.; Aktories, K.; Schulz, G. E. Conformational Changes and Reaction of Clostridial Glycosylating Toxins. *J. Mol. Biol.* **2008**, *377* (5), 1346–1356. <https://doi.org/10.1016/j.jmb.2007.12.065>.
- (35) Vliegthar, J.F.G. and Woods, R.J. Molecular Modeling of Retaining Glycosyltransferases, *NMR spectroscopy and computer modeling of carbohydrates: recent advances*. ACS **2006**.
- (36) Sinnott, M.L. and Jencks, W.P., Solvolysis of D-glucopyranosyl derivatives in mixtures of ethanol and 2, 2, 2-trifluoroethanol. *Journal of the American Chemical Society*, **1980**, *102*(6), 2026-2032.
- (37) Cowdrey, W.A., Hughes, E.D., Ingold, C.K., Masterman, S. and Scott, A.D. Reaction kinetics and the Walden inversion. Part VI. Relation of steric orientation to mechanism in substitutions involving halogen atoms and simple or substituted hydroxyl groups. *J. Chem. Soc.* **1937**, 257, 1252-1271.
- (38) Sinnott, M.L. and Souchart, I.J. The mechanism of action of β -galactosidase. Effect of aglycone nature and α -deuterium substitution on the hydrolysis of aryl galactosides. *Biochem. J.*, **1973**, *133*(1), pp.89-98.
- (39) Winchell, K. R.; Egeler, P. W.; Vanduin, A. J.; Jackson, L. B.; Karpen, M. E.; Cook, P. D. A Structural, Functional, and Computational Analysis of BshA, the First Enzyme in the Bacillithiol Biosynthesis Pathway. *J. Biochem.* **2016**, *55* (33), 4654–4665. <https://doi.org/10.1021/acs.biochem.6b00472>.

- (40) Newton, G. L.; Rawat, M.; La Clair, J. J.; Jothivasan, V. K.; Budiarto, T.; Hamilton, C. J.; Claiborne, A.; Helmann, J. D.; Fahey, R. C. Bacillithiol Is an Antioxidant Thiol Produced in Bacilli. *Nat. Chem. Biol.* **2009**, *5* (9), 625–627.
<https://doi.org/10.1038/nchembio.189>.
- (41) Gaballa, A.; Newton, G. L.; Antelmann, H.; Parsonage, D.; Upton, H.; Rawat, M.; Claiborne, A.; Fahey, R. C.; Helmann, J. D. Biosynthesis and Functions of Bacillithiol, a Major Low-Molecular-Weight Thiol in Bacilli. *Proc. Natl. Acad. Sci. U.S.A.* **2010**, *107* (14), 6482–6486. <https://doi.org/10.1073/pnas.1000928107>.
- (42) Gaballa, A.; Antelmann, H.; Hamilton, C. J.; Helmann, J. D. Regulation of Bacillus Subtilis Bacillithiol Biosynthesis Operons by Spx. *J. Microbiol. (N Y)* **2013**, *159* (Pt_10), 2025–2035.
- (43) Sharma, S. V.; Arbach, M.; Roberts, A. A.; Macdonald, C. J.; Groom, M.; Hamilton, C. J. Biophysical Features of Bacillithiol, the Glutathione Surrogate of Bacillus Subtilis and Other Firmicutes. *Chembiochem.* **2013**, *14* (16), 2160–2168.
- (44) Newton, G. L.; Fahey, R. C.; Rawat, M. Detoxification of Toxins by Bacillithiol in Staphylococcus Aureus. *J. Microbiol. (N Y)* **2012**, *158* (Pt 4), 1117.
- (45) Helmann, J. D. Bacillithiol, a New Player in Bacterial Redox Homeostasis. *Antioxid. Redox. Signal.* **2011**, *15* (1), 123–133.
- (46) Fahey, R. C.; Sundquist, A. R. Evolution of Glutathione Metabolism. *Adv. Enzymol. Relat. Areas. Mol. Biol.* **1991**, *64* (1), 53.

- (47) Dolphin, D., Poulson, R. and Avramovic, O. *Glutathione: Chemical, biochemical, and medical aspects*. New York: Wiley, 1989.
- (48) Thompson, M. K.; Keithly, M. E.; Harp, J.; Cook, P. D.; Jagessar, K. L.; Sulikowski, G. A.; Armstrong, R. N. Structural and Chemical Aspects of Resistance to the Antibiotic Fosfomycin Conferred by FosB from *Bacillus Cereus*. *J. Biochem.* **2013**, *52* (41), 7350–7362.
- (49) Lamers, A. P.; Keithly, M. E.; Kim, K.; Cook, P. D.; Stec, D. F.; Hines, K. M.; Sulikowski, G. A.; Armstrong, R. N. Synthesis of Bacillithiol and the Catalytic Selectivity of FosB-Type Fosfomycin Resistance Proteins. *Org. Lett.* **2012**, *14* (20), 5207–5209.
- (50) Sharma, S. V.; Jothivasan, V. K.; Newton, G. L.; Upton, H.; Wakabayashi, J. I.; Kane, M. G.; Roberts, A. A.; Rawat, M.; La Clair, J. J.; Hamilton, C. J. Chemical and Chemoenzymatic Syntheses of Bacillithiol: A Unique Low-molecular-weight Thiol amongst Low G+ C Gram-positive Bacteria. *Angew. Chem. Int. Ed.* **2011**, *50* (31), 7101.
- (51) Dinh, A.; Salomon, J.; Bru, J. P.; Bernard, L. Fosfomycin: Efficacy against Infections Caused by Multidrug-Resistant Bacteria. *Scand. J. Infect. Dis.* **2012**, *44* (3), 182–189.
- (52) Upton, H.; Newton, G. L.; Gushiken, M.; Lo, K.; Holden, D.; Fahey, R. C.; Rawat, M. Characterization of BshA, Bacillithiol Glycosyltransferase from *Staphylococcus Aureus* and *Bacillus Subtilis*. *FEBS Lett.* **2012**, *586* (7), 1004–1008.
<https://doi.org/10.1016/j.febslet.2012.02.028>.

- (53) Parsonage, D.; Newton, G. L.; Holder, R. C.; Wallace, B. D.; Paige, C.; Hamilton, C. J.; Dos Santos, P. C.; Redinbo, M. R.; Reid, S. D.; Claiborne, A. Characterization of the N-Acetyl- α -D-Glucosaminyl L-Malate Synthase and Deacetylase Functions for Bacillithiol Biosynthesis in Bacillus Anthracis. *J. Biochem.* **2010**, *49* (38), 8398–8414. <https://doi.org/10.1021/bi100698n>.
- (54) Ruane, K. M.; Davies, G. J.; Martinez-Fleites, C. Crystal Structure of a Family GT4 Glycosyltransferase from Bacillus Anthracis ORF BA1558. *Proteins: Struct., Funct. and Genet.* **2008**, *73* (3), 784–787. <https://doi.org/10.1002/prot.22171>.
- (55) Werner, R. M.; Stivers, J. T. Kinetic Isotope Effect Studies of the Reaction Catalyzed by Uracil DNA Glycosylase: Evidence for an Oxocarbenium Ion–Uracil Anion Intermediate. *J. Biochem.* **2000**, *39* (46), 14054–14064.
- (56) Chen, X.-Y.; Berti, P. J.; Schramm, V. L. Transition-State Analysis for Depurination of DNA by Ricin A-Chain. *J. Am. Chem. Soc.* **2000**, *122* (28), 6527–6534.
- (57) Kline, P. C.; Schramm, V. L. Purine Nucleoside Phosphorylase. Catalytic Mechanism and Transition-State Analysis of the Arsenolysis Reaction. *J. Biochem.* **1993**, *32* (48), 13212–13219.
- (58) Lewandowicz, A.; Schramm, V. L. Transition State Analysis for Human and Plasmodium Falciparum Purine Nucleoside Phosphorylases. *J. Biochem.* **2004**, *43* (6), 1458–1468.
- (59) Parkin, D. W. Methods for the Determination of Competitive and Noncompetitive Kinetic Isotope Effects. *Enzyme mechanism from isotope effects* 1991, *10*, 269–289.

- (60) Kline, P. C.; Schramm, V. L. Pre-Steady-State Transition-State Analysis of the Hydrolytic Reaction Catalyzed by Purine Nucleoside Phosphorylase. *J. Biochem.* **1995**, *34* (4), 1153–1162.
- (61) Horenstein, B. A.; Parkin, D. W.; Estupinan, B.; Schramm, V. L. Transition-State Analysis of Nucleoside Hydrolase from *Crithidia Fasciculata*. *J. Biochem.* **1991**, *30* (44), 10788–10795.
- (62) Scheuring, J.; Schramm, V. L. Pertussis Toxin: Transition State Analysis for ADP-Ribosylation of G-Protein Peptide Ai3C20. *J. Biochem.* **1997**, *36* (27), 8215–8223.
- (63) Scheuring, J.; Berti, P. J.; Schramm, V. L. Transition-State Structure for the ADP-Ribosylation of Recombinant Gi α 1 Subunits by Pertussis Toxin. *J. Biochem.* **1998**, *37* (9), 2748–2758.
- (64) Parikh, S. L.; Schramm, V. L. Transition State Structure for ADP-Ribosylation of Eukaryotic Elongation Factor 2 Catalyzed by Diphtheria Toxin. *J. Biochem.* **2004**, *43* (5), 1204–1212.
- (65) Berti, P. J.; Blanke, S. R.; Schramm, V. L. Transition State Structure for the Hydrolysis of NAD⁺ Catalyzed by Diphtheria Toxin. *J. Am. Chem. Soc.* **1997**, *119* (50), 12079–12088.
- (66) Rising, K. A.; Schramm, V. L. Transition State Analysis of NAD⁺ Hydrolysis by the Cholera Toxin Catalytic Subunit. *J. Am. Chem. Soc.* **1997**, *119* (1), 27–37.
- (67) Scheuring, J.; Schramm, V. L. Pertussis Toxin: Transition State Analysis for ADP-Ribosylation of G-Protein Peptide Ai3C20. *J. Biochem.* **1997**, *36* (27), 8215–8223.

- (68) Hunt, C.; Gillani, N.; Farone, A.; Rezaei, M.; Kline, P. C. Kinetic Isotope Effects of Nucleoside Hydrolase from *Escherichia Coli*. *Biochim. Biophys. Acta. Proteins Proteom.* **2005**, *1751* (2), 140–149.
- (69) Parkin, D. W.; Schramm, V. L. Effects of Allosteric Activation on the Primary and Secondary Kinetic Isotope Effects for Three AMP Nucleosidases. *J. Biol. Chem.* **1984**, *259* (15), 9418–9425.
- (70) Berti, P. J.; Schramm, V. L. Transition State Structure of the Solvolytic Hydrolysis of NAD⁺. *J. Am Chem. Soc.* **1997**, *119* (50), 12069–12078.
- (71) Singh, V.; Lee, J. E.; Núñez, S.; Howell, P. L.; Schramm, V. L. Transition State Structure of 5'-Methylthioadenosine/S-Adenosylhomocysteine Nucleosidase from *Escherichia Coli* and Its Similarity to Transition State Analogues. *J. Biochem.* **2005**, *44* (35), 11647–11659.
- (72) Birck, M. R.; Schramm, V. L. Nucleophilic Participation in the Transition State for Human Thymidine Phosphorylase. *J. Am. Chem. Soc.* **2004**, *126* (8), 2447–2453.
- (73) Sunko, D.E., Szele, I. and Hehre, W.J. Hyperconjugation and the angular dependence of beta.-deuterium isotope effects. *J. Am. Chem. Soc.* **1977**, *99*(15), pp.5000-5005.
- (74) Parkin, D. W.; Schramm, V. L. Catalytic and Allosteric Mechanism of AMP Nucleosidase from Primary, Beta.-Secondary, and Multiple Heavy Atom Kinetic Isotope Effects. *J. Biochem.* **1987**, *26* (3), 913–920.
- (75) Parkin, D. W.; Mentch, F.; Banks, G. A.; Horenstein, B. A.; Schramm, V. L. Transition-State Analysis of a Vmax Mutant of AMP Nucleosidase by the

- Application of Heavy-Atom Kinetic Isotope Effects. *J. Biochem.* **1991**, *30* (18), 4586–4594.
- (76) Lin, X.; Xiao, C.; Ling, L.; Guo, L.; Guo, X. A Dual-Mode Reactive Matrix for Sensitive and Quantitative Analysis of Carbohydrates by MALDI-TOF MS. *Talanta* **2021**, *235*. <https://doi.org/10.1016/j.talanta.2021.122792>.
- (77) Upton, H.; Newton, G. L.; Gushiken, M.; Lo, K.; Holden, D.; Fahey, R. C.; Rawat, M. Characterization of BshA, Bacillithiol Glycosyltransferase from *Staphylococcus Aureus* and *Bacillus Subtilis*. *FEBS Lett.* **2012**, *586* (7), 1004–1008. <https://doi.org/10.1016/j.febslet.2012.02.028>.
- (78) Gibb, S.; Strimmer, K. MALDIquant: A Versatile R Package for the Analysis of Mass Spectrometry Data. *Bioinform.* 2012, *28* (17), 2270–2271. <https://doi.org/10.1093/bioinformatics/bts447>.
- (79) Gibb, S.; Strimmer, K. Mass Spectrometry Analysis Using MALDIquant. *Arxiv* 2016.

Chapter 5: Summary and Future Directions

5.1 SUMMARY AND FUTURE DIRECTIONS

Kinetic isotope effect (KIE) measurements are a powerful tool to interrogate the microscopic steps in enzyme catalyzed reactions and can provide detailed information about transition state structures. However, the application of KIE measurements to study enzymatic reactions is not widely applied due to the tedious and complex analytical workflows required to measure KIEs with sufficient precision. In this thesis I described the development of a novel competitive KIE measurement method using MALDI-TOF-MS and the investigation of the transition state of glycosyltransferase enzyme BshA from *B. subtilis*.

First, we developed a method for the direct measurement of competitive KIEs using a whole molecule matrix assisted laser desorption ionization (MALDI) time of flight (TOF) mass spectrometry (MS). This approach enabled quantitative measurements of both relative isotope abundance of an analyte and fractional conversion F in single measurements without the need for purification prior to analysis. Using isotope labeled internal standard introduced during reaction to quench the enzyme reaction at multiple time points enabled the simultaneous measurement of R and F relative to the internal standard for each sample as the reaction progresses. We measured $1'$ - ^{13}C KIEs for *E. coli* β -galactosidase (LacZ) catalyzed hydrolysis of lactose, and obtained an average primary [$1'$ - ^{13}C] KIE of 1.034 ± 0.005 .

In order to prepare isotopically labelled UDP-GlcNAc substrates necessary for transition state analysis of the reaction catalyzed by the glycosyltransferase BshA, we described the use of two chemoenzymatic approaches. The first of these methods used a one-pot four-enzyme reaction, modified from the Chen lab,¹³⁴ using NahK, GlmU,

PK and IPPase to prepare UDP-GlcNAc, [1''-¹³C]UDP-GlcNAc (**3.2**), [2''-¹³C]UDP-GlcNAc (**3.3**), and [¹³C₆]UDP-GlcNAc (**3.4**) in 40-83% yields from the appropriately labeled GlcNAc precursors. We then used the reaction catalyzed by WecB to enzymatically incorporate deuterium into the into the 2''-H position of UDP-GlcNAc to produce [2''-²H]UDP-GlcNAc by carrying out the enzymatic reaction in D₂O (**3.5**). Finally, we have begun to work on the synthesis of [1''-¹⁸O]UDP-GlcNAc and describe an approach to prepare this substrate that is currently underway in the lab.

BshA is a retaining glycosyltransferase GT-4 family enzyme, typically hypothesized to utilize an a front-face S_{Ni} (A_ND_N) reaction mechanism in which the departure of the UDP leaving group and attack by the malate hydroxyl group at the anomeric position occur at the same face of the sugar in a concerted fashion, with a single TS that involves simultaneous bond formation and bond breaking.¹⁹⁶ Although direct experimental support for the S_{Ni} mechanism over a S_{N1} mechanism are limited, one way to distinguish between these two mechanistic manifolds is through the measurement of experimental KIEs. While structural studies^{196,210,211} provide some insight into the active site of BshA, there is limited information about the dynamic mechanistic details of BshA which would determine more conclusively whether it goes through the S_{Ni}-like reaction mechanism.

Using the quantitative whole molecule MALDI-TOF MS approach, we determined multiple competitive KIEs for the enzymatic reaction catalyzed by BshA. KIEs were measured using UDP-GlcNAc donor substrates containing specific isotope labels surrounding the reaction center: [1''-¹³C]UDP-GlcNAc, [2''-²H]UDP-GlcNAc

and [2''-¹³C]UDP-GlcNAc). The experimental KIE measured using [2''-¹³C]UDP-GlcNAc had a value of 1.001 ± 0.001 , which indicated that there is no isotope effect for 2''-¹³C and corroborated that C2'' position does not undergo a significant change in bonding at the TS of BshA. The experimental KIE measured using [2''-²H]UDP-GlcNAc with in a KIE value of 1.111 ± 0.003 indicated a high oxocarbenium ion-like character and hyperconjugation between H2'' and the electron-deficient C1'' of the oxocarbenium and hence, flattening of C5''-O5''-C1''-C2'' of the pyranose ring. Finally, the experimental KIE measured using [1''-¹³C]UDP-GlcNAc with a KIE value of 1.010 ± 0.011 was consistent with a stepwise D_N*A_N with discrete oxocarbenium ion intermediate at the rate determining TS.

While previous studies suggested a front-face S_Ni (D_NA_N) TS for the conjugation of UDP-GlcNAc and L-malate, our KIE results show that a stepwise mechanism resulting in the formation of a discrete, though likely short lived, oxocarbenium ion intermediate is more likely. TS information gathered on BshA with these measurements could be used for the efficient design of inhibitors for BshA. Given the observed isotope effects, incorporating positive charge in and nearby C1'' position of UDP-GlcNAc via nitrogen atoms could serve as a mimic for this oxocarbenium ion-like transition state. Since BshA is involved in *B. subtilis* bacterial infections leading to sepsis, especially in immunocompromised patients, developing alternative treatments for this infection could be of interest for the medical research community.

The application of this MALDI-TOF MS approach on analysis of LacZ and BshA has demonstrated the precision of KIE measurements comparable to precision obtained using competitive radioisotope labelling, and NMR based approaches. This

precision was obtained while improving on the limitations of the aforementioned approaches. The limitations of previous approaches included extensive purification of analytes prior to analysis, separate measurements of R and F, and requirement of large quantities of multi-isotopically labeled substrates. It is important to note that incorporating multiple labels in a single substrate, i.e. radioisotope labeling, makes synthesis of these materials extremely challenging due to their unstable nature and proclivity to degradation. Our MALDI-TOF MS based KIE measurement method bypasses all of these limitations, making it a more user-friendly approach applicable to a wider research community. Our method requires only μg quantities of substrates with a single isotope label, does not require any purification of analytes prior to analysis and allows for a simultaneous measurement of R and F in each time point of the reaction. Being that MALDI-TOF MS technology is often available at universities and it is relatively easy to get trained on this instrument, our hope is that more research labs will use this method to quickly and precisely determine transition states of the enzymes they are interested in. Furthermore, we hope that they can use this information for transition state analogue design, as a more efficient and less time-consuming strategy than high-throughput screening.

Another benefit of using MALDI-TOF MS for KIE analysis is that it can analyze small, medium and large size molecules. Hence, our method should not be limited to a specific class of enzymes. We predict application of our method to all types of enzymes – hydrolases, oxidoreductases, lyases, transferases, ligases and isomerases. Selection of matrix and optimization of ionization efficiency will be needed prior to analysis. Another important factor to consider is the analysis window. Major

contaminants or side products should not overlap with analyte peaks and ideally not appear in the analysis window at all. Possible ways to resolve these issues include ion deflection, alternative matrix selection and repurification of starting materials prior to enzymatic reaction.

Furthermore, our method could be applied to study chemical reactions as well, although optimal ionization of very small molecules < 200 m/z would be challenging due to signal suppression from the matrix and detection limits of the instrument. Another challenge with chemical reaction mixture analysis is its potential corrosiveness that would interfere with MALDI-TOF MS acquisition. The plate used for MALDI-TOF MS corrodes with very low and very high pH, so pH adjustment of the samples would be required prior to analysis.

Based on our preliminary tests on ESI-MS, we expect that our overall strategy for KIE measurements could be applied to analysis with different type of mass spectrometry instruments. ESI-MS instruments would require development of purification protocols prior to analysis, and testing of precision is recommended prior to full analysis of KIE values. Although we don't predict that extending our method onto different MS instruments would maintain its wide application, we would expect that specific reactions may benefit from a different type of ionization of their substrates or products.

Future development of this method towards automation of quenching and larger scale data analysis could increase its application and use in industry. Automation of reaction mixture quenching, and data analysis workflows would further simplify the KIE measurement process making the measurement of KIEs for TS analysis a more

experimentally accessible technique for the broader enzymology research community and industry-based research. Development of a programmable mixing instrument would automate chemical quenching of enzymatic KIE reaction mixtures with the reproducible introduction of an isotopically labeled internal standard, and hence enable the measurement of isotope ratios at multiple fractional conversions from a single enzyme reaction mixture with even higher reproducibility by reducing the variability coming from human error. In addition, development of scripts that would automate data analysis post peak integration would enable faster measurements and analysis of multiple heavy atom KIEs.

Our MALDI-TOF MS method for KIE measurements could furthermore be applied to study other retaining glycosyltransferases hypothesized to go through S_Ni -like mechanism to shed light on the nuances of the transition state of these enzymes, as well as on other glycosyltransferases and glycosyl-hydrolases whose mechanisms still remain to be elucidated. In Poulin lab, one such example includes PgaCD, a glycosyltransferase involved in the formation of bacterial biofilm. Targeting enzymes involved in biofilm formation for inhibitor design is also of interest for the medical research community, as the potential therapeutic benefits could solve the problem of persistent bacterial biofilm infections. Moreover, we hope that future research extends the application of this methodology onto inhibitor design of enzymes involved in progression and medication-resistance of other diseases such as viruses and different types of cancer.

5.2 BIBLIOGRAPHY

- (1) Chen, Y.; Thon, V.; Li, Y.; Yu, H.; Ding, L.; Lau, K.; Qu, J.; Hie, L.; Chen, X. One-Pot Three-Enzyme Synthesis of UDP-GlcNAc Derivatives. *Chem. Comm.* **2011**, 47 (38), 10815–10817. <https://doi.org/10.1039/c1cc14034e>.
- (2) Winchell, K. R.; Egeler, P. W.; Vanduinen, A. J.; Jackson, L. B.; Karpen, M. E.; Cook, P. D. A Structural, Functional, and Computational Analysis of BshA, the First Enzyme in the Bacillithiol Biosynthesis Pathway. *J. Biochem.* **2016**, 55 (33), 4654–4665. <https://doi.org/10.1021/acs.biochem.6b00472>.
- (3) Parsonage, D.; Newton, G. L.; Holder, R. C.; Wallace, B. D.; Paige, C.; Hamilton, C. J.; Dos Santos, P. C.; Redinbo, M. R.; Reid, S. D.; Claiborne, A. Characterization of the N-Acetyl- α -D-Glucosaminyl L-Malate Synthase and Deacetylase Functions for Bacillithiol Biosynthesis in Bacillus Anthracis. *J. Biochem.* **2010**, 49 (38), 8398–8414. <https://doi.org/10.1021/bi100698n>.
- (4) Ruane, K. M.; Davies, G. J.; Martinez-Fleites, C. Crystal Structure of a Family GT4 Glycosyltransferase from Bacillus Anthracis ORF BA1558. *Proteins: Structure, Function and Genetics* **2008**, 73 (3), 784–787. <https://doi.org/10.1002/prot.22171>.